AD-A173 603

ON THE BUCKLING OF SANDWICH BEAMS
CONTAINING AN UNBONDED REGION

by

Carl Joseph Frushon, B.S.

THESIS

Presented to the Faculty of the Graduate School of

The University of Texas at Austin

in Partial Fulfillment

of the Degree of

Master of Science in Engineering

THE UNIVERSITY OF TEXAS AT AUSTIN

May 1986

86 11 4 092

REPORT DOCUMENTATION PAGE		READ INSTRUCTIONS BEFORE COMPLETING FORM
1. REPORT NUMBER AFIT/CI/NR 86- 185T	2. GOVT ACCESSION NO. AD A1736 03	3. RECIPIENT'S CATALOG NUMBER
4. TITLE *(and Subtitle)* On The Buckling Of Sandwich Beams Containing An Unbonded Region		5. TYPE OF REPORT & PERIOD COVERED THESIS/DISSERTATION/
		6. PERFORMING ORG. REPORT NUMBER
7. AUTHOR(s) Carl Joseph Frushon		8. CONTRACT OR GRANT NUMBER(s)
9. PERFORMING ORGANIZATION NAME AND ADDRESS AFIT STUDENT AT: The University of Texas		10. PROGRAM ELEMENT. PROJECT, TASK AREA & WORK UNIT NUMBERS
11. CONTROLLING OFFICE NAME AND ADDRESS		12. REPORT DATE 1986
		13. NUMBER OF PAGES 117
14. MONITORING AGENCY NAME & ADDRESS*(if different from Controlling Office)*		15. SECURITY CLASS. *(of this report)* UNCLASS
		15a. DECLASSIFICATION/DOWNGRADING SCHEDULE

16. DISTRIBUTION STATEMENT *(of this Report)*

APPROVED FOR PUBLIC RELEASE; DISTRIBUTION UNLIMITED

17. DISTRIBUTION STATEMENT *(of the abstract entered in Block 20, if different from Report)*

18. SUPPLEMENTARY NOTES
APPROVED FOR PUBLIC RELEASE: IAW AFR 190-1

LYNN E. WOLAVER 3 Oct 86
Dean for Research and
Professional Development
AFIT/NR

19. KEY WORDS *(Continue on reverse side if necessary and identify by block number)*

20. ABSTRACT *(Continue on reverse side if necessary and identify by block number)*

ATTACHED ...

DD $_{1\ JAN\ 73}^{FORM}$ 1473 EDITION OF 1 NOV 65 IS OBSOLETE

ABSTRACT

This study involves a combined experimental and analytical analysis of the stability of a sandwich beam (overall length of 16.5 inches) with a partially unbonded faceplate. For simplicity, the beam considered was simply supported. Fully bonded beams as well as beams with unbonded lengths ranging from 0.5 to 5.0 inches were tested.

Two failure regimes were observed. A distinct collapse load was evident in experiments with short unbond lengths ($\leq$ 2.0 inches). The loading histories of beams with longer unbond lengths ($\geq$ 3.0 inches) were found to be characterized by a limit load. In all cases, a transition from a symmetric to a nonsymmetric buckling shape occurred. The presence of the unbonded region was found to drastically reduce the load-carrying capacity of the sandwich structure. A power-law relationship was found between the unbond length and maximum load.

The unbonded sandwich beam was modeled as an assembly of three beams. This structure was assumed to be initially geometrically perfect. A solution was found numerically and began when the load within the unbonded faceplate was greater than the Euler buckling load for that section. Limit loads were predicted for all unbond lengths. The model was found to predict the failure load of a sandwich beam (unbond lengths $\geq$ 2.0 inches) to within 12.5%.

Possible improvements and extensions of both the experimental and analytical aspects of the investigation were discussed.

ACKNOWLEDGMENTS

The author wishes to take this opportunity to express his indebtedness to his advisor, Dr. Stelios Kyriakides, whose hours of patience, interest, expertise, and good humor were instrumental in the author's acquisition of knowledge in this field of study. Sincere thanks must be extended to Dr. Kenneth Liechti for his guidance, advice, and the use of his video recording and analyzing equipment, all of which greatly contributed to this research. Encouragement and assistance from the other ASE/EM faculty, staff, and fellow graduate students were highly valued. Thanks are also due to the United States Air Force for affording the author the opportunity to obtain the degree of Master of Science in Engineering.

In addition, the author wishes to warmly acknowledge the continuous support and encouragement from his family and friends. Finally, a very special thanks goes to Debra for her love, patience, and understanding.

Accesion For		
NTIS CRA&I	☑	
DTIC TAB	☐	
Unannounced	☐	
Justification		
By		
Distribution /		
Availability Codes		
Dist	Avail and/or Special	
A-1		

iii

ABSTRACT

This study involves a combined experimental and analytical analysis of the stability of a sandwich beam (overall length of 16.5 inches) with a partially unbonded faceplate. For simplicity, the beam considered was simply supported. Fully bonded beams as well as beams with unbonded lengths ranging from 0.5 to 5.0 inches were tested. $>$ or $=$ $<$ or $=$

Two failure regimes were observed. A distinct collapse load was evident in experiments with short unbond lengths ($\leq$ 2.0 inches). The loading histories of beams with longer unbond lengths ($\geq$ 3.0 inches) were found to be characterized by a limit load. In all cases, a transition from a symmetric to a nonsymmetric buckling shape occurred. The presence of the unbonded region was found to drastically reduce the load-carrying capacity of the sandwich structure. A power-law relationship was found between the unbond length and maximum load.

The unbonded sandwich beam was modeled as an assembly of three beams. This structure was assumed to be initially geometrically perfect. A solution was found numerically and began when the load within the unbonded faceplate was greater than the Euler buckling load for that section. Limit loads were predicted for all unbond lengths. The model was found to predict the failure load of a sandwich beam (unbond lengths $\geq$ 2.0 inches) to within 12.5%. $>$ or $=$

Possible improvements and extensions of both the experimental and analytical aspects of the investigation were discussed.

iv

TABLE OF CONTENTS

vi

viii

NOMENCLATURE

b	beam width
c	core thickness
D	flexural rigidity
D_i	flexural rigidity of beam section $i = 1, 2, 3$
d_a	$c + t_a$
d_f	$c + t_f$
E_a	Young's Modulus of the adhesive
E_c	Young's Modulus of the core (through the thickness)
E_f	Young's Modulus of the faceplate
G_W	core shear modulus
h	sandwich beam thickness
I_a	adhesive 2nd moment of area
I_f	faceplate 2nd moment of area
k_c	elastic foundation stiffness
L	beam length
L_o	test specimen length $(L + l_r)$
l	critical wrinkling half-wavelength
l_i	length of beam section $i = 1, 2, 3$
l_r	length of end fixture
M	moment
M_i	moment of beam section $i = 1, 2, 3$
N	load
N_B	critical buckling load
N_C	critical shear crimping load
N_D	critical intra-cell dimpling load
N_E	Euler buckling load
N_S	shear component of buckling
N_W	critical faceplate wrinkling load
N_Y	critical faceplate yielding load

P	axial load (Nb)
P_i	axial load in beam sections $i = 1, 2, 3$
r	distance from faceplate/adhesive interface to neutral axis of beam section 2
s	cell diameter of hexagonal honeycomb core
t_a	adhesive thickness
t_f	faceplate thickness
u_i	load in beam section $i = 1, 2, 3$ (normalized by the first Euler buckling load for a clamped-clamped beam)
V	shear force
$W3_o$	deflection of unbonded faceplate mid-point
w	out-of-plane deflections along z-axis
w_b	deflections due to bending
w_i	displacements of beam section $i = 1, 2, 3$ along z-axis
w_s	deflections due to shear
x_i	coordinates of beam section $i = 1, 2, 3$
α	critical dimpling load constant
α_s	shear stress shape factor
γ	shear strain
Δ	axial displacement of beam ends
δ	deflection of the interface from the unloaded position
δ_o	deflection of the end fixture from the unloaded state
θ	beam slope at the interface of the unbond
θ_o	beam slope at the interface of the end fixture
ν	Poisson's ratio
ρ	density of the core
σ	normal stress
σ_y	yield stress (0.2% strain offset)
τ	shear stress

LIST OF TABLES

LIST OF FIGURES

Chapter 1

INTRODUCTION

Throughout the history of the aerospace industry, Man's ambition to fly faster, farther, and higher has produced many sophisticated and expensive flight vehicles. Today, pure desire to achieve these goals is insufficient motivation for producing newer craft. A variety of factors, from economical feasibility to availability of resources, have come to significantly influence the design and manufacturing processes.

Thus, the role of the design engineer has changed from "making an aircraft fly," to "making it inexpensive and fly more efficiently." In the area of structural design, analysis has come to place more emphasis on developing lighter, stronger and more versatile, yet specialized materials. Aircraft once chiefly made from plywood and then aluminum are now manufactured with large amounts of fiberglass and carbon fiber epoxy-resin composites.

Another "new" material which is becoming more widely used in aircraft and space vehicles is the sandwich structure. Although not a recent innovation--the concept of sandwich construction has been accredited to Fairbairn (1849) [1]--its wider use has been affected by newly developed lightweight core and faceplate materials and improved adhesives and bonding methods.

Prior to discussing some of the advantages, disadvantages, uses, and failure characteristics of the sandwich structure, a proper definition is in order.

1.1 DEFINITION OF A SANDWICH STRUCTURE

A sandwich structure was identified by the American Society for Testing Materials as "A laminar construction comprising a combination of alternating dissimilar simple or composite materials assembled and intimately fixed in relation to each other so as to

1

use the properties of each to attain specific structural advantages for the whole assembly" [2]. In aerospace applications, a typical sandwich construction usually contains two similar faceplates which are adhesively bonded to a core (fig. 1.1).

The faceplates are typically made from strong, thin, stiff materials such as aluminum, fiberglass, or graphite-epoxy fiber composites. However, the core is usually much thicker, more flexible, and less dense than the faceplates. Cores for aerospace applications are often made from aluminum, resin-reinforced paper, glass, or stainless steel and titanium alloys, and are shaped in hexagonal honeycomb or corrugated configurations. The volume of the honeycomb core is typically 90 to 99 percent open space [3].

Once the faceplates are securely bonded to the core, this structure behaves like an "I" beam. The faceplates, being the primary load-carrying members, are comparable to the "I" beam flanges, while the core, which separates and supports this skin, is similar to the web.

Like the web, the honeycomb core carries the majority of the shearing stresses. Since the faceplates carry most of the bending load as tensile and compressive stresses, the stiffness of the beam can be greatly increased by spreading the faceplates farther apart. The translation of the faceplates' moment of inertia away from the centroid of the entire structure is the mechanism which causes this increase in the beam flexural rigidity (D) (See Appendix A), without significantly increasing the weight of the structure.

To further emphasize this point, consider a solid metal laminate of thickness t and a sandwich panel with core thickness t and overall thickness 2t. The sandwich will exhibit a 7 fold increase in stiffness, and an increase in strength over the solid plate by a factor of 3.5, with only a 5% increase in weight. Increasing the sandwich core thickness so that the overall height is now 4t, increases the stiffness by 37 times, and the strength by

9.25 times above the solid laminate. This stronger and significantly stiffer sandwich panel still only increased in weight by 9% [3].

The advantages of a sandwich construction are thus obvious. Large strength-to-weight and stiffness-to-weight ratios are the primary and most important properties of the sandwich structure. In addition, the core supports the faceplates and keeps them parallel over the entire region of the structure, adding to the torsional stiffness. Finally, the flexible core allows freedom to easily manufacture curved panels, and the core can be machined into a variety of shapes for special applications.

1.2   SANDWICH STRUCTURE APPLICATIONS

In the aerospace industry, sandwich structures have been marginally used in aircraft since the WWII "Mosquito." Today however, new applications are continuously being conceived for use in both military and civilian vehicles--from wing tips and speed brakes in the McDonnell-Douglas F-15 and F-18 tactical fighters, entire control surfaces in the DC-10, Rockwell's B-1B bomber and Boeing's 767, Rotodomes of the AWACS surveillance aircraft, Sikorsky's UH-60 helicopter main rotor blades [3], DC-9-80 engine nacelles, Airbus A-310 empennage [4], to the design of entire aircraft wings [5] and the entire monocoque fuselage of the Avtek 400 turboprop aircraft, which because of its sandwich fuselage boasts the ability to carry six persons across the country on a single tank of fuel [6].

Uses of sandwich structures are not limited to aircraft structural components. They are also found in airplane bulkheads and seats where weight savings will additionally increase overall performance. Outside the aerospace industry, sandwich panels are used for tooling structures, molds, energy absorption, and packaging. In addition, these structural panels are used in buildings, from homes to high-rise office buildings [7-9].

In the future, use of the sandwich structure should greatly increase with further applications to space-based technologies. Lightweight sandwich structures could be easily carried aboard the space shuttle for construction of spacestation bulkheads, storage areas, equipment platforms, and deep-space vehicles. In fact, a sandwich shell structure is presently being considered for the fuel tank of the second generation (single-stage-to-orbit) Space Transportation System [10].

1.3   SANDWICH STRUCTURE PROBLEM AREAS

This versatile sandwich structure is not the solution to every problem where high-strength and low-weight structures are needed. It too suffers from deficiencies, as do all structural materials. In the area of design, some difficulties arise in calculating sandwich loading characteristics because of the complex and little-understood relationship between the adhesive and honeycomb [11].

Faulty bonds and damage to the structure during the manufacturing process can lead to reduced load-carrying abilities [2]. In addition, solvents within the adhesive may vaporize during the curing process and become trapped within the honeycomb cells. After a period of time, the core may warp, the resins may leach, the organic materials can deteriorate, and in cold environments ice may form and damage the bonds [12].

During use, safety inspections of sandwich components prove quite cumbersome because critical damage usually occurs within the structure. In addition, there are presently no quick and efficient methods for determining the integrity of sandwich constructions. Ultrasonic testing may be used, but getting the sandwich submersed in water can be difficult, especially if it is part of a 767 wing. Still, this method of testing is not efficient in detecting voids within the adhesive bond [2]. While portable ultrasonic and x-ray techniques are available, maintaining inspections of a fleet of

aircraft, which widely use sandwich components, can be a formidable task. Other methods for testing the quality of the sandwich can be more accurate, but are usually destructive.

In the Avtek 400 [6], 25% of the labor cost to rivet and fasten components together was saved because the aircraft was glued together. However, should the need arise to replace a defective section of sandwich construction, repair can be very difficult. Although methods exist [2], ensuring that the structure will be capable of identical loading conditions can be a tedious task.

1.4 PURPOSE OF THIS RESEARCH

There are several modes of failure for a sandwich structure (see chapter 2). A majority of the analytical and experimental work to determine these modes has been performed by the U.S. Department of Agriculture's Forest Products Laboratory--from effects of shear deformation [13], to simply supported panel buckling [14].

Within the confines of this study, it was desired to examine the effects of an unbonded region on the overall buckling of a sandwich plate. Motivation for this work stems from the fact that this seems to be one of the most critical failure modes experienced by sandwich structures on flight vehicles (e.g., ice may form within a sandwich panel and cause delamination of a faceplate). If the structure happens to be a primary load-carrying member or control surface of an aircraft, failure can cause catastrophic loss of equipment and life.

In addition, apparent lack of significant analysis on this important failure topic necessitates discussion of this failure mode. As a first step, it was thought prudent to narrow the scope of this analysis to the study of the effects of an unbonded region on the buckling failure of a sandwich beam. Once a basic understanding of this failure mode is accomplished, extensions to the more useful and general plate problem will be less laborious.

Chapter 2
EXPERIMENTAL PROCEDURE

Experimentation was important in establishing the effect of the presence of an unbonded area on sandwich beam buckling. In order to achieve this goal, a careful examination of major alternate modes of sandwich beam failure was necessary. Within this chapter, an overview of the steps necessary to construct and test this composite structure is presented. Described are the design and construction of the sandwich beam and its simple-support joints, the testing apparatus used, the measurements of the sandwich component material properties, and the data acquisition and reduction techniques used.

2.1   SPECIMEN DESIGN

The sandwich beam considered in this study consisted of an aramid-fiber honeycomb core to which two aluminum faceplates were bonded using a film adhesive (fig. 1.1). Figure 2.1 shows the geometry and reference frame orientation for this structure.

Sandwich beams and plates loaded axially or transversely can fail in several different modes [15]. Five of these failure conditions were important to this analysis: overall buckling, faceplate yielding, intra-cell dimpling, faceplate wrinkling, and shear crimping (fig. 2.2). To establish the effect of an unbond on sandwich buckling, the structure must be designed such that all other failure modes do not precede buckling. Thus, a close examination of all five failure modes was needed to determine a safe experimental regime.

For this preliminary design study, Bernoulli/Euler beam theory was used, along with several conventional assumptions.

(1) Plane sections remained plane and perpendicular to the neutral axis.

6

(2) The neutral axis was assumed inextensional.

(3) The beam slope $w' = dw/dx \ll 1$ at all points along the beam.

(4) Stress in the beam width, or "y" direction, was zero.

(5) All materials were linearly elastic.

(6) The faceplate and core were assumed to behave isotropically, although the core was actually an orthotropic material.

2.1.1 Faceplate Yielding.

As is customary, the axial load was assumed to be carried exclusively by the faceplates. Thus, the maximum allowable axial load per unit beam width is bounded by the yield load of the faceplates. The following relationship was readily derived:

$$N_Y = 2\, t_f\, \sigma_y \qquad (2.1)$$

The plot of this equation (fig. 2.3) demonstrates the obvious increase in yielding load due to increasing faceplate thickness.

2.1.2 Intra-cell Dimpling.

Faceplate dimpling is a localized, intra-cell buckling instability of the sandwich faceplates (fig. 2.2b). When viewed on a scale the order of the core cell diameter, dimpling can be easily visualized as a plate-buckling mode. This failure mode is controlled by the honeycomb cell diameter and by the faceplate thickness. Using plate-buckling theory, the critical load equation can be derived [16] as:

$$N_D = \frac{\alpha t_f\, E_f}{(1 - \nu^2)} \left[\frac{t_f}{s}\right]^2 \qquad (2.2)$$

From this theory, the value for α was found to be 4.642. According to the Military Handbook, Construction of Sandwich

Composites [17], an empirical formula for this failure mode determined α to be 2. The empirical formula was chosen to determine the critical loads. Figure 2.4, the plot of eq. 2.2 with α - 2, showed that the critical dimpling load decreased as the cell size increased or the faceplate thickness decreased.

2.1.3 Shear Crimping.

Shear crimping occurs if the core is insufficiently thick or its shear modulus is small. Essentially this failure results when the shearing stress within the core becomes larger than the shear strength of the core. Since the core is bonded to the faceplates, shearing may wrinkle or crush the core within the failure area (fig. 2.2c).

The critical shear crimping failure load is linearly related to the core thickness and its shear modulus [15]:

$$N_C - c \ G_w \qquad (2.3)$$

The parametric plot of this equation can be found in fig. 2.5. Note that as the core thickness or shear modulus decreased, so did the critical load. Another trend indicated that, for a particular cell size, a decrease in shear modulus was the result of decreasing core density. In addition, as the cell size increased while holding the core density fixed, the shear modulus also decreased.

2.1.4 Faceplate Wrinkling.

Wrinkling is a localized buckling of the sandwich faceplates in short, sinusoidal waves (fig. 2.2d). The behavior of the faceplates closely resembles the buckling of a beam on an elastic foundation. A first-order approximation of the critical wrinkling loads is typically found by modeling the core as a linearly elastic Winkler foundation [18]. Appendix B contains the derivation of the following equation:

$$N_W = t_f E_f \left[\frac{2 \ t_f E_c}{3 \ c \ E_f} \right]^2 \qquad (2.4)$$

In this mode, core and faceplate properties play an important role in failure. Since the faceplates are sufficiently thick, overall buckling does not occur. It is the core compressive modulus and thickness that greatly influence wrinkling, as does the spring stiffness in an elastic foundation.

From the graph of the above equation (fig. 2.6), this dependence can be easily seen. Decreasing faceplate thickness had the obvious decreasing effect of the critical wrinkling load. A decrease in the failure load also resulted if the core thickness was increased while the core compressive modulus was held constant. Finally, note that as the core modulus decreased, the load also decreased.

2.1.5   **Overall Buckling.**

Buckling of an isotropic, geometrically straight, axially loaded beam depends upon the column's flexural rigidity, boundary conditions, and length. Typically shear deformations are small and neglected in most buckling analysis. However, because of the type of core used in this sandwich structure, shear deformations may significantly contribute to the buckling failure, and are thus considered in this analysis.

From the derivation in Appendix B, it was found that the critical buckling load can be expressed as:

$$N_B = \frac{N_E}{[1 + N_E/N_S]} \qquad (2.5)$$

where,
$$N_E = \frac{\pi^2 \ D}{L^2} \ , \qquad N_S = \frac{G_w d_f^2}{c}$$

A parametric plot of this equation (fig. 2.7) shows that increasing beam length or decreasing faceplate thickness will

decrease the failure load. However, the greatest effects on the critical buckling load arose from changes in the core thickness and shear modulus. Increasing the core thickness by 50% was found to increase the failure load by approximately the same amount. This was due to the added flexural rigidity that resulted when the faceplates were moved farther apart.

On the other hand, a 47% increase in the shear modulus (G_w) also increased the buckling load by about 50% at small beam lengths, while at larger beam lengths only a 15% increase in load occurred. This exemplifies the fact that this sandwich beam is subject to large shear deformations, especially at shorter beam lengths.

2.1.6 Sandwich Beam Geometry.

Beam geometry was not fixed by determining an efficient combination of parameters that satisfied the failure criteria. It would have been impractical to choose the sandwich dimensions on this basis. Rather than fixing geometry from the failure criteria alone, commercial availability and economic feasibility of materials were also considered.

Thus, a Nylon Fiber Reinforced Honeycomb core (NOMEX) was chosen from HEXCEL. Aluminum 2024-T3 was picked for the sandwich faceplates because of its high strength (σ_y = 40 ksi, E_f = 10^7 psi) and common use in sandwich construction. Table 2.1 lists the properties of these materials in detail.

With these properties fixed, the five failure criteria were parametrically plotted to determine faceplate thickness and beam length. Figures 2.8 and 2.9 show the failure criteria plots for 0.457 and 0.506 inch core thicknesses, respectively. Each graphs the failure loads per unit beam width for the five failure modes versus beam length and faceplates thickness.

It is interesting to note that only the overall buckling load was affected by changing the beam length. As anticipated,

this load decreased with increasing beam length. Since it was desirable to have the largest possible margin between buckling and the other failure modes, a large beam length should have been chosen. However, dimensions of the oven used to cure the specimen, limited the beam length to 13.0 inches. Although longer beams are more desirable, fig. 2.8 and 2.9 show that a 13.0 inch beam would ensure a 620-lb/in margin between buckling and other failure modes if a 0.020-inch faceplate thickness was used.

2.2   DESIGN OF BEAM SUPPORTS

End fixtures were designed to provide support and transmit the axial load to the specimen. Simple supports were chosen because of the simplicity they added to both experiments and analysis without loss of generality.

Since the sandwich faceplates carried the compressive loads, they were made to extend 3/4-inch beyond the core to allow bonding of the end fixtures (fig. 2.10 and 2.11). The end supports were made from steel.

The fixture was machined to fit snugly between the aluminum faceplate extensions. This ensured that the faceplates would remain parallel at the loading points, thus avoiding failure at the interfaces. The supports were carefully machined to close tolerances so that support center lines would be aligned with those of the specimen to prevent eccentric loading of the column during testing. To aid the transmission of the axial force from the end fixture to the faceplates, aluminum grips were bonded to the exterior of the faceplate extensions and to the angled stop of the fixture.

At the tip of the support, the end was rounded to allow free rotation. The loading block, which was attached to the testing apparatus by means of a threaded hole, had a "v" trench into which the rounded end fixture rested. These were well lubricated to reduce friction.

2.3 SPECIMEN FABRICATION

The sandwich beam was constructed by bonding the honeycomb core to the aluminum faceplates by means of a film adhesive. Within this section is a description of the procedures used to prepare the various components and assemble the test specimen.

2.3.1 Component Preparation.

The three sandwich components--the aluminum faceplates, the aramid fiber honeycomb core, and the film adhesive--needed preparation before curing. This was necessary to ensure a sufficiently strong bond that would not allow failure other than the desired buckling mode.

(a) Aluminum 2024-T3 Faceplates.

Faceplate preparation began by cutting the 3.0 x 14.5 inch plates from the aluminum 2024-T3 sheet. Each beam faceplate was cut along the same orientation to ensure minimum variation of material properties. A shearing machine was used to cut the aluminum, and then all plates were milled to obtain geometrically identical faceplates with square edges.

After cutting, the aluminum surfaces to be bonded to the core were lightly sanded with emery cloth and cleaned with acetone. Finally, penciled lines were used to mark the 3/4-inch extensions and the boundary of the unbond. The marks for the unbond were laid out so that the unbonded area would be centered on one face of the sandwich beam.

(b) Aramid Fiber Reinforced Honeycomb Core.

This hexagonal-celled honeycomb core "consists of DuPont's NOMEX aramid-fiber paper treated with a heat resistant phenolic resin. It features high strength and toughness in a small cell size, low density nonmetallic core" [19]. The core was manufactured in blocks and then cut into sheets [15].

From these sheets, the 3.0 x 13.0 inch beams were cut. Care was taken to insure that the cell arrangement was such that the core "w" direction was parallel to the beam length (fig. 2.1). The core was cut by hand using a sharp knife and straight edge to make it square. Finally, the honeycomb was blown with compressed air to remove any loose particles or fibers.

(c) Film Adhesive.

The film adhesive used was manufactured by American Cyanamid and had a designation FM-300. It was shipped in rolled form with protective plastic on either side. To prolong its lifetime, it was stored at -40° F. Because this temperature made the adhesive brittle, it was necessary to allow the film to warm to room temperature before handling.

Once warm, the adhesive was carefully cut into 3.0 x 13.0 inch sections. For the faceplate with an unbond, two identical sections were cut in such a way that their lengths, including the unbond length, would add to 13.0 inches. Care was taken to minimize contamination of the adhesive which could degrade the integrity of the bond.

2.3.2 Beam Assembly.

The sandwich was assembled as shown in fig. 2.12. Lines marked on the aluminum faceplates served as guides while positioning the adhesive. One of the protective backings was removed from the 13.0-inch adhesive strip, and the film was carefully centered on the clean aluminum plate. The adhesive was pressed into place and stuck since it was slightly tacky.

On each side of the unbond, adhesive film was positioned and aligned. To prevent seeping into the unbond area and to reduce local deformation of the faceplate, a piece of 0.0035-inch teflon was centered between the core and faceplate of the unbond. It was cut to the exact length of the unbond by 2.5 inches wide.

As soon as the adhesive and teflon were situated, the honeycomb core was placed on top of the unbonded faceplate and centered. The other faceplate was then positioned on the core. A T-square was used to ensure that both faceplates were aligned and square. Next, the entire structure was lightly pressed by hand to make the core stick to the adhesive to prevent the faceplates from slipping while being transported to the oven. Finally, aluminum spacers were placed between the faceplate extensions to keep the them parallel during the curing cycle.

2.3.3 Curing Cycle.

The adhesive curing process entailed heating the sandwich for a specified time. A press with carefully aligned heating platen was used to apply the necessary temperature and pressure to the specimen (fig. 2.13).

The sandwich was placed on the lower platen. Steel spacers were positioned on either side of the beam to prevent the core from being crushed. The lower platen was hydraulically raised until the specimen just touched the upper platen. This slight contact pressure was maintained throughout the curing cycle and until the specimen completely cooled.

The platen temperature was monitored and controlled by a thermocouple temperature controller. The adhesive curing cycle (fig. 2.14) required bringing the sandwich temperature up to 350° F and holding it there for one hour. Upon completion of this cycle, the specimen was allowed to cool overnight.

2.3.4 Attachment of End Fixtures.

Once the specimen cooled, the end fixtures were attached. The aluminum extensions and end supports were first lightly sanded with emery cloth and then cleaned with acetone. Figure 2.15 shows the specimen ready for the attachment of the end supports.

Next, a five-minute, two-part liquid epoxy was mixed and

applied to the contact surfaces of the fixtures and grips. These were then joined to the aluminum extensions and hand-pressed to remove excess adhesive.

Wood blocks were used to evenly distribute the c-clamp load. The assembly remained clamped for one hour to ensure bonding of the surfaces. After the adhesive dried, any hardened excess glue was carefully removed.

2.3.5 Preparation of the Unbond for the Shadow-moire Method.

A Shadow-moire Method [20] was used to measure the out-of-plane displacement of the unbonded faceplate during testing. To eliminate glare from the shiny aluminum, the surface was dulled by shot peening the unbonded region of the faceplate. This process entailed using a small pressurized jet of water containing fine sand particles to erode the surface to a rougher state. Care was taken to protect the exposed honeycomb core during this procedure.

2.4 MEASUREMENT OF FLEXURAL RIGIDITIES

The flexural rigidity (D) of a composite beam is calculated by summing the contributions from each constituent. This was done for the three sections of the sandwich beam used in this analysis (Appendix A)--the fully bonded sandwich specimen (D_1), the section of core with only one faceplate attached (D_2), and the unbonded aluminum faceplate (D_3).

To verify the accuracy of the calculated rigidities, separate experiments were performed to directly measure these properties. The stiffness of section one (D_1) was measured by a four-point bending test, and a cantilever bending experiment was used for section two (D_2).

2.4.1 Four-Point Bending: D_1

One method of directly measuring the flexural rigidity of a beam is to apply a pure moment to its ends and measure the

displacement at the center of the beam. The following equation was derived from beam theory and used to determine the value for the flexural rigidity of this section:

$$w(L/2) = \frac{M_o L^2}{8 D_1} \qquad (2.6)$$

To perform this test, a four-point bending device (fig. 2.16) was constructed. It was capable of applying pure moments to the central section of the beam. To allow rotation during bending, four well-lubricated rollers were used to apply the load to the sandwich specimen. An aluminum strip was placed between each roller and the beam to distribute the load applied to the specimen.

A fully bonded sandwich beam specimen (table 2.3) was positioned between the upper and lower sets of rollers. Load was applied to this system at the center of the upper section of aluminum. For this loading, the uniform moment in the central beam section was calculated to be one half the applied load times the lengthwise distance (q) between the lower and upper rollers. Substituting this into eq. 2.6 yielded:

$$P = \left(\frac{16 D_1}{q L^2}\right) w(L/2) \qquad (2.7)$$

This experiment was performed on an MTS testing machine using displacement control. Figure 2.16 shows the four point bending device attached to the MTS and set-up to begin testing the sandwich specimen.

An eddy-current displacement transducer (proximeter) was fixed to the upper aluminum block and used to measure the downward displacement at the center of the beam. The slope from the experimental plot of the applied load versus $w(L/2)$ displacement (eq. 2.7) yielded the value for flexural rigidity of section one ($D_1 = 31288.47$ in-lb).

The experimental value for D_1 was found to be 31.8% larger

than the theoretical value (table 2.2). This significant difference may be a result of an incorrect assumption in the role that the adhesive layer played in the flexural rigidity of the system.

2.4.2 Cantilever Bending: D_2

The unbonded region of the sandwich beam can be considered as two separate beams--the unbonded aluminum faceplate (section three) and the core with one bonded faceplate (section two). The flexural rigidity for section three (D_3) was directly calculated from EI. On the other hand, D_2 needed to be experimentally found and compared to theoretical calculations as was done with D_1.

A specimen was manufactured with one faceplate and adhesive layer absent (table 2.3). The stiffness of this sandwich was significantly less than that for the fully bonded beam because of the missing faceplate and adhesive layer. Since the expected loads would be small, an end-loading cantilever device was used to measure D_2 (fig. 2.17).

The following relationship between tip load and displacement was found from beam theory:

$$P = -\left(\frac{3\ D_2}{L^3}\right) w(L) \tag{2.8}$$

The experiment was also performed on an MTS testing machine in the displacement control mode. A vertical aluminum support was used to clamp the specimen like a cantilevered beam. This support could be translated to choose any desired beam length. A beam length of 4.0 inches was used for this test.

To achieve a greater accuracy in results, a 300-lb load cell was used instead of the MTS's 20,000-lb cell. A wedge was used to apply the point load at the beam tip.

The experiment was performed with the aluminum faceplate placed up so it would bend as the section does in the unbonded

sandwich beam. D_2 was determined from the initial tangent of the experimental load versus tip displacement plot. Table 2.2 contains the measured values for D_2. It was found that the predicted value for D_2 was 43% lower than the experimentally recorded value. These errors may be attributed to the effect of the adhesive on the flexural rigidity of the structure.

2.5   OTHER PROPERTY MEASUREMENTS

To validate any theoretical predictions of failure loads, the core shear stress shape factor and Young's Modulus for the film adhesive and aluminum faceplates were also experimentally found.

2.5.1   Shear Stress Shape Factor.

Determination of the shear stress shape factor (α_s) was necessary to verify the value assumed while deriving the overall buckling failure equation (Appendix B). In a homogeneous beam, the stress distribution is usually parabolic. In this composite beam, however, it was assumed that the shear stress across the core thickness was uniform.

This shape factor determines the amount of shear contribution to the deflection of a buckling column. In order to find the magnitude of this contribution, a three-point bending experiment was performed (fig. 2.18). Dimensions for this test specimen are listed in table 2.3.

Similar to the four-point bending test, the three-point bending experiment differed only in the application of load. Instead of using the upper aluminum plate to distribute the load to two points, the load was applied directly to the beam's center.

The deflection equation for this loaded beam included a shear deflection term, along with the usual bending component. By measuring the displacement at the beam's midsection and plotting it versus the applied load, the shear stress shape factor (α_s) was determined from the slope of the following equation:

$$w(L/2) = -\frac{P\ L^3}{48\ D_1}\left\{ 1 + \frac{12\ D_1\ \alpha_s}{L^2\ A\ G_w} \right\} \tag{2.9}$$

where,

$$A = b\ d_f^2/c \qquad \text{(see ref. [21])}$$

The experimental value for α_s was found to be within 1.9% of the predicted value (table 2.2).

2.5.2 Modulus of Aluminum 2024-T3.

The Young's modulus for the aluminum faceplate was determined by performing a simple tension test. A standard "dog-bone" specimen was cut from the aluminum sheet in the same direction as the length of the beam faceplates. The test area was 4.0 x 0.409 inches.

Strain gages and an extensometer were used to measure the axial strain of the specimen as it was loaded on the testing machine (displacement control). The Young's Modulus was determined to be 9.951×10^3 ksi, and the 0.2% strain offset yield stress, 42.68 ksi (table 2.1).

2.5.3 Modulus of FM-300 Adhesive.

A similar tension test was performed on the adhesive. The specimen was made by curing six layers of the FM-300 adhesive in an aluminum mold that was lined with teflon. The curing cycle was identical to the one used in the lay-up procedures for the sandwich beam specimens (fig. 2.14).

The adhesive test coupon was loaded in tension on the MTS machine using displacement control. The elastic modulus of the adhesive was found to be approximately 463.5 ksi (table 2.1).

2.6 EXPERIMENTAL APPARATUS

An MTS closed-loop servo-hydraulic testing device was used to perform the sandwich buckling and material property experiments. Figure 2.19 is a photo of the MTS equipment

arrangement, and fig. 2.20 shows a schematic representation of the testing and data collection system. Experimental apparatus preparation included configuring the MTS loading device and specimen support network and aligning the various displacement measuring devices.

2.6.1 The Testing Machine.

The MTS is a versatile materials-testing machine with a 22 kips loading capacity (tension or compression). Applied loads were measured via a load cell (maximum error of $\pm$ 0.10 %) that was calibrated using dead weights. Since the MTS load cell had a capacity of 20,000 pounds, external load cells with 300 and 500 pound limits were used to obtain more accurate results when small loads were expected.

Axial displacements of the hydraulic actuator were measured using a linearly variable differential transducer (LVDT), an internal component of the MTS system. It had a range of $\pm$ 3.0 inches with a $\pm$ 0.80% maximum error. Because axial displacements of only a few thousandths of an inch were expected before the sandwich column buckled, the actuator had to be positioned within 0.002 inch of the range zero for these measurements to be accurately recorded.

The MTS is capable of operating under load, strain, or displacement control. A function generator controls the actuator movement through various loading functions (ramp, sine, haversine, etc.). In addition, rate of loading can be selected to provide additional control over experimental operating conditions.

The rate of loading was determined by the function generator TIME and SPAN settings. According to the MTS operation manuals [22], the loading rate was found from the following equation:

$$\text{Rate} = \frac{\text{Total output}}{\text{Total time}} = \frac{\text{SPAN}}{\text{TIME}} \quad \text{(volt/sec)} \qquad (2.10)$$

2.6.2 Specimen Loading Configuration.

As mentioned earlier, the hydraulic actuator (fig. 2.19) needed to be positioned as close to the zero range as possible. This was done by raising the crossbeam support until the LVDT output indicated a zero voltage with the sandwich specimen fitting between the loading blocks.

The upper loading block was attached directly to the load cell suspended from the crossbeam support. Attached to the actuator was the second loading block. A ball joint was placed between the block and actuator, allowing free 360° rotation of the block.

This joint proved invaluable in aligning the specimen prior to testing, ensuring that a uniform load was applied through the center line of the specimen. The ball joint, loading blocks, and specimen end fixtures were well lubricated to reduce friction.

2.6.3 Measuring Instrumentation.

Various instruments were used to monitor the specimen during testing. The MTS or an external load cell was used to measure the axial load being applied to the sandwich beam. An internal MTS LVDT measured the axial displacement applied to the sandwich beam. These measurements were recorded using an X-Y plotter.

Two spring-loaded LVDT's were placed on opposite sides of the specimen to detect changes in the mid-point deflections of the unbonded beam section (fig. 2.21). Displacements from section two and three mid-points, $\hat{w}_2(0)$ and $\hat{w}_3(0)$ respectively, were recorded on an X-Y Y plotter versus axial load.

Finally, a Shadow-moire Method [20] was used to measure the out-of-plane displacements of the unbonded aluminum faceplate. Figures 2.22 and 2.23 schematically depict the set-up of this technique.

For sandwich buckling experiments with an unbond, a ruled

screen was positioned in front of the shot peened, unbonded aluminum faceplate (fig. 2.24). This grating screen contained 200 lines per inch and was placed so that the lines were parallel to the width of the beam. A 1500-watt quartz halogen light source was used to illuminate the master grating from an incidence angle. Two lenses were positioned between the light source and moire screen to collimate the beam of light. The light passing through the lined grating cast shadows on the unbonded surface and produce fringes when observed from a viewing angle.

A video camera system was used to record the changing fringe pattern (out-of-plane displacement of the unbond), along with a digital readout of the load cell voltage, as the sandwich was tested. This tape was later analyzed with a video analyzer (fig. 2.25) to determine the buckling faceplate shape at particular loads.

2.7   EXPERIMENT EQUIPMENT PREPARATION

The testing machine was warmed up prior to each experiment by sinusoidally cycling the actuator for 15 minutes. Displacement control was used to load the test specimens. A maximum stroke displacement of 1/4 inch was set for all experiments, with a loading rate of approximately 0.001 inch every 15 seconds.

Once the machine was sufficiently warmed, the actuator was moved to zero, and the specimen was carefully fitted between the loading blocks. The section midpoint LVDT's were positioned perpendicular to the specimen and zeroed. In addition, the moire screen was placed in its holder and adjusted so that the fringes would appear parallel to the beam width.

Both plotters were readied, and the scales were adjusted to yield the largest plots possible. Finally, after the VCR was activated, the function generator started to begin ramping the actuator displacement.

Recording equipment was continuously monitored throughout

the experiment for detection of any problems. In addition, visual observations were made of the beam edge of the unbonded section to determine if a failure mechanism could be observed.

After maximum load occurred, the displacement was continued until the load decreased. The function generator was then stopped manually, and the load removed from the specimen. Recording instruments were turned off and the buckled column removed from the MTS.

Chapter 3
EXPERIMENTAL RESULTS

The primary objective of the experimental program was to establish the failure mechanisms of partially unbonded sandwich beams subjected to axial compression. In order to achieve this goal, thirteen specimens were manufactured and tested under the guidelines presented in the previous chapter. These test specimens were geometrically identical with the exception of the unbond length.

Physical dimensions of the sandwich specimens are listed in table 3.1. Overall, common dimensions were fixed to a 3.00 ± 0.02 in. specimen width (b), and a beam length (L) of 13.00 ± 0.05 in. With the end fixtures attached, the overall structure length (L_o) was 16.50 ± 0.05 in. The unbond lengths (L_u) ranged from 0.0 to 5.0 inches.

Data was collected from these experiments in order to quantify the failure of the unbonded sandwich beam and to validate the results obtained from the theoretical models. The effect of increasing unbond length on the buckling load, the mode of buckling, and the failure mechanism were the three main parameters of interest investigated.

3.1 LOADING HISTORY

An MTS closed-loop, servo-hydraulic testing machine was used to load the simply supported test specimens (fig. 2.19 and 2.20). The first two sandwich beams tested utilized the load-control feature of the MTS. These specimen--a fully bonded beam (specimen one), and one which contained a 3.0-inch unbond (specimen two)--were found to fail catastrophically at some critical load.

In order to capture the load-deformation characteristics of the columns in more detail (especially near the critical load),

24

displacement-controlled loading was necessary and was used in all subsequent tests. This made it possible to make observations of the failure mode and to determine the initial post-buckling history of the sandwich specimen. A loading rate of approximately 0.004 in/min was used for all experiments.

The actuator was ramped to a maximum "breakpoint" displacement of 0.25 in. Stroke displacements for experiments one and two were found to be only 0.047 in. and 0.005 in., respectively. The margin between the experimental and "breakpoint" displacement was necessary for accurately placing the specimen between the loading blocks.

Once the specimen was positioned, the function generator was activated, starting the displacement ramp. At first contact, loading was interrupted, and all measuring equipment was re-zeroed. The test was then resumed, and the loading continued until the column failed or until a well-defined limit load was obtained.

3.2 EXPERIMENTAL MEASUREMENTS

Four sets of data were collected in each experiment--the load versus the applied axial displacement, the load versus the midpoint deflections of beam sections two and three, $\hat{w}_2(0)$ and $\hat{w}_3(0)$ (fig. 2.21), and the displacement families of out-of-plane deflections along the unbond length obtained from the Shadow-moire Method.

3.2.1 Load versus Stroke Displacement.

Figures 3.1--L_u from 0.0 to 0.5 inches--and 3.2--L_u from 1.0 to 5.0 inches--plot the axial load (P_1) versus the applied axial displacement (Δ or actuator translation), for each performed experiment. According to load cell specifications, measurements of the load (in the test regime) were accurate to within $\pm$ 0.5 lbs. On the other hand, actuator displacements were measured to within $\pm$ 0.0005 inches.

The initial nonlinearity observed in these loading histories was due to "settling" of the test fixtures and specimen. Response curves from beams having unbonded lengths of 2.0 inches or less were characterized by a <u>distinct failure</u> point, beyond which the columns load-carrying capacity was significantly reduced. Loading histories of beams with longer unbonded sections were characterized by <u>limit loads</u>. (Note that the distinct failure for one 3.0-in. unbond specimen was a result of controlling the load during testing.) These columns were found to retain their load-carrying abilities for deflections well beyond the displacement measured at the limit load.

3.2.2 Load versus $W3_o$ Displacement.

Two LVDT's positioned at the midpoints of beam sections two and three monitored the respective displacements $\hat{w}_2(0)$ and $\hat{w}_3(0)$ during testing (fig. 2.21). Subtracting $\hat{w}_2(0)$ from $\hat{w}_3(0)$ yielded the relative displacement of the section three midpoint from the core ($W3_o$).

Figure 3.3 contains the $W3_o$ displacements for experiments with a 1.0, 3.0, 4.0, and 5.0-in. unbond (test specimens 4, 10, 11, and 9 respectively). The midpoint displacement of the unbonded faceplate did not begin as loading was initiated. Instead it began at a load which may be linked to the buckling load of the unbonded faceplate. This idea will be expanded further in the theoretical discussion of this structure (chapter 4).

3.2.3 $\hat{w}_3(x)$ Displacement Shapes from the Shadow-moire Method.

The Shadow-moire Method, see ref. [20], was used to determine the overall shape of the unbonded faceplate as the sandwich beam was loaded. The changing fringe pattern was recorded on a VCR system. Figure 3.4 shows photos taken from the VCR of fringe patterns for four loads of the 5.0-in. unbonded specimen. Notice the increase in fringe density as the load increased. The

photo at the right was taken at the limit load.

A video image analyzer was used to plot the intensity of the fringe pattern versus scan position. Lined tape was placed on each beam and used to calibrate the scan position with the actual lengthwise position on the specimen. Figure 3.5 exhibits fringe intensity plots, made by the analyzer and recorded on an X-Y plotter, corresponding to the four loads at which the photos in fig. 3.4 were taken.

Each curve corresponded to a different shape as determined by the load applied to the sandwich beam. From these plots the minima and maxima represent the whole and half fringe numbers, respectively, corresponding to the shape displacements. Table 3.2 lists the data from each experiment used to find the order of the moire fringe displacements. The equation which related the fringe order (N), grating pitch (p), point-source incidence angle (α), and viewing angle (β) to the out-of-plane displacement (w) was found from [20] to be (fig. 2.23):

$$w = \frac{N\,p}{\tan\alpha + \tan\beta} \tag{3.1}$$

Using the fringe data for each load, the $\hat{w}_3(x)$ displacement shapes were calculated and plotted. These curves were then digitized on an IBM-PC AT and for each unbond were combined to form a three-dimensional plot. Figures 3.6 through 3.10 contain these plots for specimens 4, 3, 10, 11, and 9, with unbond lengths of 1.0 through 5.0 inches, respectively.

The horizontal axis represents the length along the unbond from top $(-l_3/2)$ to bottom $(+l_3/2)$ (see fig. 4.1). $w_3(x)$ displacement was plotted along the vertical axis, with the positive direction indicating displacements away from the core of the structure. Each plot was found at the same position on the unbond but at different loads. Thus, the third axis showed the increase in the applied load P_1.

Since it was desired to determine the deflections of the unbonded faceplate from its unloaded position, all displacements were referenced to the top edge of the unbonded region. The deformation profiles were found to be almost symmetric about the mid-span of the beams during initial loading. At higher loads the shapes became progressively less symmetric. This indicated that a transition from the symmetric buckling mode to a nonsymmetric one may have occurred. Since the last curve plotted was at or just prior to maximum load, the transition was not a result of the specimen reaching maximum load.

3.2.4 Maximum Load versus Unbond Length.

Table 3.3 lists the maximum loads found for each specimen tested. These results were plotted to determine the effect of sandwich beam unbond length on the maximum load supported by the structure. Figure 3.11 shows a plot of these results.

It was found that the maximum load rapidly decreased as the unbond length was increased. Plotting these results on a fully logarithmic scale (fig. 3.12) indicated that for unbond lengths larger than 1.5 inches, a power-law relationship exists between unbond length and maximum load. This can be expressed as follows:

$$P_{1max} = \alpha(L_u)^\beta \qquad (3.2)$$

The coefficients of this equation were found by a least squares fit to be $\alpha = 1275.85$ and $\beta = -1.8172$ (table 5.2). The fit of these experimental results had a correlation factor of -0.9962. This factor was based upon the ratio of the abscissa and ordinate standard deviations. A correlation of ± 1.0 would indicate an exact data fit with positive or negative slope. Thus, eq. 3.2 can predict the maximum load for sandwich beams with similar geometries and with unbond lengths between 1.5 and 5.0 inches to within 8.8% of the measured value.

3.3 SPECIMEN FAILURE OBSERVATIONS

Visual observations of the sandwich specimen were made during loading to augment and support physical measurements. Several details observed during testing proved useful for interpreting and verifying results from the collected data. Observations concentrated on determining the failure mechanism of both fully bonded and unbonded specimens.

3.3.1 Fully Bonded Specimens.

Two fully bonded specimens were tested. The first experiment (specimen one) was run using load control. Displacement control was used for the second (specimen eight). A similar failure was noted in each of these sandwich beams.

Figure 3.13 shows the failure shape of specimen one. The predicted failure load for this beam was found to be 2297.4 lbs. The load actually measured was 3480 lbs. Using the experimentally measured flexural rigidity D_{1ex} (see 2.4.1) in eq. 2.5 still resulted in a low prediction of the failure load (table 3.4). The most accurate failure estimation was achieved by using D_{1ex} and an equation derived from classical stability analysis. This approach yielded a load (P_{cr} = 3454.2 lbs.) which was within 2.5% of the experimental failure loads.

Although specimen two was over-collapsed because the experiment was load controlled as mentioned earlier, both fully bonded columns appear to have failed similarly. In addition, the failure load measured in experiment eight was also close to the predicted at 3540 lbs.

3.3.2 Specimens with an Unbonded Faceplate.

Photos in figs. 3.14 through 3.16 document some of the observations made of sandwich beams with an unbonded faceplate. Specimen three, with a 2.0-inch unbond, was held in the expected symmetric failure mode and compared to the collapsed 3.0-inch

unbond specimen two (fig. 3.14). Notice that specimen two exhibited the same general failure shape as the fully bonded beam (fig. 3.13). Also observe that the core of the 3.0-in. unbond failed at the left unbond interface (fig. 3.14a).

It was uncertain whether the core failure caused the change in the collapsed mode shape or if both were a result of over-compression due to the test being performed in the load-controlled configuration. However, observations from other beam tests strongly indicated that transition to the nonsymmetric mode was gradual for large unbond lengths, but more sudden and occurring at or just prior to maximum load for short unbonded faceplates.

From experiment six (0.5-inch unbond) crushing of the core and some permanent deformation of the aluminum faceplates occurred as a result of the sudden transition. Figure 3.15 shows the symmetric shape of 3.0-inch unbond specimen ten prior to any noticeable change in shape. This photo roughly corresponded to the moire shape plot (fig. 3.8a) with a load of approximately 160 lbs. In contrast, a photo of specimen nine with a 5.0-inch unbond (fig. 3.16), taken just prior to maximum load (fig. 3.10a), exhibited the nonsymmetric shape.

Close examination of the unbond interface of all specimens with unbond lengths larger than 1.5 inches did not indicate any obvious failure of the honeycomb core. Thus, the transition in mode shape was most likely caused by either the fact that the unbond was itself an imperfection of the beam, or imperfections of the unbonded faceplate may have caused eccentric loading of the structure.

3.3.3 Imperfect Specimens.

Two of the sandwich beams tested contained large, observable imperfections in the unbonded region, with the maximum displacement in the warped core approximately 8.6% of the core thickness. These two specimens (twelve and thirteen) were tested

and were found to reach maximum loads 7.9% and 24.2% lower than similarly tested sandwich beams. Since this study was not concerned with the effects of imperfections, results from these experiments were not used in this analysis.

Chapter 4

AN ANALYTICAL MODEL FOR THE BUCKLING OF
UNBONDED SANDWICH BEAMS

In a paper discussing the failure in laminated graphite/epoxy plates by delamination buckling, Chai et al. [23] developed a set of equations to describe the stability, growth, and arrest of local delaminations. Their work provided a foundation for the unbonded sandwich beam models derived within this chapter.

A general model and a simplified version were developed in an attempt to describe the buckling failure of axially loaded sandwich beams containing an unbonded faceplate section. These theoretical models were derived by considering the equilibrium of such a beam with a buckled faceplate, as shown in figure 4.1.

4.1   PROBLEM FORMULATION

The structure was idealized as a long, simply supported column of length L. This column consisted of two faceplates of equal thickness t_f, bonded to a honeycomb core of thickness c. One of the faceplates was not bonded to the core over a length L_u, which was symmetrically located as shown in figure 2.12.

Under the action of the compressive axial load P_1, the unbonded section buckled. The failure configuration was <u>assumed</u> to be symmetric about the beam midspan. Several additional, customary assumptions were made:

(a) Axial loads were carried strictly by the faceplates.

(b) The neutral axis (N.A.) of the faceplate was considered inextensional.

(c) Plane sections through the faceplate thickness, and perpendicular to the N.A. prior to deformation, remain normal during deformation.

(d) The strains were assumed to be small.

32

    (e)   Deflections and rotations of all components were also assumed to be small.

    (f)   The unbonded section <u>did not delaminate</u> during deformation.

    (g)   All beam constituents were linearly elastic.

Equilibrium Equations.

For convenience, the sandwich structure was analyzed in three separate sections as shown in fig 4.1. From this figure, the following section equilibrium equations were readily derived:

$$M_1(x_1) = M_o + P_1[w_1(x_1) - \delta_o] \tag{4.1}$$

$$M_2(x_2) = M_2 + P_2[w_2(x_2) - \delta] \tag{4.2}$$

$$M_3(x_3) = M_3 + P_3[w_3(x_3) - \delta] \tag{4.3}$$

Constitutive Equations.

The moment (M_i) in each section was related to the displacement (w_i) as follows:

$$M_i = -D_i\left(\frac{d^2 w_i}{dx^2}\right), \qquad i = 1,2,3 \tag{4.4}$$

where D_i is the flexural rigidity of the ith member. Substituting eq. 4.4 into eq. 4.1-4.3, the following expression for the displacements (w_i) can be obtained:

$$w_i(x_i) = A_1 \sin(k_i x_i) + A_2 \cos(k_i x_i) + A_3$$
$$k_i^2 = P_i/D_i \qquad i = 1,2,3 \tag{4.5}$$

Boundary and Compatibility Conditions.

The following section boundary and compatibility conditions were found to hold: (see fig. 4.1; invoke symmetry about the beam midspan):

Section 1:

$$
\begin{array}{ll}
w_1(0) = \delta_o, & w_1'(0) = \theta_o \\
w_1(1_1/2) = \delta, & w_1'(1_1/2) = \theta
\end{array} \tag{4.6}
$$

Section 2 & 3:

$$w_i'(0) = 0 \quad , \quad \begin{array}{l} w_i(-l_i/2) = \delta \\ w_i'(-l_i/2) = \theta \end{array} \qquad i = 2,3 \qquad (4.7)$$

By substituting boundary conditions 4.6 and 4.7 and eq. 4.1-4.4 into eq. 4.3, the following displacement expressions were obtained:

$$w_1(x_1) = \frac{\theta l_1}{2u_1 \cos u_1} \left\{ \sin\left(\frac{2u_1 x_1}{l_1}\right) \right\} + \delta_o \qquad (4.8)$$

$$w_i(x_i) = \frac{\theta l_i}{2u_i \sin u_i} \left\{ \cos\left(\frac{2u_i x_i}{l_i}\right) - \cos u_i \right\} + \delta \qquad (4.9)$$

$$i = 2,3$$

where,

$$\delta_o = \frac{l_r \theta}{2 \cos u_1} \qquad \text{(see fig. 4.1)} \qquad (4.10)$$

$$\delta = \left(\frac{\theta l_1}{2 u_1}\right) \tan u_1 + \delta_o \qquad (4.11)$$

$$u_i = (l_i/2)(P_i/D_i)^{1/2} \qquad i = 1,2,3 \qquad (4.12)$$

Interface Continuity.

Axial and moment equilibrium at the interface of the three sections required that:

$$P_1 = P_2 + P_3 \qquad (4.13)$$

$$M_1 = M_2 + M_3 + P_3\left(\frac{h - t_f}{2}\right) - P_2\left(\frac{c}{2} + r\right) \qquad (4.14)$$

(The distance, r (fig. 4.2), from the aluminum faceplate/adhesive joint to the neutral axis, was taken to be 0.00976 inches.) Using eq. 4.4-4.12 in eq. 4.13 and 4.14 yielded:

$$\frac{D_1 u_1^2}{l_1^2} - \frac{D_2 u_2^2}{l_2^2} - \frac{D_3 u_3^2}{l_3^2} = 0 \qquad (4.15)$$

$$\frac{D_3 u_3^2}{l_3^2} (h - t_f) \; - \; \frac{2 D_2 u_2^2}{l_2^2} \left(\frac{c}{2} + r \right) \; - \; \theta \left[\left(\frac{D_1 u_1}{l_1} \right) \tan u_1 \right.$$

$$\left. + \; \frac{l_r D_1 u_1^2}{l_1^2 \cos u_1} \; - \; \left(\frac{D_2 u_2}{l_2} \right) \cot u_2 \; - \; \left(\frac{D_3 u_3}{l_3} \right) \cot u_3 \right] \; = \; 0 \qquad (4.16)$$

Beam Shortening due to Bending.

Two additional equations were determined from the fact that the beam shortened as a result of bending deformations (fig. 4.2).

$$\frac{1}{2} \int_0^{l_3/2} (w_3')^2 \, dx_3 \; = \; \frac{1}{2} \int_0^{l_2/2} (w_2')^2 \, dx_2 \; + \; e \qquad (4.17)$$

$$\Delta \; = \; 2 \left[\frac{1}{2} \int_0^{l_1/2} (w_1')^2 \, dx_1 \; + \; \frac{1}{2} \int_0^{l_2/2} (w_2')^2 \, dx_2 \; + \; g \right] \qquad (4.18)$$

where, $e = \theta(h - t_f)$, $g = e/2$

Equation 4.17 related the amount of shortening in sections two and three, since $l_2 = l_3$. The amount that the entire sandwich beam shortened (Δ) was found from eq. 4.18. Using eq. 4.17 and 4.18 with eq. 4.8 to 4.12 produced the following two equations:

$$\theta \left[\frac{l_3}{\sin^2 u_3} \left\{ 1 - \frac{\sin 2u_3}{2u_3} \right\} - \frac{l_2}{\sin^2 u_2} \left\{ 1 - \frac{\sin 2u_2}{2u_2} \right\} \right]$$

$$- \; 8 \left\{ \frac{h - t_f + c}{2} + r \right\} \; = \; 0 \qquad (4.19)$$

$$\theta^2 \left[\frac{l_1}{4 \cos^2 u_1} \left\{ 1 + \frac{\sin 2u_1}{2u_1} \right\} + \frac{l_2}{4 \sin^2 u_2} \left\{ 1 - \frac{\sin 2u_2}{2u_2} \right\} \right]$$

$$- \; \frac{l_r}{2} \left[1 - \left(1 - \frac{\theta^2}{\cos^2 u_1} \right)^{1/2} \right] \; + \; 2\theta \left(\frac{c}{2} + r \right) \; - \; \Delta \; = \; 0 \qquad (4.20)$$

The system of equations 4.15, 4.16, 4.19, and 4.20 was used to solve for the five unknowns u_1, u_2, u_3, θ, and Δ. Due to the nonlinear nature of these equations, a numerical iterative scheme was employed to determine the solution.

4.2   NUMERICAL SOLUTION USING NEWTON'S METHOD

The system of aforementioned nonlinear equations were solved numerically using a variation of Newton's method [24]--which employed a modification of the POWELL-HYBRID method. Due to the nature of the problem, it was found convenient to prescribe the interface angle θ and solve for the normalized loads with eq. 4.15, 4.16 and 4.19. The final equation (eq. 4.20) was used after a solution was determined in order to find the axial displacement Δ.

Convergence of the Newton scheme greatly depended upon the initial guess of the unknown values. According to ref. [23], a first guess for u_3 would be π. This was reasonable since the unbonded faceplate was essentially a clamped beam, and the loads were normalized by the Euler buckling load for this type of beam. To avoid the singularity which develops at this load, the initial guess for u_3 was taken to be an incremental amount (ϵ) larger than π. Initial values for u_2, u_1, and θ were made by trial and error until a solution was found in which all quantities increased.

4.3   SIMPLIFIED MODEL

Solution of the nonlinear system of equations presented above required a considerable computational effort. Thus it was desired to develop a simplified model which could be utilized without loss of generality.   Table 2.2 presented evidence for such a simplification.

An examination of this table indicated that the bending stiffness for section one was approximately 2000 times larger than the other sections. In effect, section one can be considered a rigid beam, with the other two constituents having different, yet finite rigidities (fig. 4.3). Development of this model followed a procedure identical to the one used in the general case.

It was found that the boundary and compatibility conditions for the unbonded beam sections (eq. 4.7) were still valid. However, the conditions for section one (eq. 4.6) needed alteration

to reflect the now infinite rigidity of this section.

Modified Section 1:

$$w_1(0) = 0 \quad , \qquad w_1'(0) = \theta$$
$$w_1(\hat{1}_1/2) = \delta \quad , \qquad w_1'(\hat{1}_1/2) = \theta \qquad (4.21)$$

where,
$$\hat{1}_1 = 1_1 + 1_r$$

Section equilibrium indicated that displacement eq. 4.9 holds for this simplification, while eliminating eq. 4.8. The equation for the interface displacement δ was found to reduce to:

$$\delta = \hat{1}_1 \, \theta/2 \qquad (4.22)$$

Interface equilibrium produced equations identical to eq. 4.13 and 4.14. In addition, the beam shortening relationship eq. 4.17 also remained the same. Combining eq. 4.15 with eq. 4.16 eliminated the unknown load u_1 as follows:

$$\theta \left[\frac{D_2 u_2}{1_2} \cot u_2 \; + \; \frac{D_3 u_3}{1_3} \cot u_3 \; - \; \hat{1}_1 \left\{ \frac{D_2 u_2^2}{1_2^2} \; + \; \frac{D_3 u_3^2}{1_3^2} \right\} \right]$$
$$\frac{D_3 u_3^2}{1_3^2} (h - t_f) \; - \; \frac{2 D_2 u_2^2}{1_2^2} \left(\frac{c}{2} + r \right) \; = \; 0 \qquad (4.23)$$

Finally, the assumption that beam section one was rigid altered eq. 4.20 to:

$$\frac{\theta^2 1_2}{4 \sin^2 u_2} \left\{ 1 - \frac{\sin 2 u_2}{2 u_2} \right\} \; + \; \frac{\hat{1}_1}{2} \left[1 - \left(1 - \theta^2 \right)^{1/2} \right]$$
$$+ \; 2\theta \left(\frac{c}{2} + r \right) \; - \; \Delta \; = \; 0 \qquad (4.24)$$

For this simplified theory, it was only necessary to solve eq. 4.19 and 4.23 using Newton's method. This meant that only initial guesses for u_2, u_3, and θ were required to initiate the solution process. Thus, computational effort was reduced along with the energies for estimating the initial solution.

4.4   Comparison of Analytical Models.

The equations derived for the two analytical models were used to calculate load and displacement data for direct comparison with experimental results and to relate additional properties not directly measured. It was found that results calculated from both the simplified and general models were almost identical. For example, the general model was used to calculate various data for a 5.0-inch unbond sandwich (figs. 4.4-4.6). If similar responses were found from the simplified model and plotted on these figures, visual differences would be indiscernible.

Computations for other sandwich beams (L_u from 1.0 to 5.0 inches) demonstrated that both the general and simplified models were similar. The displacement shapes of constituent sections two and three were also found to be nearly identical. For section one, however, the shapes were slightly different since the simplified model assumed that this component of the beam was rigid.

Returning to fig. 4.4, this plot of load (P_1) and overall axial displacement (Δ), demonstrated two important characteristics of the analytical models. First, the loading histories for all unbond lengths from 1.0 to 5.0 inches were not complete--solutions were found only after u_3 = π. This was a result of assuming that the initial geometry of the sandwich beam was perfect. And more importantly, it was found that the analytical models predicted limit loads for all unbond lengths.

In addition, since the load in the three beam sections were related (eq. 4.13) and the overall load (P_1) reached a limit, the loading in section two also reached a limit (fig. 4.5)--the load in section three was still increasing. A careful examination of fig. 4.4 and 4.5 indicates that the limit load within section two occurred at a displacement prior to the limit load for the overall beam. Figure 4.6 emphasized the fact that the displacement of the unbond midspan ($W3_o$) did not begin until the buckling load in section three (u_3 = π) was reached.

Finally, the general model was used to plot the buckling shape of a sandwich beam with a 5.0-in. unbond (fig. 4.7). Half of the symmetric beam was plotted, excluding the left end fixture. Three loaded configurations are shown for comparison. Note that displacements were amplified approximately 12.5 times and the beam dimensions were scaled so that the shapes could be easily identified. The first beam shape was found at the initial load of the solution. The second represented the shape found when the load within section two reached a limit. And finally, the third indicated the beam displacements at the time of maximum (limit) load.

Chapter 5

COMPARISON OF EXPERIMENTAL AND THEORETICAL RESULTS

Thus far, this analysis has followed two separate paths. One concerned with the design, construction, and experimentation of sandwich beams containing an unbonded section, and the other with the development of analytical models to establish the response and stability of the structure.

In this chapter, data from theory and experiment will be compared in the following areas: load and axial displacement, $W3_o$ displacements, buckling shapes of the unbonded faceplate, load versus unbond length, and critical bending moments. This comparison was used to critically review the assumptions made while deriving the analytical models and to identify areas and reasons for disagreements between the two.

5.1 COMPARISON OF BUCKLING AND FAILURE LOADS

It is important to note that the problem formulation, as presented in chapter 4, assumed that the sandwich beam structure was initially geometrically perfect. As a result, all analytical load-displacement responses start after the unbonded aluminum faceplate reached its buckling load ($u_3 - \pi$). Thus, direct comparison of the experimental and theoretical loading histories was not possible.

All of the tested columns exhibited, to varying degrees, pre-buckling transverse deflections. These were primarily caused by initial geometric imperfections, which are always present in real structures. Another notable deficiency in the analytical models may be in the assumption that the linearized form of the curvature-displacement relationship could be adopted ($w' \ll 1$).

From experimental results of beams with long unbond lengths, it was found that this assumption may have been violated.

This was due to the fact that the maximum lateral deflection of the unbonded faceplate exceeded the thickness of the plate by a factor of more than five. Thus, the comparisons which follow must be viewed with these limitations in mind.

5.1.1 Load versus Axial Displacement.

Loading histories (load versus axial displacement) experimentally recorded were plotted in figs. 3.1 and 3.2. Due to the previously mentioned reasons, only the limit loads obtained analytically were shown in these plots. Comparison of the predicted and measured failure loads indicate three distinct unbond length regimes which should be discussed separately: fully bonded beams, those with short unbond lengths ($L_u \leq 2.0$ in.), and those with longer unbonded specimens ($L_u \geq 3.0$ in.).

(a) Fully Bonded Sandwich Beams.

The buckling load of a simply supported sandwich column with rigid end fixtures can be shown to be directly proportional to the bending rigidity (table 3.4). Due to difficulties in accurately predicting the flexural rigidity of the column, the measured value had to be used. With it, the buckling load could be predicted to within 2.5% of the experimental failure load.

If flexural rigidity (D) testing is not possible, design using a calculated value of D in the above procedure, in the Euler buckling equation, or in eq. 2.5 (table 3.4) will yield failure loads between 26.8% to 52.1% lower than will actually occur--as long as a careful manufacturing process is employed. This margin of safety ensures that only buckling failure will not occur.

(b) Sandwich Beams with Short Unbonded Regions.

In the regime of short unbond length specimens ($L_u \leq 2.0$ in.), figs. 3.1 and 3.2 indicate that distinct failure loads occur. During testing, visual observations of these columns

revealed that some type of core failure may have occurred at, or near, the maximum load. Accurate analytical predictions for these failure loads were not possible. The analysis developed yielded buckling loads substantially higher than those measured experimentally (table 5.1).

To obtain a more practical model then, it will be necessary to eliminate a majority of the errors caused by stiff assumptions imposed upon the analytical models. This can be achieved by revaluating the assumptions used and incorporating:

(a) A failure criterion for the core at the interface of the fully bonded and unbonded sections.

(b) An extended analysis which includes the initial imperfections of the unbonded faceplate.

(c) <u>Sandwich Beams with Long Unbonded Regions</u>.

For beams with unbond lengths longer than 2.0 inches (fig. 3.2), comparison between theoretical and experimental failure loads indicated that the analytical models were accurate to within 12.5% (table 5.1). It was found that the experimental loading histories, for the columns with 3.0, 4.0 and 5.0-in. unbonded regions, were characterized by limit loads. This validated the theoretical conclusion that a limit in the loading history was a buckling attribute of an unbonded sandwich beam.

In addition, finding an experimental limit load response also supported the deficiencies identified in the analytical models. Since the only variable which separates the distinct failure and limit load responses was the unbond length, failure of the short unbond regions may result from either geometric imperfections or failure of the core.

5.1.2 **Load versus $W3_o$ Displacement.**

From analytical results, the $W3_o$ displacement (fig. 2.21)

should begin when the load within section three reached the buckling load of the unbonded section ($u_3 - \pi$). In the experiments, $W3_0$ displacements began well below this load (fig. 3.3). This was attributed to the presence of initial geometric imperfections within the sandwich specimens. Also because of this difference, the theoretical predictions of the $W3_0$ displacement at critical limit load were found to be much smaller than those measured experimentally.

5.2   QUALITATIVE DISCUSSION OF BUCKLING SHAPES

Out-of-plane displacement shapes of the unbonded faceplate were found from the experimental moire fringe data and calculated from the theoretical equations. These shapes were plotted in figs. 3.6-3.10 for comparison.

In the case of the 1.0-in. unbond (fig. 3.6), the beam failed well before the limit load was reached. As a result, direct comparison of the faceplate deformations was not possible. For unbond lengths from 2.0 to 5.0 inches (figs. 3.7-3.10), the failure loads were within 12.5%. It was found, however, that the magnitudes of the experimental displacement shapes were up to four times larger than those predicted from the analytical models.

The buckling shapes for these unbonded faceplates were qualitatively compared. Figures 3.7-3.10 indicate that the experimental and analytical deformation shapes were similar. Finally note that the transition in buckling mode--from symmetric to nonsymmetric, and found in all tested specimens--was not predicted by the theoretical models. Again, these differences were mainly due to the lack of geometric imperfection sensitivity of the analytical models.

5.3   MAXIMUM LOAD VERSUS UNBOND LENGTH

Plots of maximum load versus sandwich unbond length (fig. 3.15 and 3.16) indicated that the analytical models were capable of

predicting the limit load to within 12.5% for unbond lengths from 2.0 to 5.0 inches (table 5.1). If the 4.0-in. specimen was excluded, since it had an observable, initial displacement imperfection shape, estimations were within 7.7% of the measured loads.

In addition, it was found that a full logarithmic plot of this data (fig. 3.16) indicated a direct power-law relationship (eq. 3.2) between maximum load (P_{1max}) and unbond length (L_u). Constants for this equation, for both experimental and theoretical data, can be found in table 5.2. The analytical data indicated an almost exact fit (L_u from 1.0 to 5.0 inches). A power-law fit of experimental results (L_u between 1.5 and 5.0 inches) was found to predict failure loads to within 8.8%.

5.4   CRITICAL BENDING MOMENTS

In the design analysis of the fully bonded sandwich beam (chapter 2), yielding of the aluminum faceplates was not to occur until well after buckling failure. For the unbonded specimens tested, additional stresses were expected within the buckling faceplate. In order to determine if any yielding occurred, possibly causing the transition in mode failure shape or beam collapse load, it was necessary to examine critical bending moments at the maximum load.

Critical areas of the failing sandwich beam were considered to be along the interface and midspan of the unbonded section. Thus, the moments were calculated from the analytical model at the interface, M_2 and M_3, and unbond midsection, M_{2o} and M_{3o} (fig. 4.1). The moments were found at the theoretical limit loads. Since these loads were close to those measured for long unbond lengths, and higher at shorter unbond lengths, meeting the yielding criteria for the aluminum faceplates would indicate a margin of safety for the experimentally tested beams.

From the critical moments, the maximum stresses within the

faceplate were calculated. The yielding stress for the aluminum used was found to be approximately 42.68 ksi (table 2.1). Thus all stresses at the critical moments should be below this value. Table 5.3 listed the predicted maximum stresses found within the critical areas.

It was theoretically determined that all stresses were at most 65.3% below the yielding stress of the aluminum. The largest stresses were found to be within the unbonded faceplate, with the greatest magnitude occurring in the 1.0-inch unbond (14.82 ksi) and decreasing for longer unbond lengths. Thus, it was concluded that the transition in failure mode shape and actual buckling of the structure was not a result of yielding of the load-carrying aluminum faceplates.

Chapter 6
CONCLUDING REMARKS

A combined experimental and analytical study has been performed to establish the effect of a partially unbonded faceplate on the stability of sandwich beams. The sandwich structure considered was comprised of a lightweight aramid-fiber honeycomb core to which two aluminum 2024-T3 faceplates were bonded using a film adhesive.

In what follows the important experimental and analytical conclusions from the study are summarized. In addition, improvements and extensions of both the analytical models as well as the experimental work are suggested.

6.1   EXPERIMENTAL FINDINGS

In the experimental part of this work, the geometry of the beam was kept constant and the length of the unbonded section was varied. The beam geometry and properties of the constituents were chosen such that buckling would precede all other major failure modes--faceplate yielding, intra-cell dimpling, shear crimping, and faceplate wrinkling.

A total of 13 sandwich beam specimens were tested, two of which were fully bonded. The remainder contained an unbonded region which was always located symmetrically about the midspan of the beam. Experiments were performed over a range of unbond lengths from 0.5 to 5.0 inches. Both ends of the specimens were simply supported.

Each beam was axially loaded until either a distinct failure developed or until a limit load was obtained and surpassed. The majority of the tests were conducted using displacement control so that the load-deformation characteristics of the beam near the critical load could be identified.

46

Results from two fully bonded specimen indicated that a buckling instability developed which was then followed by catastrophic collapse of the structure. These failure loads were found to be within 2.5% of the load estimated by a classical beam stability analysis. However, in order to obtain this accuracy, it was necessary to use an experimentally determined bending rigidity.

The presence of an unbonded section along the length of the beam was found to drastically reduce the capacity of the structure to support axial loads. For example, an unbonded section with a 0.5 inch length caused a 46.4% reduction in failure load from the fully bonded case. In addition, it was found that a 98.2% load reduction occurred if the unbond length was 5.0 inches. Thus, as the unbond length was increased, the load carrying capacity decreased. Failure load (P_{1max}) was found to be related to the unbond length (L_u) by a least squares power-law fit. This relationship could predict the failure load of a sandwich beam (L_u between 1.5 and 5.0 inches) to within 8.8%.

Two distinct failure modes were observed in the loading histories of the beams tested. For unbond lengths of 2.0 inches or less, the column was found to fail suddenly and catastrophically. Calculations of the critical stresses within the unbonded region of the sandwich beam indicated that yielding of the aluminum faceplates did not occur. However, visual observations of these sandwich beams indicated that some type of core failure occurred at or near the maximum load.

A second failure mode was identified for sandwich unbond lengths of 3.0 inches or greater. For these specimens, a limit load characterized the loading histories. The deformation of the unbonded sections of the sandwich beams were initially symmetric about the beam midspan with the unbonded faceplate deflecting away from the honeycomb core. At some point in the loading history a transition in this deformation pattern--where the two sections started deforming in an nonsymmetric mode--was noted. This

occurred for <u>all</u> unbonded sandwich beams tested. This transition was sudden and occurred at or just prior to the maximum load for beams with short unbonded sections. For longer unbonded regions, the transition from the symmetric shape was much more gradual and occurred well before the limit load. Failure of the core was not observed in the specimens with long unbonded lengths.

6.2   ANALYTICAL FINDINGS

Analytical models were concurrently developed with the objective of predicting the observed unbonded beam instabilities. The structure was modeled as a beam comprised of three different sections--a fully bonded segment, the unbonded faceplate, and the opposite faceplate with the core attached--with compatibility and continuity enforced at the interface.

Among other more customary assumptions, it was assumed that this structure had an initially perfect geometry and that only symmetric failure shapes were possible. The measured flexural rigidities of the constituent sections were used in the analysis because of large uncertainties found in their predicted values.

The bending rigidities of the beam segments within the unbonded region were up to 2000 times lower than the value measured for the fully bonded section. It was found that because of the significantly large stiffness, deflections of the fully bonded beam segments contributed little to the displacements of the interior unbonded sections. Thus it was possible to assume that this section was rigid, which greatly simplified the solution process.

It was found that the responses of the models, for all unbond lengths, were characterized by limit loads. Because of the assumed initially perfect geometry, results were only obtained just prior to and after the limit load. In addition, while all predicted displacements were much lower than those measured, the models could accurately estimate experimental failure loads to within 12.5% (unbond lengths from 2.0 to 5.0 inches).

6.3   EXPERIMENTAL/ANALYTICAL IMPROVEMENTS AND EXTENSIONS

Throughout this analysis, modeling and experimental deficiencies have been noted. The primary cause for the observed differences between the predicted and measured results were due to the restrictions placed on the analytical model. It was found that the assumption which modeled the sandwich beam as initially geometrically perfect led to underestimations of all displacement measurements. In addition, the assumed inextensionality and linear curvature-displacement relationships also contributed to the observed differences between the calculated and measured deflections. Thus, for more accurate predictions of the loading histories and displacements, a modification of the analytical equations will be necessary. As a first step, geometric imperfections of the unbonded faceplate should be incorporated. If satisfactory results are not found, the addition of large rotations should be considered.

Experimentally, the displacement-measuring techniques can be improved. Use of an external LVDT for determining the axial displacement of the sandwich specimen will remove settling errors associated with the loading apparatus. Improvements in the Shadow-moire Method are necessary. Increasing the light source and camera angles will increase the accuracy of the measured faceplate displacements. Better alignment of the moire grating plate and continuous measurement of the distance between the plate and specimen will help determine a fixed reference for all fringe patterns. In addition, using the Shadow-moire Method on both sides of the unbond will yield the complete displacement profiles for the specimen. These will be useful in developing a better perspective of the transition in buckling shapes encountered.

While it was desired to determine the buckling failure of a sandwich plate with an unbond, further work on the unbonded beam is necessary prior to extending this analysis to the more general plate problem. Measurement of geometric imperfections and their

inclusion into the analytical models is one such area. In addition, the causes for the failure observed within the core of shorter unbonded sections will have to be established. It would also be useful to examine variations in loading--such as eccentrically loading the sandwich beam--nonsymmetric and other buckling modes, and possible crack growth in the core or adhesive interface.

In conclusion, this study has considered several methods for predicting the failure loads of sandwich beams with an unbonded region and has gained some insight as to the instability of this structure. However, unanswered questions remain, and new ones have arisen. It is anticipated that with additional analysis, the causes of failure--both catastrophic and limit load--and the reasons for buckling shape transition will be determined and analytically predicted.

APPENDIX A

FLEXURAL RIGIDITY CALCULATIONS

Flexural rigidity (D) is defined as the product of the materials Young's Modulus (E) and the second moment of area (I). Determination of D for beam sections one and two (fig. 4.1) was necessary to accurately predict failure loads.

Fully Bonded Beam: D_1

According to ref. [1], a simple approximation of flexural rigidity (per unit width of beam), for a fully bonded sandwich beam, contained contributions from the core and faceplates only (fig. 2.2).

$$D_1 = \frac{E_c c^3}{12} + \frac{2E_f t_f^3}{12} + \frac{2E_f t_f d_f^2}{4} \qquad (A.1)$$

A simplification was then made in eq. A.1 since $t_f \ll 1$ and $E_c \ll E_f$ (i.e. $E_c \approx 0$):

$$D_1 = \frac{E_f t_f d_f^2}{2} \qquad (d_f = c + t_f) \qquad (A.2)$$

Using dimensions and properties from table 2.1, it was found that D_1 equalled 23731.28 in·lb. In order to compare this approximation with experimental results, contributions from all components were found:

$$D_1 = D_c + D_{f1} + D_{f2} + D_{a1} + D_{a2} \qquad (A.3)$$

$$D_c = 0 \qquad (A.4)$$

$$D_{f1} = \frac{E_f t_f^3}{6} = 13.94 \text{ in·lb} \qquad (A.5)$$

$$D_{f2} = \frac{E_f t_f d_f^2}{2} = 23123.25 \text{ in·lb} \qquad (A.6)$$

51

$$D_{a1} = \frac{E_a t_a^3}{6} = 0.17 \text{ in.lb} \tag{A.7}$$

$$D_{a2} = \frac{E_a t_a d_a^2}{2} = 593.92 \text{ in.lb} \tag{A.8}$$

Totaling the contributions in A.4 through A.8 using A.3 showed that D_1 was equal to 23731.28 in.lb, and was not significantly larger than the value determined by eq. A.2. However, comparison with the experimentally determined value for D_1 (table 2.2) indicated that a significant discrepancy existed in the method used to predict flexural rigidity for a sandwich beam. It was unclear as to the exact reason for these large errors.

Beam with one faceplate: D_2

The flexural rigidity for beam section two--only one faceplate bonded to the core--was found in a similar procedure. Adhesive contributions to D_2 were again included. For this section, it was necessary to determine the location of the new neutral axis. This was accomplished by integrating the stress distribution through the beam section and setting the resulting force equal to zero.

$$N = \int_t \sigma \, dz = 0 \tag{A.9}$$

Again assuming that $E_c = 0$ and the thickness of the adhesive ($t_a = 0.013$ in.) was uniform, the approximate location of the neutral axis was found to be within the aluminum faceplate a distance $r = 0.00976$ in. from the adhesive interface (fig. 4.2).

The flexural rigidity was found by summing the contributions from each component, as before:

$$D_2 = D_c + D_{f1} + D_{f2} + D_{a1} + D_{a2} \tag{A.10}$$

$$D_c = 0 \tag{A.11}$$

$$D_{f1} = \frac{E_f t_f^3}{12} = 6.97 \text{ in.lb} \tag{A.12}$$

$$D_{f2} = E_f t_f \left(\frac{t_f}{2} - r \right)^2 = 0.03 \text{ in.lb} \qquad (A.13)$$

$$D_{a1} = \frac{E_a t_a^3}{12} = 0.09 \text{ in.lb} \qquad (A.14)$$

$$D_{a2} = E_a t_a \left(\frac{t_a}{2} + r \right)^2 = 1.59 \text{ in.lb} \qquad (A.15)$$

Summing the contributions using eq. A.10, the flexural rigidity for beam section two was approximated as $D_2 = 8.68$ in.lb.

APPENDIX B
FAILURE CRITERIA DERIVATIONS

Two sandwich beam failure modes are explained further within this section: overall column buckling including the effects of shear deformations, and faceplate wrinkling.

Column Buckling with Shear Deformations.

Buckling deformations in sandwich beams are primarily caused by bending deflections (w_b) and shear deformations (w_s) (fig. B.1). The bending contribution was derived from fig. B.2 and Bernoulli/Euler beam theory:

$$\frac{d^2 w_b}{dx^2} = \frac{-M(x)}{D_1} \qquad (B.1)$$

From fig. B.3, shear angle (γ) was found to be:

$$\gamma = \frac{d_f}{c} \frac{dw_s}{dx} \qquad (B.2)$$

Integrating γ through the core thickness (c) produced an equation for shear force (V). Using B.2 and introducing a geometry dependent shape factor (α_s), as proposed by Timoshenko since the shear was not constant through the core, yielded:

$$\frac{dw_s}{dx} = \frac{V}{\alpha_s G d_f} \qquad (B.3)$$

Using symmetry, equilibrium produced:

$$V = N \, dw/dx \qquad (B.4)$$

$$M(x) = -N \, [\, \delta - w(x)] \qquad (B.5)$$

Differentiating the resulting equation found by substituting eq. B.4 into B.3, gave:

$$\frac{d^2w_s}{dx^2} - \left(\frac{N}{\alpha_s Gd_f}\right)\frac{d^2w}{dx^2} \qquad (B.6)$$

The beams total deflection was defined (fig. B.1) as:

or,
$$w = w_b + w_s \qquad (B.7)$$

$$\frac{d^2w}{dx^2} - \frac{d^2w_b}{dx^2} + \frac{d^2w_s}{dx^2}$$

Combining eq. B.1, and B.5 through B7 yielded the following differential equation:

$$\frac{d^2w}{dx^2} + k^2w(x) - k^2\delta \qquad (B.8)$$

where,

$$k^2 - \frac{N}{D\left[1 - \dfrac{N}{\alpha_s Gd_f}\right]} \qquad (B.9)$$

Using boundary conditions,

$$w(0) - 0 \qquad w'(0) - 0 \qquad w(L/2) - \delta \qquad (B.10)$$

in the general solution of eq. B.8,

$$w(x) - C_1 \sin kx + C_2 \cos kx + \delta \qquad (B.11)$$

yielded,

$$k - (2n - 1)\frac{\pi}{L} \qquad (B.12)$$

Since concern was for the first buckling load, (n - 1) eq. B.12 and B.9 gave:

$$N_{cr} - \frac{\pi^2 D}{1^2}\left\{1 - \frac{N_{cr}}{\alpha_s Gd_f}\right\} \qquad (B.13)$$

Shear stress distribution was used to determine the shape factor (α_s). From strength of materials, it was found for a composite beam that:

$$\tau = \frac{V}{D}\left[\frac{E_f d_f t_f}{2} + \frac{E_c}{2}\left(\frac{c^2}{4} - z^2 \right) \right] \tag{B.14}$$

From ref. [1], since $E_c \ll E_f$ and $t_f \ll c$, eq. B.14 reduced to:

$$\tau = V/d_f \tag{B.15}$$

Since $\tau = G\gamma$ and from eq. B.2 and B.3, it was found that $\alpha_s = d_f/c$. Using this result in eq. B.13, the equation for critical buckling load (per unit width) was found:

$$N_B = \frac{N_E}{1 + N_E/N_S} \tag{B.16}$$

where,

$$N_E = \pi^2 D/L^2$$
$$N_S = Gd_f^2/c$$

Faceplate Wrinkling.

Only symmetric wrinkling was considered, since sandwich design was based upon the lowest loads of the various failure modes (fig. 2.3d). Using symmetry, the structure can be modeled as a beam on a linearly elastic spring foundation [3]. The spring constant was found to be:

$$k_c = 2E_c/c \tag{B.17}$$

From beam theory, the equation of motion for this model was determined.

$$\frac{d^4w}{dx^4} + \left(\frac{N}{E_f I_f} \right)\frac{d^2w}{dx^2} + \left(\frac{k_c}{E_f I_f} \right) w = 0 \tag{B.18}$$

Substituting the assumed solution,

$$w(x) = C_1 \sin\left(\frac{\pi x}{1} \right) \tag{B.19}$$

into eq. B.18 yielded:

$$N = E_f I_f (\pi/1)^2 + k_c (\pi/1)^2 \qquad (B.20)$$

Minimizing eq. B.20 (i.e. dN/dl = 0) produced the equation for critical half-wavelength (fig. 2.3d):

$$l_{cr} = \pi \left[\frac{E_f I_f}{k_c} \right]^{1/4} \qquad (B.21)$$

Substituting eq. B.21 into B.20 lead to the equation for the critical wrinkling load:

$$N_W = t_f E_f \left[\frac{2 E_c t_f}{3 E_f c} \right]^{1/2} \qquad (B.22)$$

REFFRENCES

1. Fairbairn, W., "An Account of the Construction of the Britannia and Conway Tubular Bridges," John Weale et al., London, 1849.

2. *Composite Construction for Flight Vehicles*, MIL-HDBK-23, Part 1, USGPO, Washington D.C., Oct. 1959.

3. *HEXCEL Honeycomb*, HEXCEL Corporation, 1983.

4. Langston, P.R., "Design and Use of KEVLAR in Aircraft Structures," *Composites: Design and Manufacturing for General Aviation Aircraft*, SAE, General Aviation Aircraft Meeting and Exposition, Wichita, KS, pp. 41-55, April 1985.

5. Neubert, H.D., and Kiger, R.W., "Modern Composite Aircraft Technology," *Sport Aviation*, pp. 55-63, Sept. 1976.

6. DeMeis, R., "Avtek 400: light is right," *Aerospace America*, V. 23, No. 8, pp. 62-66, Aug. 1985.

7. Minnford, J.D., and Vader, E.M., "Aluminum-Faced Sandwich Panels and Laminates," *Adhesives Age*, V. 18, No. 2, pp. 30-35, Feb. 1975.

8. Becker, W.E., *U.S. Sandwich Panel: Manufacturing/Marketing Guide*, Technomic Publishing Co., Stamford, CT, 1968.

9. U.S. Forest Products Laboratory, "Characteristics of Load-Bearing Sandwich Panels for Housing," USDA, 1973.

10. Shideler, J.L., Swegle, A.R., and Fields, R.A., "Honeycomb Sandwich Structure for Future Space Transportation Systems with Integral Cryogenic Tankage," *Journal of Spacecraft and Rockets*, V. 21, No. 3, pp. 246-252, May/June 1984.

11. Grimes, G.C., "The Adhesive-Honeycomb Relationship," Applied Polymer Symposia No. 3, Hoboken, NJ, 1965, <u>Structural Adhesives Bonding</u>, pp. 157-190, Wiley & Sons, NY, 1966.

12. Parkinson, R.E., "Selection of Materials for Architectural Sandwich Panels," ASTM, *Symposium on Structural Sandwich Constructions*, Los Angeles, CA, Sept. 1956.

13. Ericksen, W.S., and March, H.W., "Effects of Shear Deformation in the Core of a Flat Rectangular Sandwich Panel," FPL Report No. 1583-B, Revised Nov. 1958.

14. Jahnke, W.E., and Kuenzi, E.W., "Buckling of Simply Supported Rectangular Sandwich Panels Subjected to Edgewise Bending," FPL Report No. 1868, Mar. 1959.

15. "The Basics on Bonded Sandwich Construction," TSB124, HEXCEL, 1984.

16. Column Research Committee of Japan, ed., <u>Handbook of Structural Stability</u>, pp. 3-121, Corona, Tokyo, 1971.

17. *Construction of Sandwich Composites*, Military Handbook, Vol. 23A, USGPO, Revised 1984.

18. Yusuff, S., "Theory of Wrinkling in Sandwich Construction," *Journal of the Royal Aeronautical Society*, Vol. 59, No. 529, pp. 30-36, Jan. 1955.

19. "Mechanical Properties of HEXCEL Honeycomb Materials," TSB120, HEXCEL, 1981.

20. Chiang, F.P., "Moire Methods of Strain Analysis," *Manual on Experimental Stress Analysis*, SESA, 3rd ed., A.S. Kobayiashi, ed., Chapter VI, pp. 51-69, 1978.

21. Allen, H.G., <u>Analysis and Design of Structural Sandwich Panels</u>, Pergamon Press, London, 1969.

22. Material Test System Reference Manual, MTS Systems Corporation, Minneapolis, MN, 1978.

23. Chai, H., Babcock, C.D., and Knauss, W.G., "One Dimensional Modelling Of Failure in Laminated Plates by Delamination Buckling," *International Journal of Solids & Structures*, Vol. 17, No. 11, pp. 1069-1083, 1981.

24.   Garbow,   B.S.,   Hillstrom,   K.E.,   and   More,   J.J.,
        "Documentation   for   MINPACK   Subroutine   HYBRD1,"   Argonne
        National Laboratory, Mar. 1980.

Additional General References

25.   Plantema, F.J., Sandwich Construction: The Bending and
        Buckling of Sandwich Beams, Plates, and Shells, Wiley &
        Sons, NY, 1966.

26.   Hoff, N.J., The Analysis of Structures, Wiley & Sons, NY,
        1956.

27.   Webber, J.P.H., Kyriakides, S., and Lee, C.T., "On the
        wrinkling of honeycomb sandwich columns with laminated
        cross-ply faces," Journal of the Royal Aeronautical
        Society, V. 80, pp. 263-272, June 1976.

28.   Webber,   J.P.H.,   "Least-weight   design   of   carbon   fibre
        honeycomb   sandwich   columns,"   Journal   of   the   Royal
        Aeronautical Society, V. 83, pp. 314-319, Aug. 1979.

29.   Chapman, R.G., "Compression Tests on Dural-Balsa Sandwich
        Panels," R.A.E. Report No. S.M.E. 3326, Aug. 1945.

30.   Webber, J.P.H., and Pearce, T.R.A., "Buckling of Sandwich
        Panels with Laminated Face Plates," The Aeronautical
        Quarterly, V. XXIII, pp. 147-160, May 1972.

31.   Lo,   K.H.,   and   Conway,   H.D.,   "Effects   of   Interface
        Conditions on the Bending of Laminated Beams," ASME,
        Journal of Applied Mechanics, V. 43, pp 495-496, June 1975.

32.   Webber, J.P.H., "Governing Equations for Thick Sandwich
        Shells with Honeycomb Cores and Laminated Faces," The
        Aeronautical Quarterly, V. XXV, pp. 270-286, Nov. 1974.

33.   Reissner, E., "On Small Bending and Stretching of Sandwich-
        Type Shells," International Journal of Solids & Structures,
        V. 13, pp. 1293-1300, Dec. 1977.

34.   Brush, D.O., and Almroth, B.O., <u>Buckling of Bars, Plates, and Shells</u>, Mc Graw-Hill, NY, 1975.

35.   Oden, J.T., and Ripperger, E.A., <u>Mechanics of Elastic Structures</u>, 2nd ed., Mc Graw-Hill, NY, 1981.

36.   Jones, R.M., <u>Mechanics of Composite Materials</u>, Mc Graw-Hill, NY, 1975.

37.   Dally, J.W., and Riley, W.F., <u>Experimental Stress Analysis</u>, 2nd ed., Mc Graw-Hill, NY, 1978.

38.   Beer, F.P., and Johnston, E.R., <u>Mechanics of Materials</u>, Mc Graw-Hill, NY, 1981.

39.   Ralston, A., and Rabinowitz, P., <u>A First Course in Numerical Analysis</u>, Mc Graw-Hill, NY, 1978.

40.   Chajes, A., <u>Principles of Structural Stability Theory</u>, Prentice-Hall, NJ, 1974.

FACEPLATES	Aluminum 2024-T3
	$t_f = 0.0203 \pm 0.0001$ in
	$E_f = 9.951 \times 10^3$ ksi
	$\sigma_{y\ 0.2\%} = 42.68$ ksi
CORE	Aramid Fiber Hexagonal Celled Honeycomb: HRH 10-1/8-3.0(2)
	$s = 0.125 \pm 0.002$ in
	$\rho_c = 3.054$ pcf
	$E_c = 20.0$ ksi
	$G_W = 3.5$ ksi
	$G_L = 7.0$ ksi
ADHESIVE	FM 300 Film Adhesive
	$t_a = 0.013 \pm 0.001$ in
	$E_a = 463.5$ ksi
TEFLON SPACER	
	$t_t = 0.0035 \pm 0.0002$ in

Table 2.1 SANDWICH BEAM COMPONENT PROPERTIES

	MEASURED	PREDICTED
D_3	-	6.97 in·lb
c = 0.457 in D_1 D_2 α_s	31288.47 in·lb 15.27 in·lb 1.0245	23731.28 in·lb 8.68 in·lb d/c = 1.0444
c = 0.506 in D_2	14.363 in·lb	8.68 in·lb

Table 2.2 SANDWICH BEAM SECTION MEASUREMENTS

4-pt Bending	$L = 12.02 \pm 0.01$ in $b = 1.507 \pm 0.001$ in $h = 0.496 \pm 0.001$ in $q = 2.52 \pm 0.005$ in $r = 6.00 \pm 0.005$ in $s = 0.49 \pm 0.005$ in
Cantilever Bending	$L = 4.00 \pm 0.005$ in $b = 1.50 \pm 0.005$ in $h = 0.477 \pm 0.001$ in
3-pt Bending	$L = 12.02 \pm 0.01$ in $b = 1.50 \pm 0.005$ in $h = 0.496 \pm 0.001$ in $r = 5.50 \pm 0.005$ in $s = 0.50 \pm 0.005$ in

Table 2.3 FLEXURAL RIGIDITY TEST SPECIMEN DIMENSIONS

SPECIMEN NO.	L_u (in)	THICKNESS	
		CORE c (in)	OVERALL h (in)
1	0.000	0.457	0.495
2	3.000	0.457	0.498
3	2.001	0.457	0.498
4	0.995	0.457	0.498
5	1.504	0.457	0.498
6	0.500	0.457	0.498
7	1.504	0.457	0.497
8	0.000	0.457	0.496
9	5.000	0.506	0.547
10	3.012	0.506	0.548
11	4.020	0.506	0.548
12*	4.010	0.506	0.546
13*	2.998	0.506	0.545

Note: All measurement uncertanties are ± 0.001 in.
  * Imperfect Beam

Table 3.1   SANDWICH BEAM TEST SPECIMEN DIMENSIONS

SPECIMEN NO.	L_u (in)	GRATING PITCH (lines/in)	α (deg)	β (deg)	$W_{n=1}$ (in)
2	3.0	120	20.0	7.0	0.0171
3	2.0	120	20.0	12.0	0.0145
4	1.0	200	18.0	24.0	0.0065
5	1.5	200	19.0	18.0	0.0075
6	0.5	200	19.0	18.0	0.0075
7	1.5	200	20.0	23.0	0.0063
8	0.0	200	20.0	25.0	0.006
9	5.0	200	20.5	14.0	0.008
10	3.0	200	17.0	22.0	0.007
11	4.0	200	17.0	22.0	0.007

Note: Displacement errors are approximately $\pm 1/2\ W_{n=1}$

Table 3.2 SHADOW MOIRE DATA

L_u (in)	P_{1max} (lbs)
0.0	3480.0
	3540.0
0.5	1898.0
1.0	914.0
1.5	574.0
	582.0
2.0	390.0
3.0	185.5*
	190.0
4.0	95.0*
5.0	65.4*

NOTE: * Core thickness c − 0.506 in
       All Others   c − 0.457 in

Table 3.3 SANDWICH BEAM FAILURE LOADS

FAILURE EQN.	P_{cr} (lbs)	
	D_1 theory	D_1 exper
EULER	2580.9	3402.8
STABILITY EQUILIBRIUM	2619.9	3454.22
BEAM THEORY W/SHEAR	1717.6	2046.5

Note: End fixtures included in beam length.

$$\text{EULER:} \quad P_{cr} = b \, D_1 \, (\pi/L_o)^2$$

$$\text{STABILITY EQUILIBRIUM:} \quad \tan[kl(1 - \eta)] = 1/(kl\eta)$$

$$\text{where} \quad k^2 = P_{cr}/(D_1 b)$$

$$1 = L_o/2 \, , \quad \eta 1 = 1.75 \text{ in.}$$

BEAM THEORY W/ SHEAR: see eqn. 2.5

where,

D_1 theory $= 23731.28$ in·lb
D_1 exper $= 31288.47$ in·lb
$L_o = 16.5$ in
$b = 3.0$ in

Experimental failure loads: 3480 lbs (specimen one)
3540 lbs (specimen eight)

Table 3.4 FULLY BONDED BEAM FAILURE LOADS

L_u (in)	P_{1max} (lbs)				
	EXPERIMENT	ANALYTICAL MODEL			
		GENERAL		SIMPLIFIED	
		c (in)	error	c (in)	error
0.0	3480.0 3540.0	-	-	-	-
0.5	1898.0	10519.0	454.2%	6633.87	249.5%
1.0	914.0	1661.75	81.8%	1664.62	82.1%
1.5	574.0 582.0	741.85	29.1%	742.71	29.4%
2.0	390.0	419.17	7.5%	419.48	7.6%
2.5	-	269.47	-	269.62	-
3.0	185.5* 190.0	187.97*	1.3%	188.05*	1.4%
3.5	-	138.79	-	138.84	-
4.0	95.0*	106.77*	12.4%	106.80*	12.4%
4.5	-	84.87	-	84.86	-
5.0	65.4*	69.08*	5.6%	69.09*	5.6%

NOTE: * Core thickness   c = 0.506 in
All Others   c = 0.457 in

Table 5.1   SANDWICH BEAM FAILURE LOADS
EXPERIMENTAL & THEORETICAL

L_u DATA SET (in)	β	LOG α	α	CORRELATION* FACTOR
Experimental 1.5 to 5.0	-1.8172	3.1058	1275.9	-0.99615
Theoretical 1.0 to 5.0	-1.97622	3.21849	1653.8	-0.99999

* Correlation Factor $= 1 - \sigma_x^2 / \sigma_y^2$
where σ_x and σ_y are the summation of standard deviation
of error estimate of the absissa and ordinate.

$$P_{1max} = \alpha (L_u)^\beta$$

Table 5.2 LEAST SQUARES FIT

L_u (in)	σ_2 (psi)	σ_{2o} (psi)	σ_3 (psi)	σ_{3o} (psi)
1.0	12.13	22.78	14819.24	14819.48
1.5	18.40	34.21	12124.24	12124.91
2.0	21.98	40.48	9871.39	9872.53
2.5	24.52	44.71	8288.96	8290.60
3.0	27.09	48.92	7216.13	7218.36
3.5	29.60	52.89	6422.83	6425.73
4.0	31.84	56.28	5788.30	5791.89
4.5	35.23	61.60	5376.17	5380.74
5.0	38.34	66.28	5010.68	5016.28

Table 5.3 CRITICAL STRESSES IN THE ALUMINUM FACEPLATES
AT THEORETICAL LIMIT LOAD
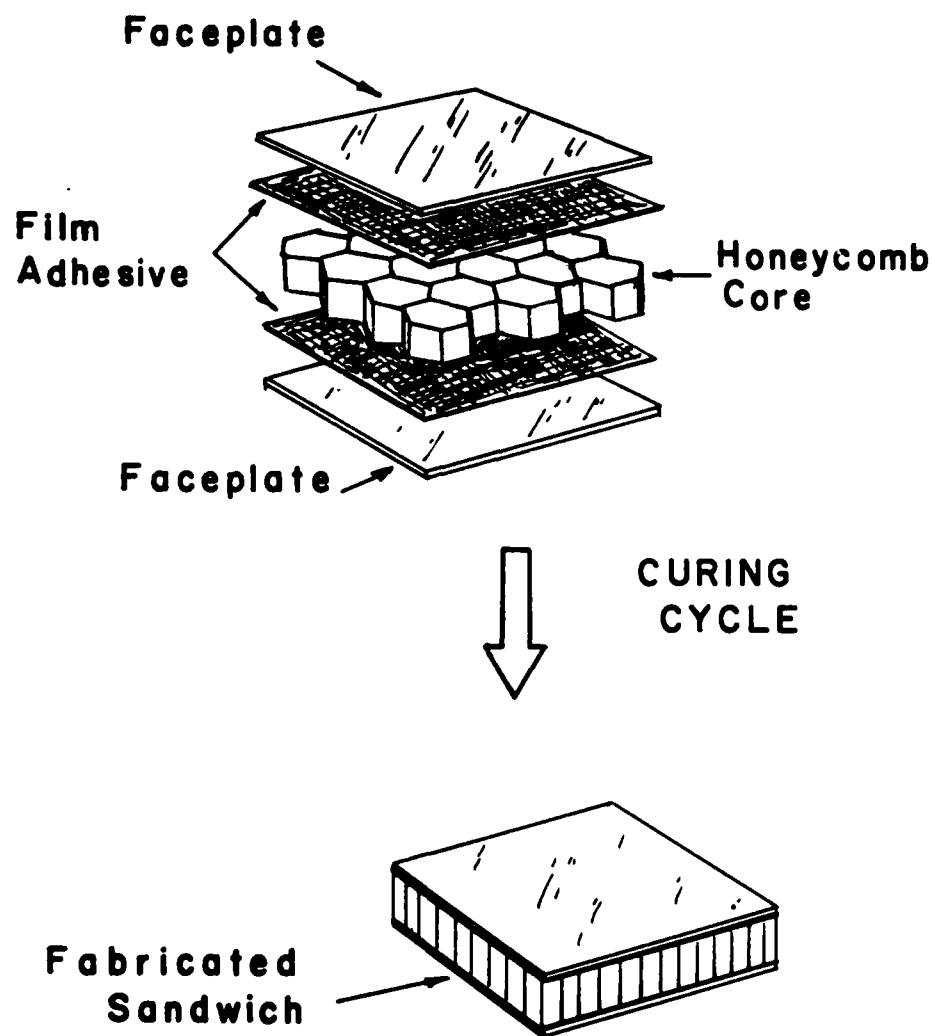
FIG   1.1   SANDWICH BEAM CONSTRUCTION
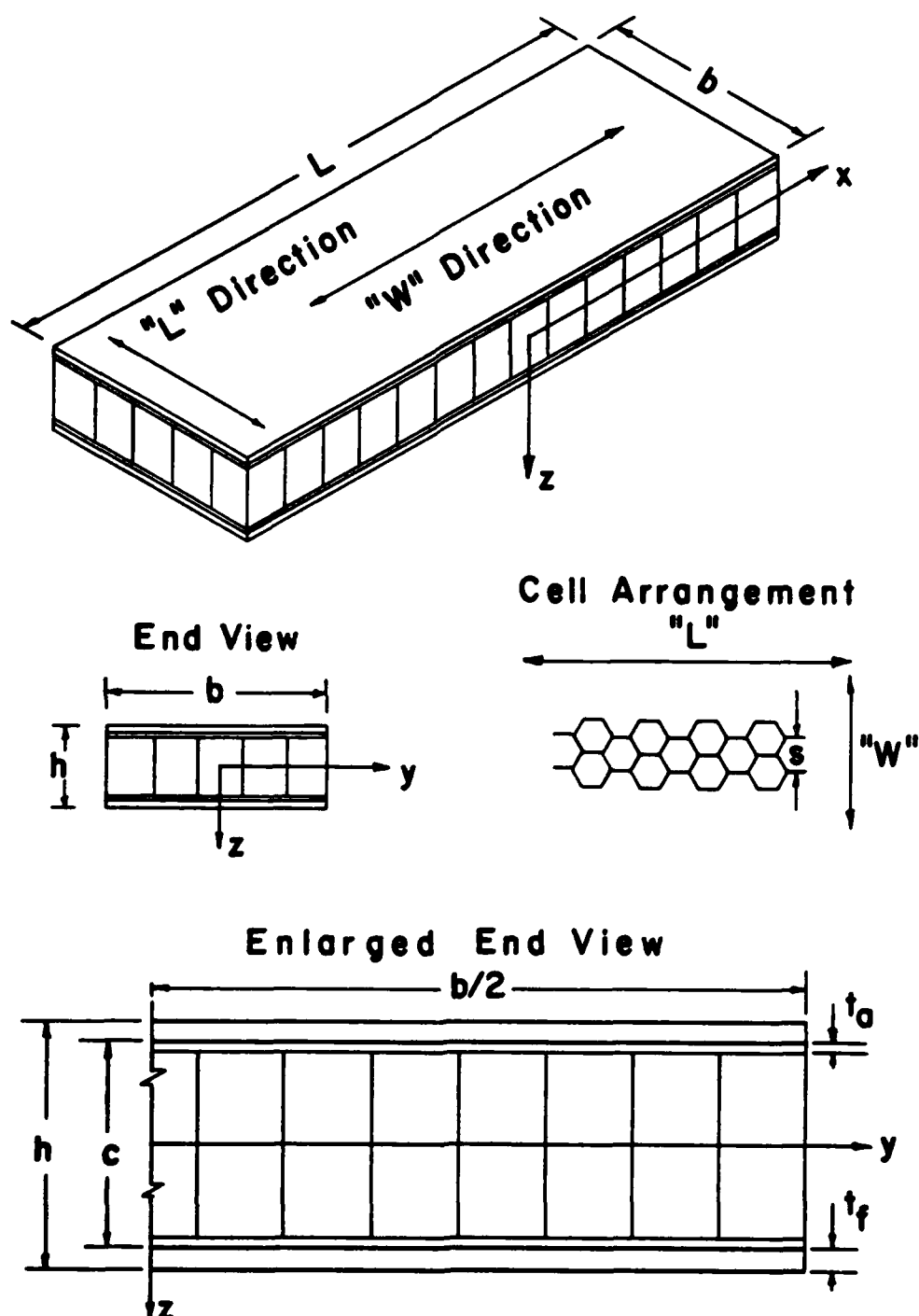
FIG 2.1   SANDWICH BEAM LAY-UP AND
GEOMETRIC PARAMETERS

A. FACEPLATE YIELDING

B. INTRA-CELL DIMPLING

C. SHEAR CRIMPING

D. FACEPLATE WRINKLING

E. OVERALL BUCKLING
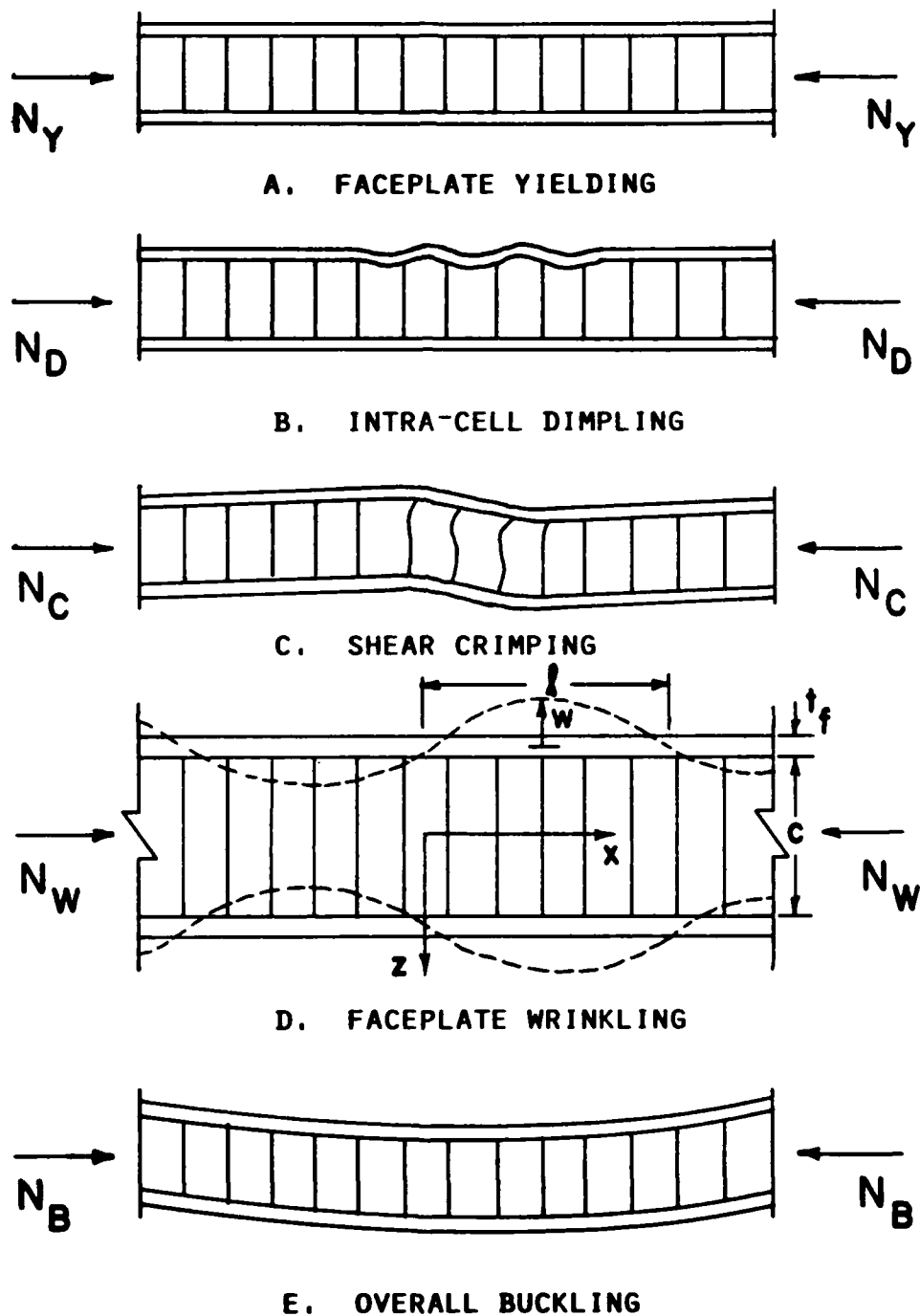
FIG 2.2 SANDWICH BEAM FAILURE MODES
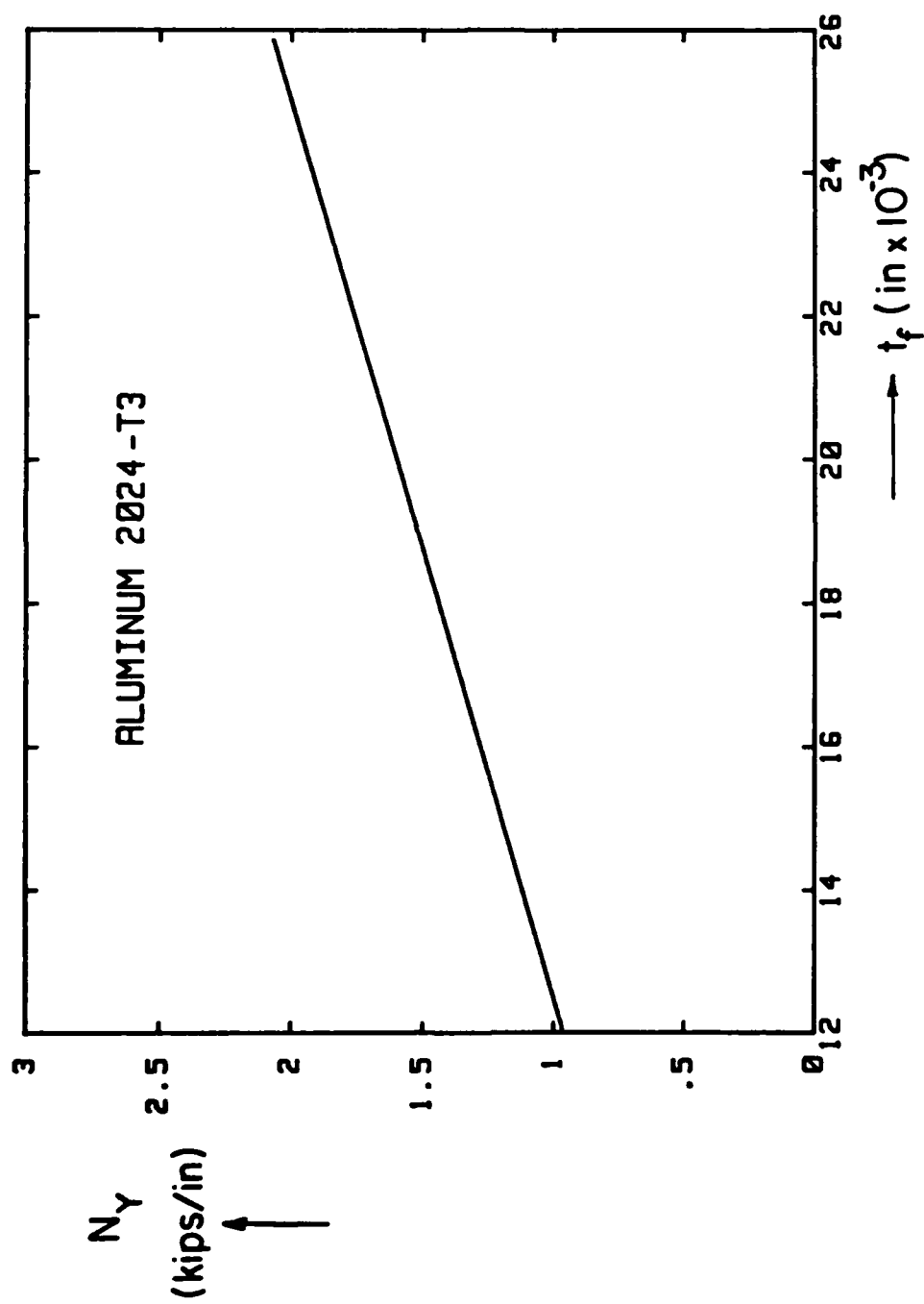
FIG 2.3 FACEPLATE YIELDING LOAD VERSUS FACEPLATE THICKNESS
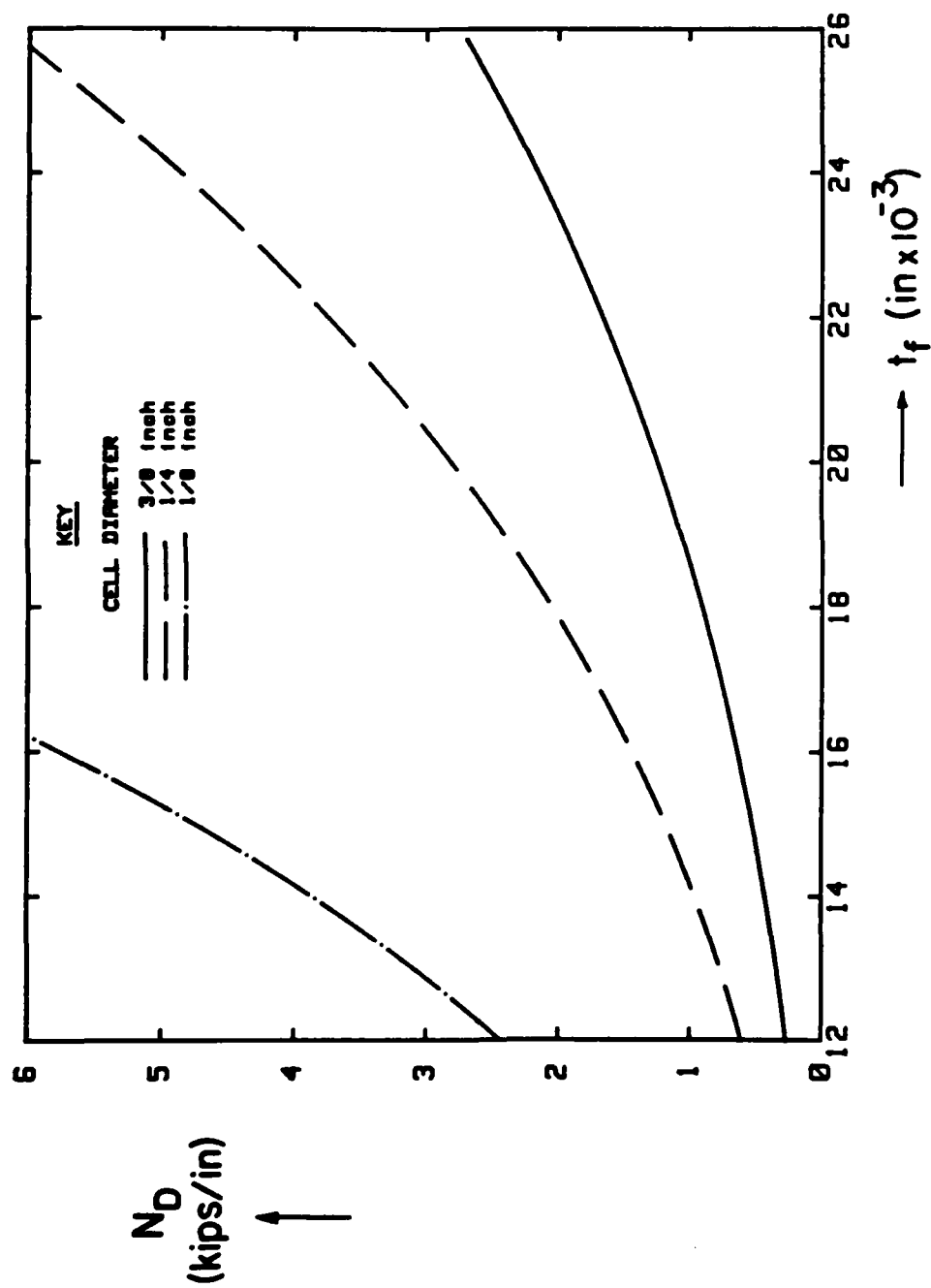
FIG 2.4 CRITICAL DIMPLING LOAD VERSUS FACEPLATE THICKNESS
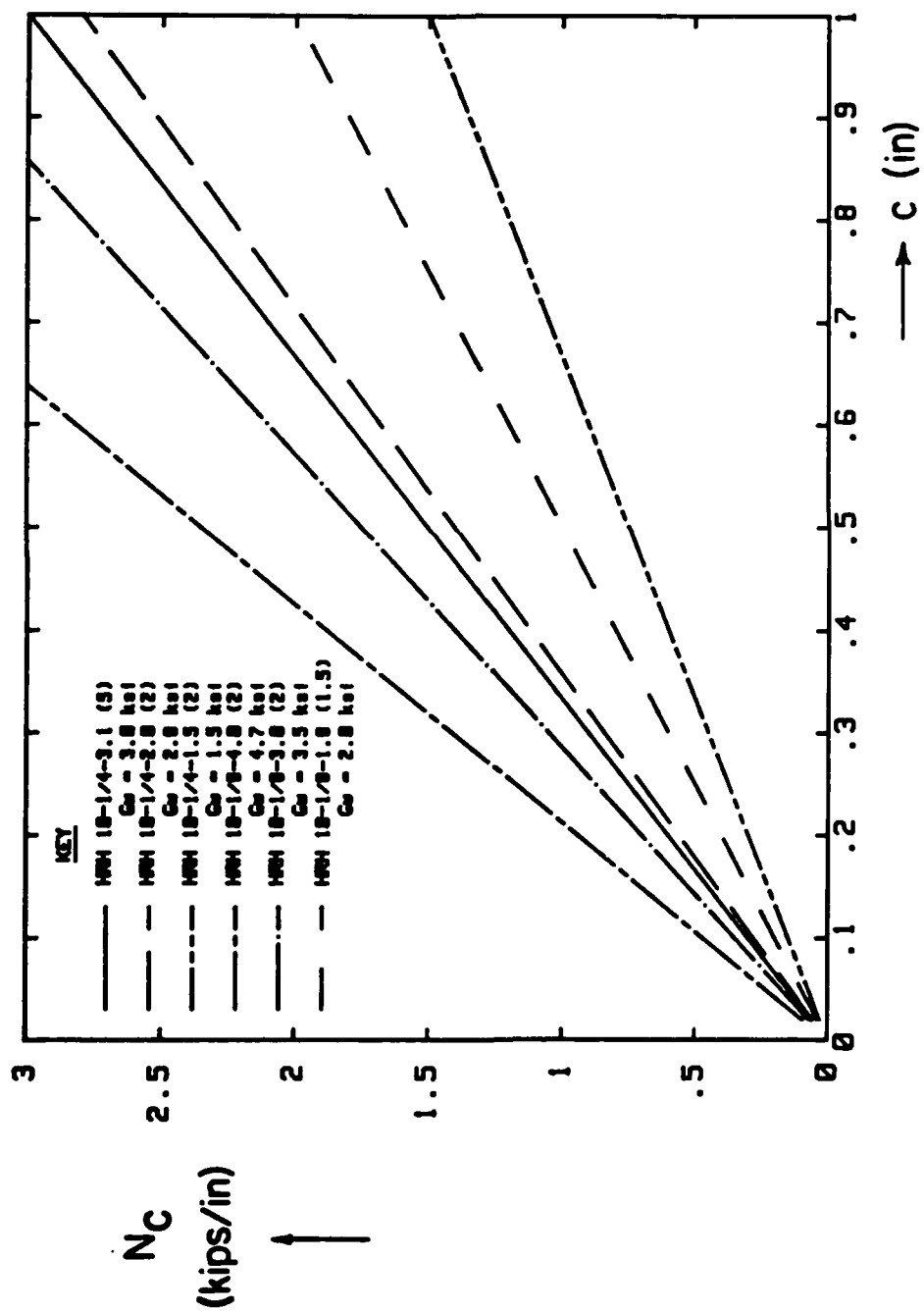
FIG 2.5 CRITICAL SHEAR CRIMPING LOAD VERSUS CORE THICKNESS
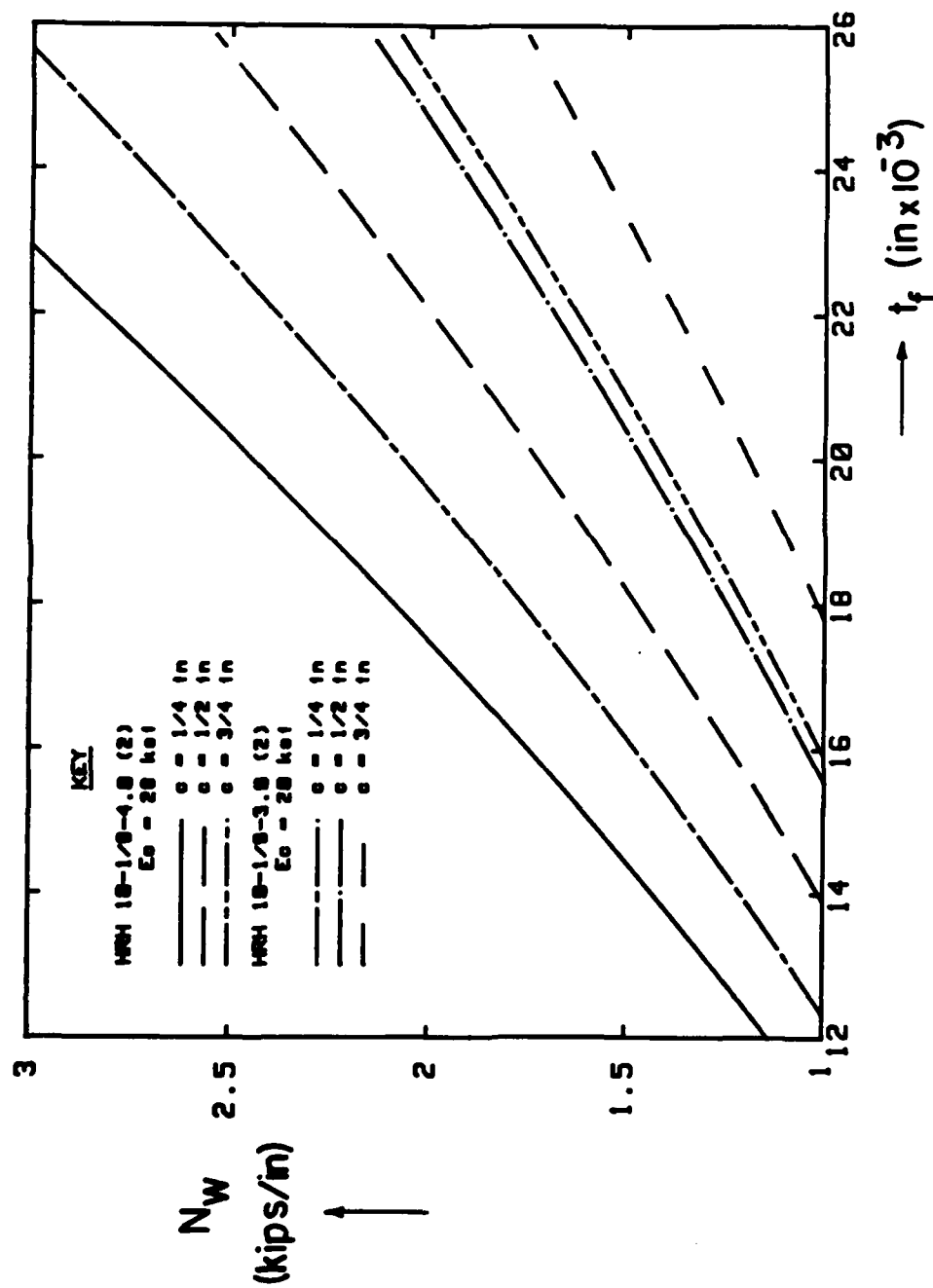
FIG 2.6 CRITICAL WRINKLING LOAD VERSUS FACEPLATE THICKNESS

KEY

C = 8.5 inch
Go = 3.5 ksi

—— t = 8.828 in
···· t = 8.825 in

—— C = 8.75 inch
      Go = 3.5 ksi
      t = 8.828 in

—·— C = 8.5 inch
      Go = 2.8 ksi
      t = 8.828 in

N_B

(kips/in)

→ L (in)
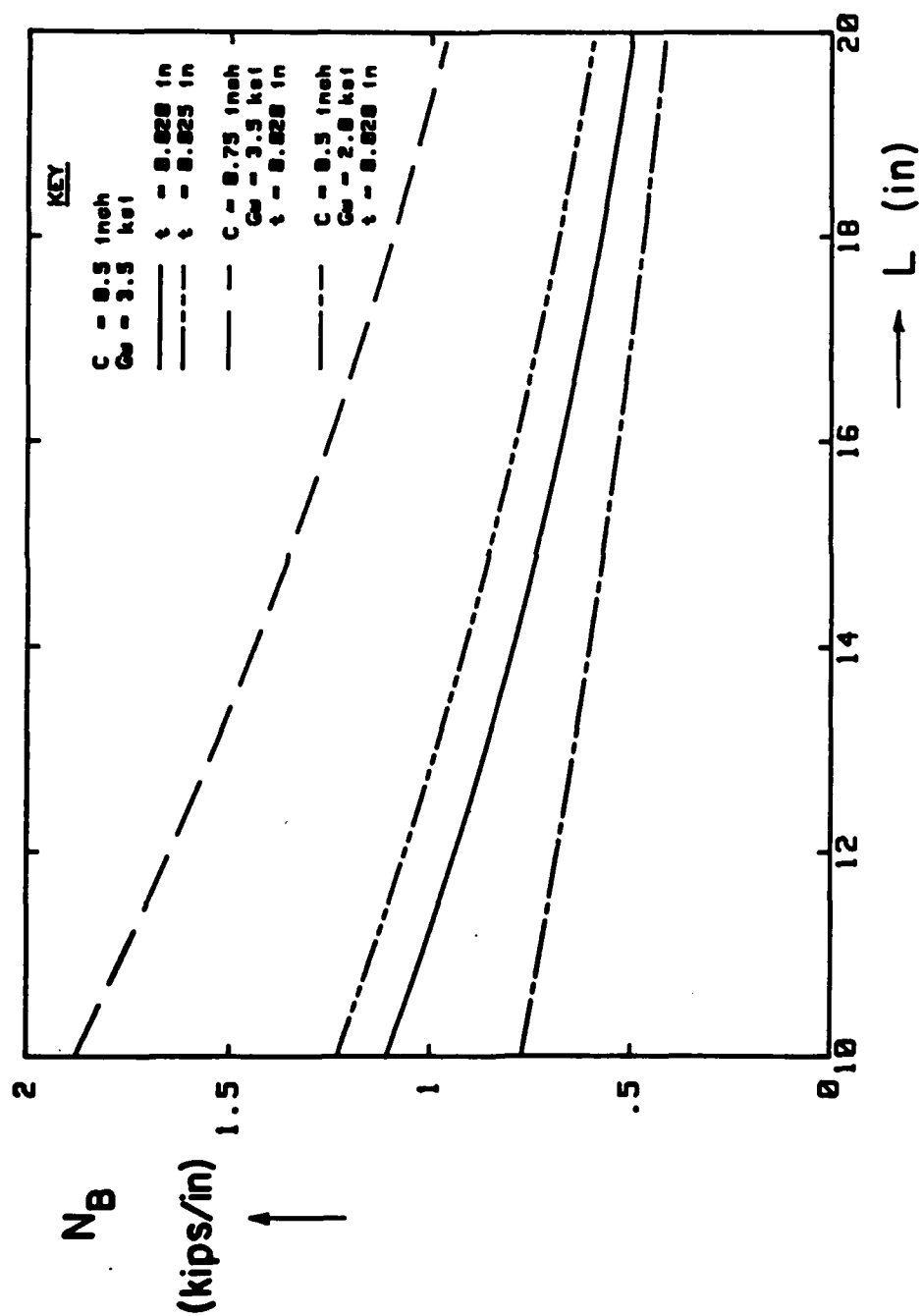
FIG 2.7   CRITICAL OVERALL BUCKLING LOAD VERSUS BEAM LENGTH
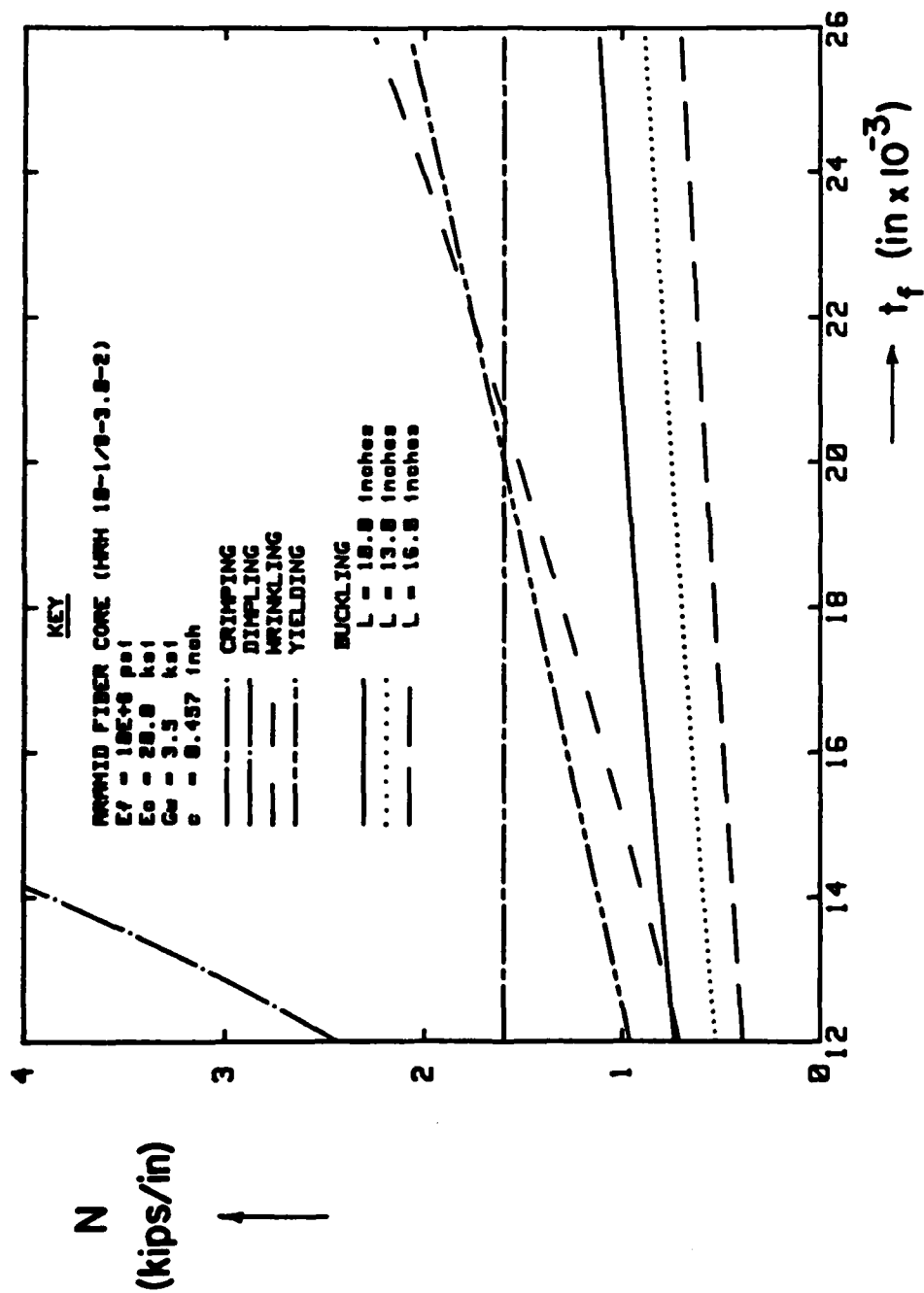
FIG 2.8 FAILURE CRITERIA PLOT: c = 0.457 IN. (3 BEAM LENGTHS)
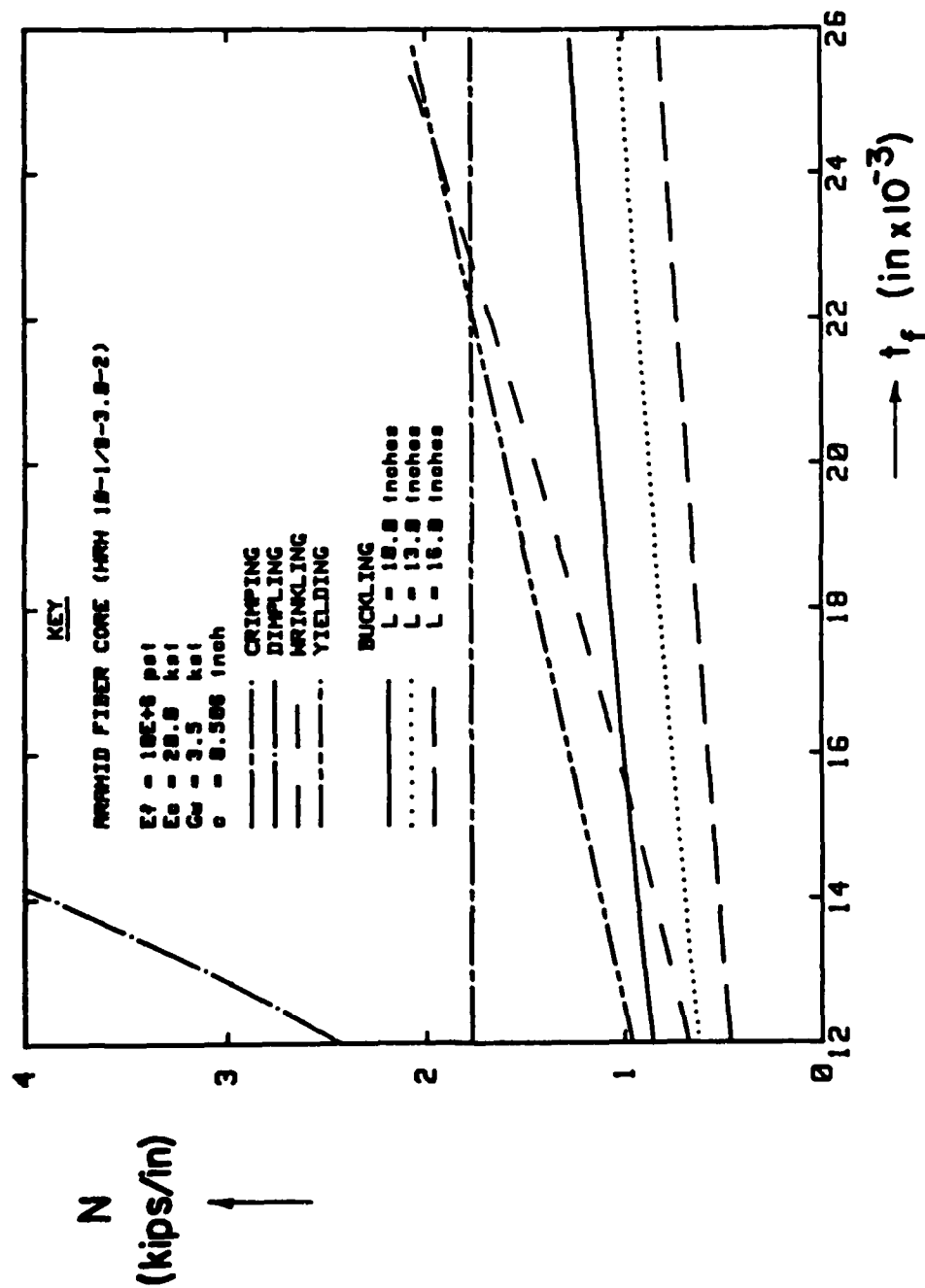
FIG 2.9 FAILURE CRITERIA PLOT: c = 0.506 IN. (3 BEAM LENGTHS)

END VIEW

1.5"

0.25"

0.1875"R

0.125" t

1.75"

0.75"

C

1x14x1 Tap

0.25"

0.5"

TOP VIEW

SIDE VIEW

1.5"

0.25"

Loading
Block

End
Fixture

3"

4"
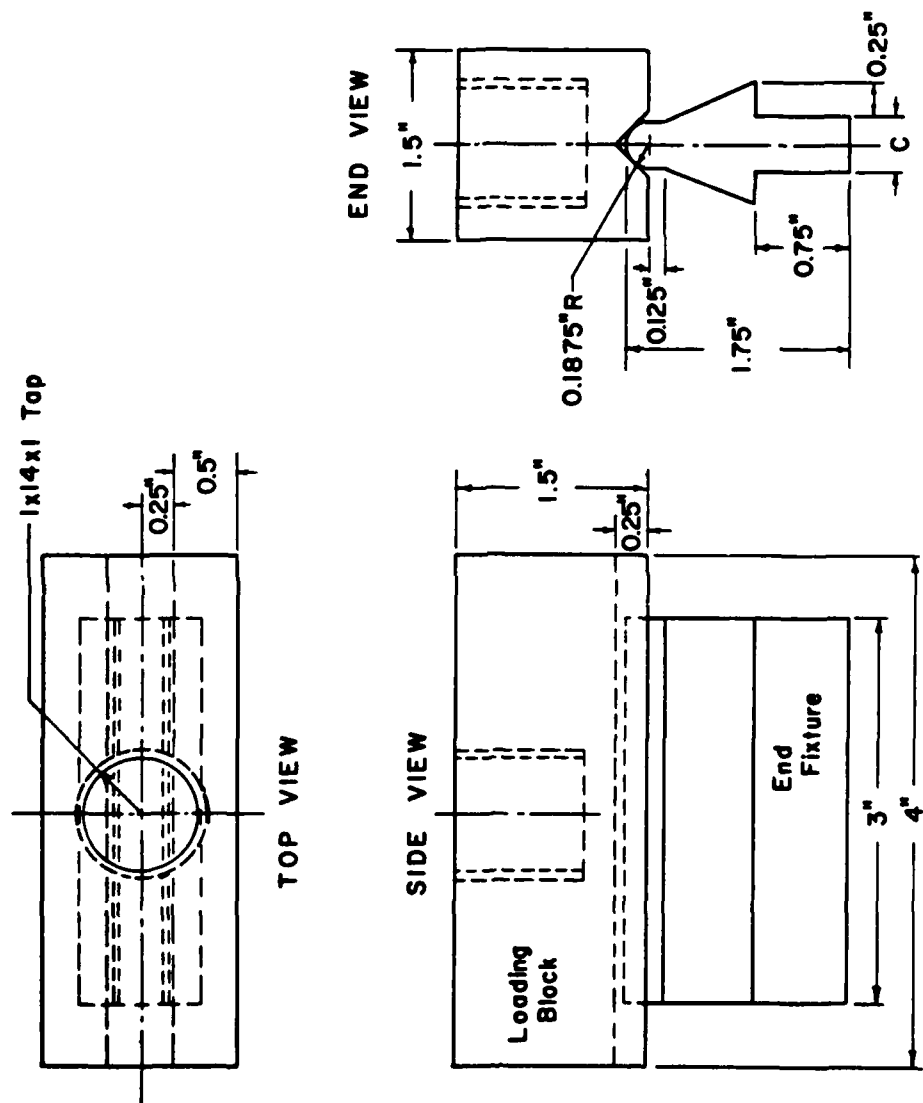
FIG 2.10 MECHANICAL DRAWING OF SIMPLE-SUPPORT END FIXTURES
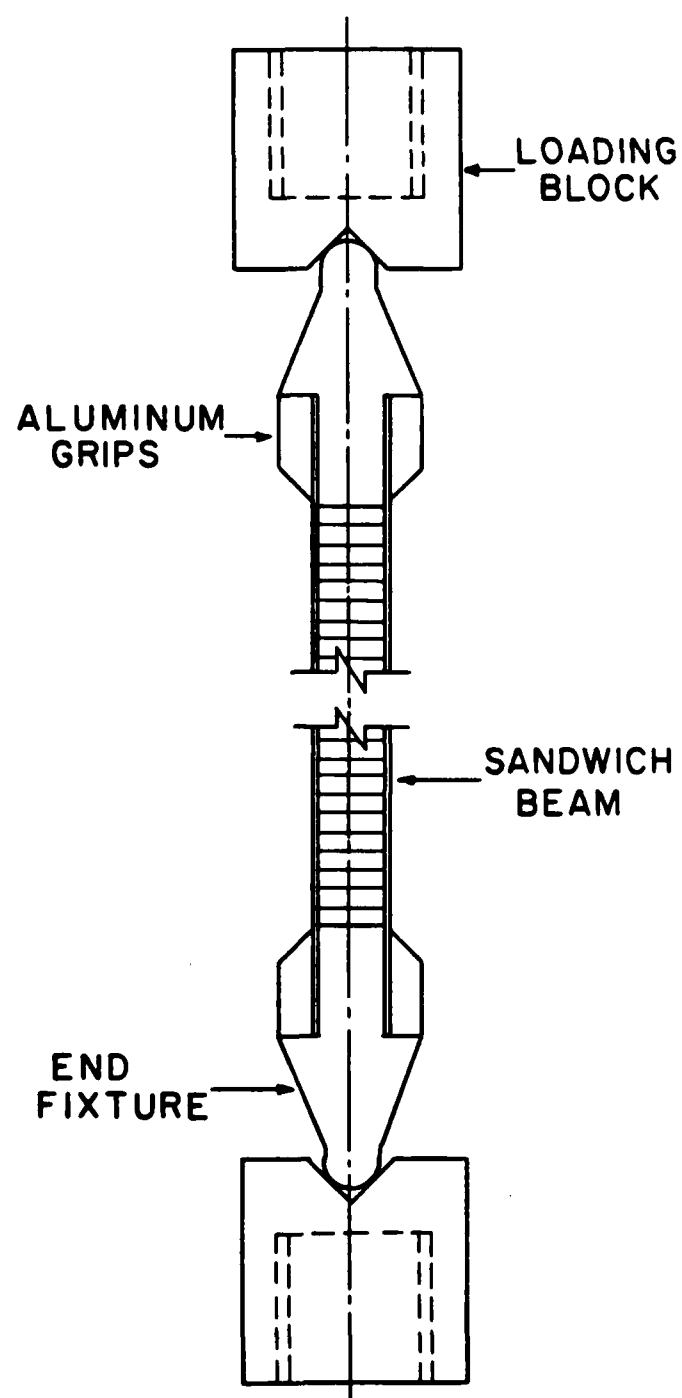
FIG 2.11 SCHEMATIC OF SPECIMEN AND END FIXTURE ASSEMBLY
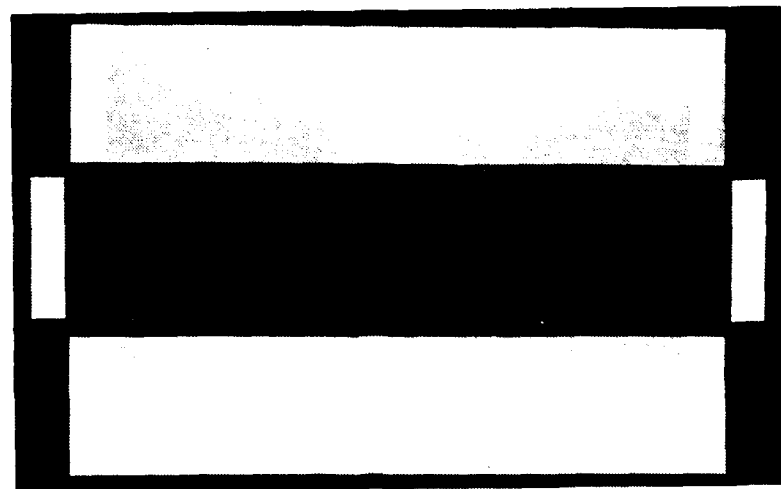
FIG 2.12   SPECIMEN COMPONENTS PRIOR TO ASSEMBLY

Thermocouple

Temperature

Controller

Platen

Specimen

Hydraulic Actuator
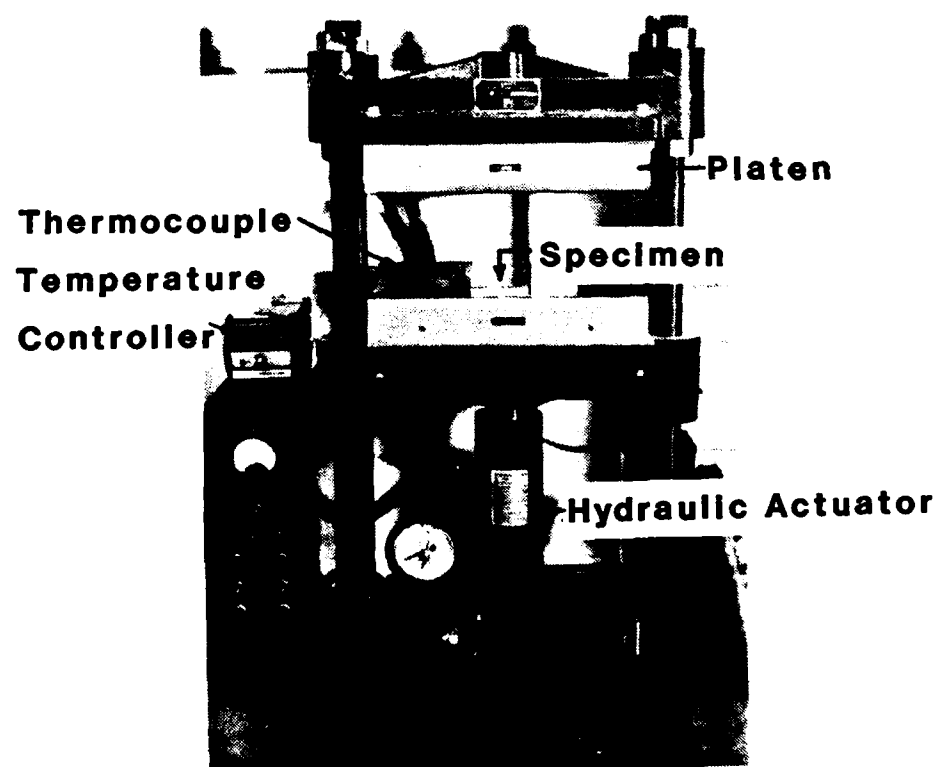
FIG 2.13   HEATED PLATEN PRESS USED FOR
CURING THE SANDWICH STRUCTURE
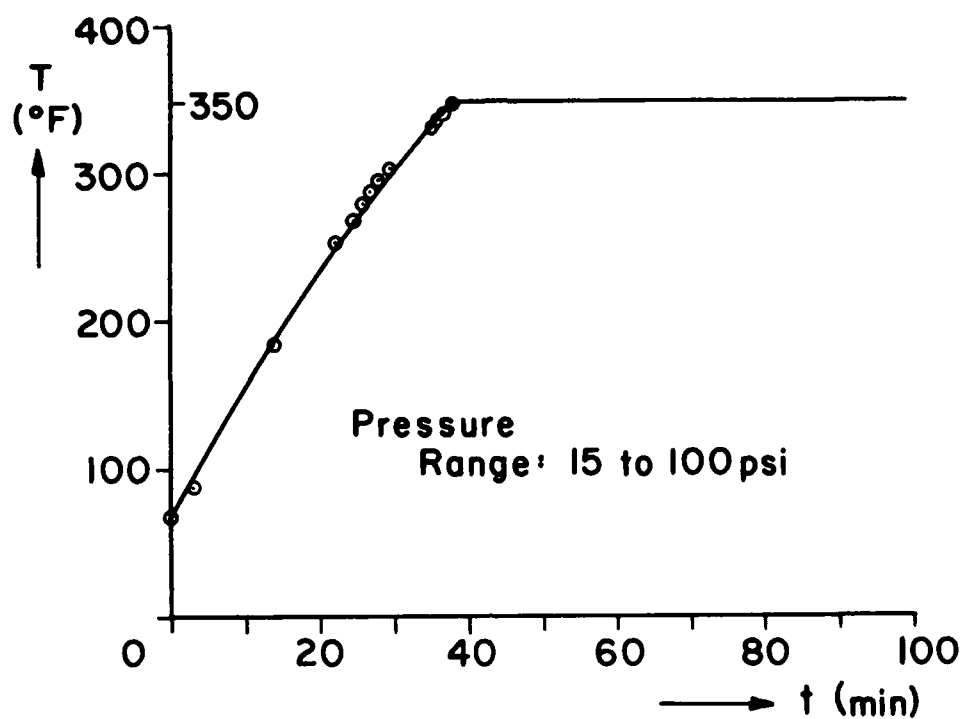
FIG 2.14 ADHESIVE TEMPERATURE CURING CYCLE

FIG 2.15 CURED SPECIMEN PRIOR TO ATTACHMENT
OF END FIXTURES
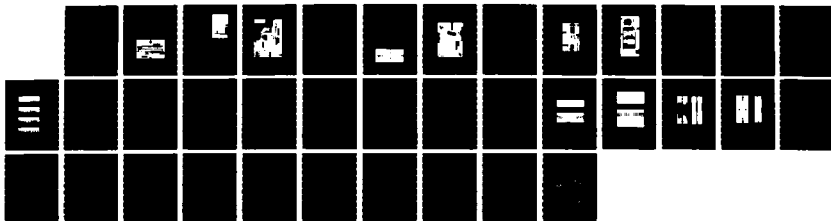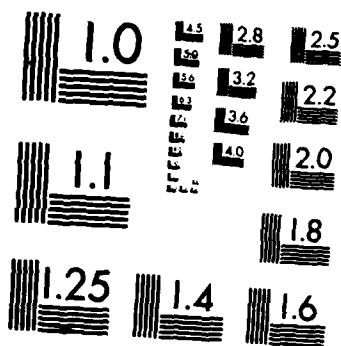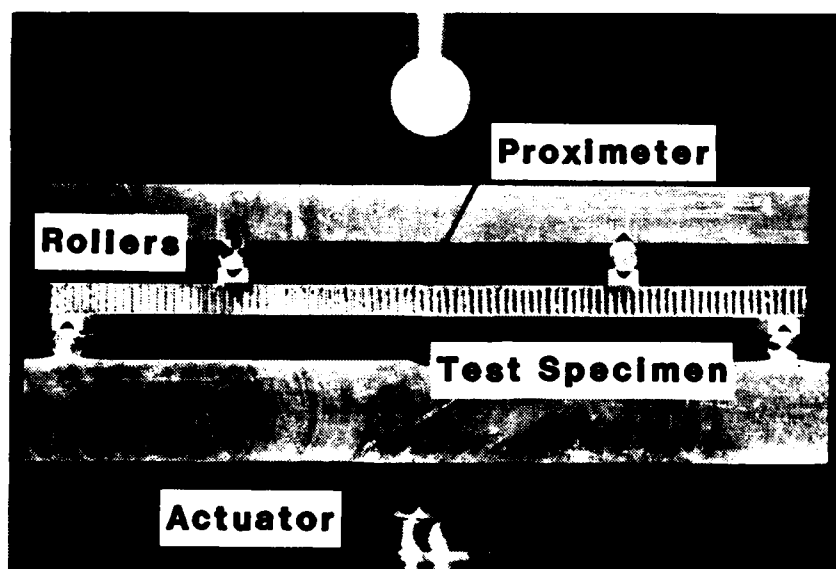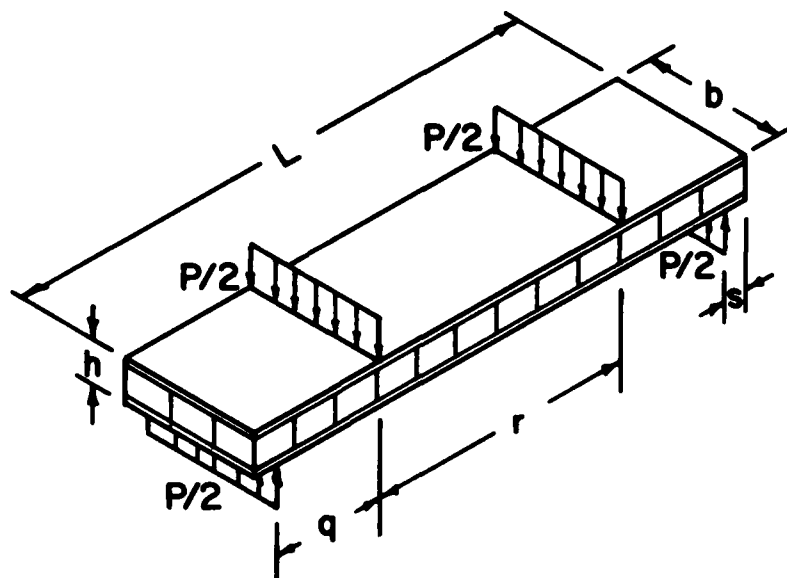
FIG 2.16   SANDWICH BEAM FOUR-POINT BENDING
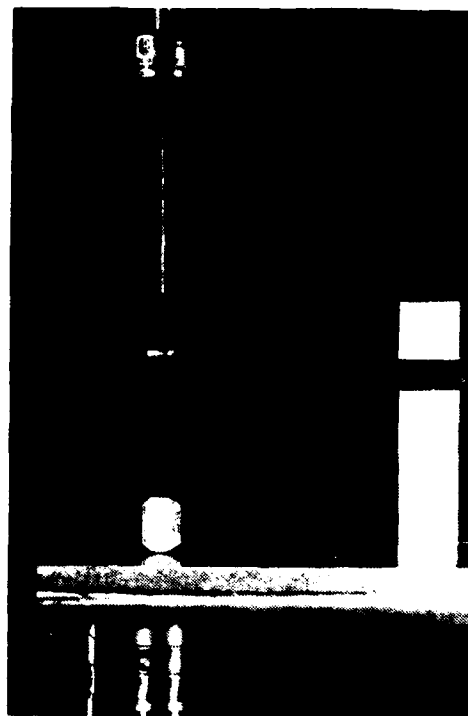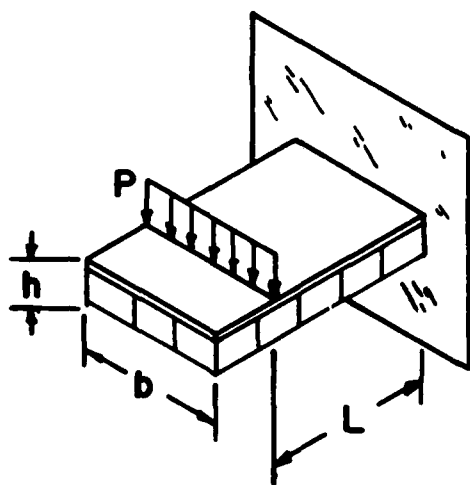
FIG 2.17   SANDWICH BEAM CANTILEVER BENDING
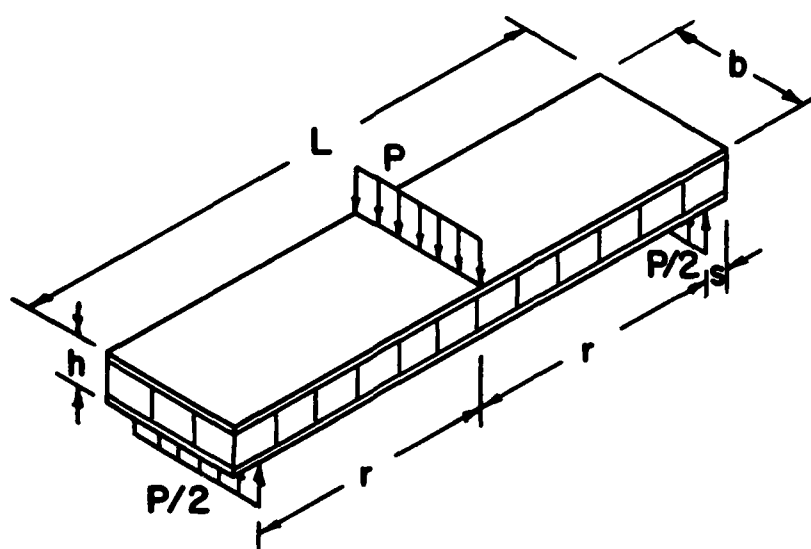
FIG 2.18   THREE-POINT BENDING SCHEMATIC
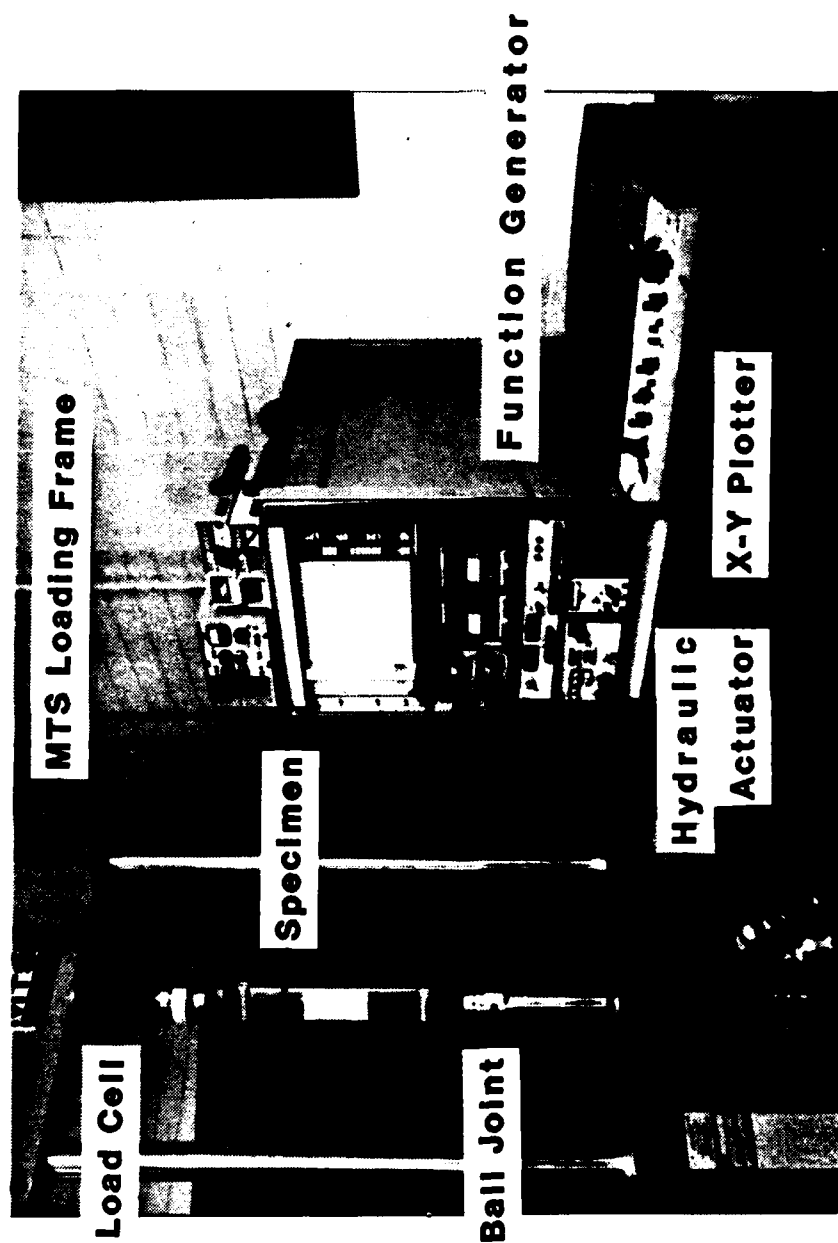
FIG 2.19 MTS EQUIPMENT ARRANGEMENT
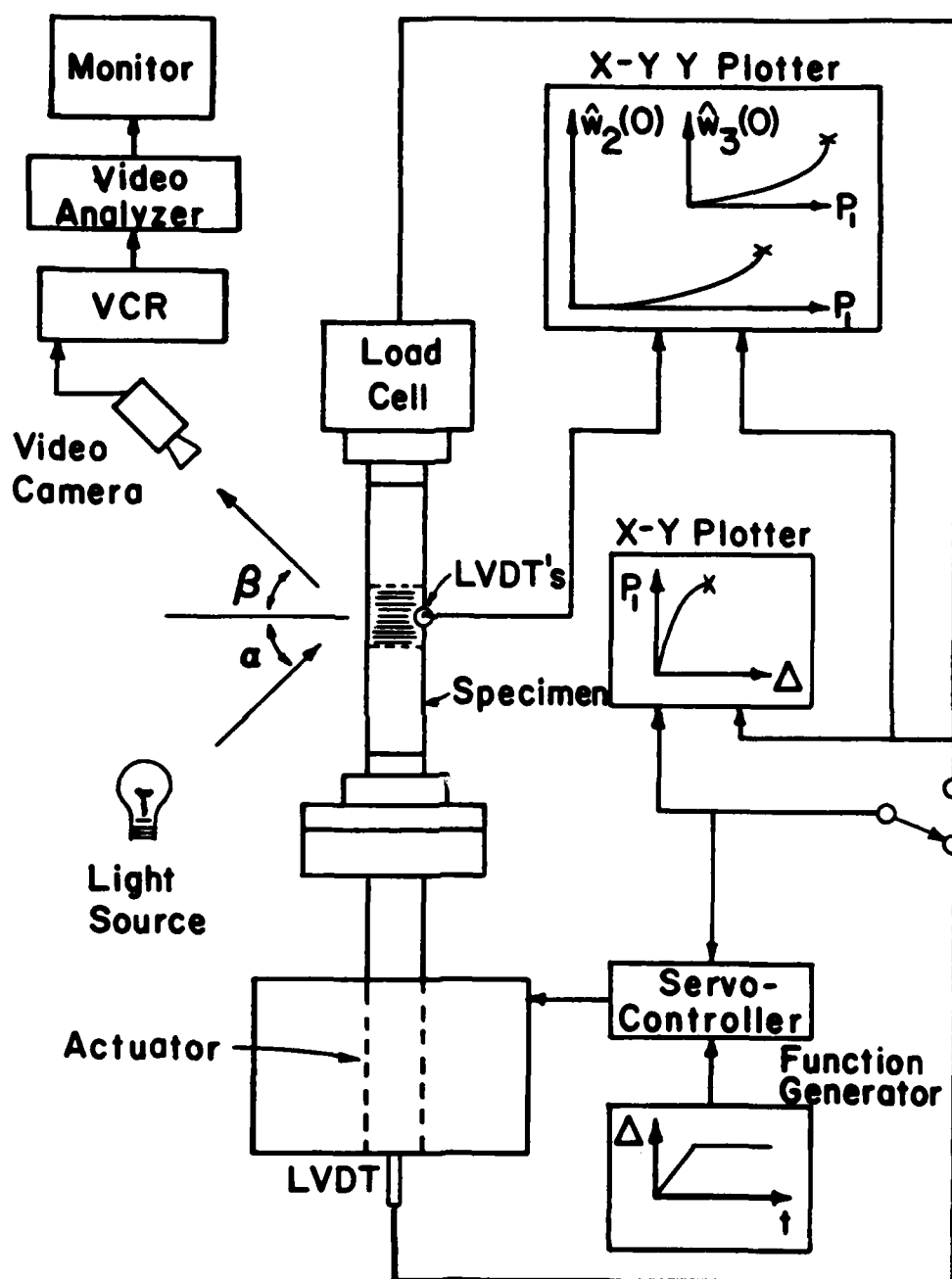
FIG 2.20 EXPERIMENTAL EQUIPMENT &
DATA RECORDING SCHEMATIC
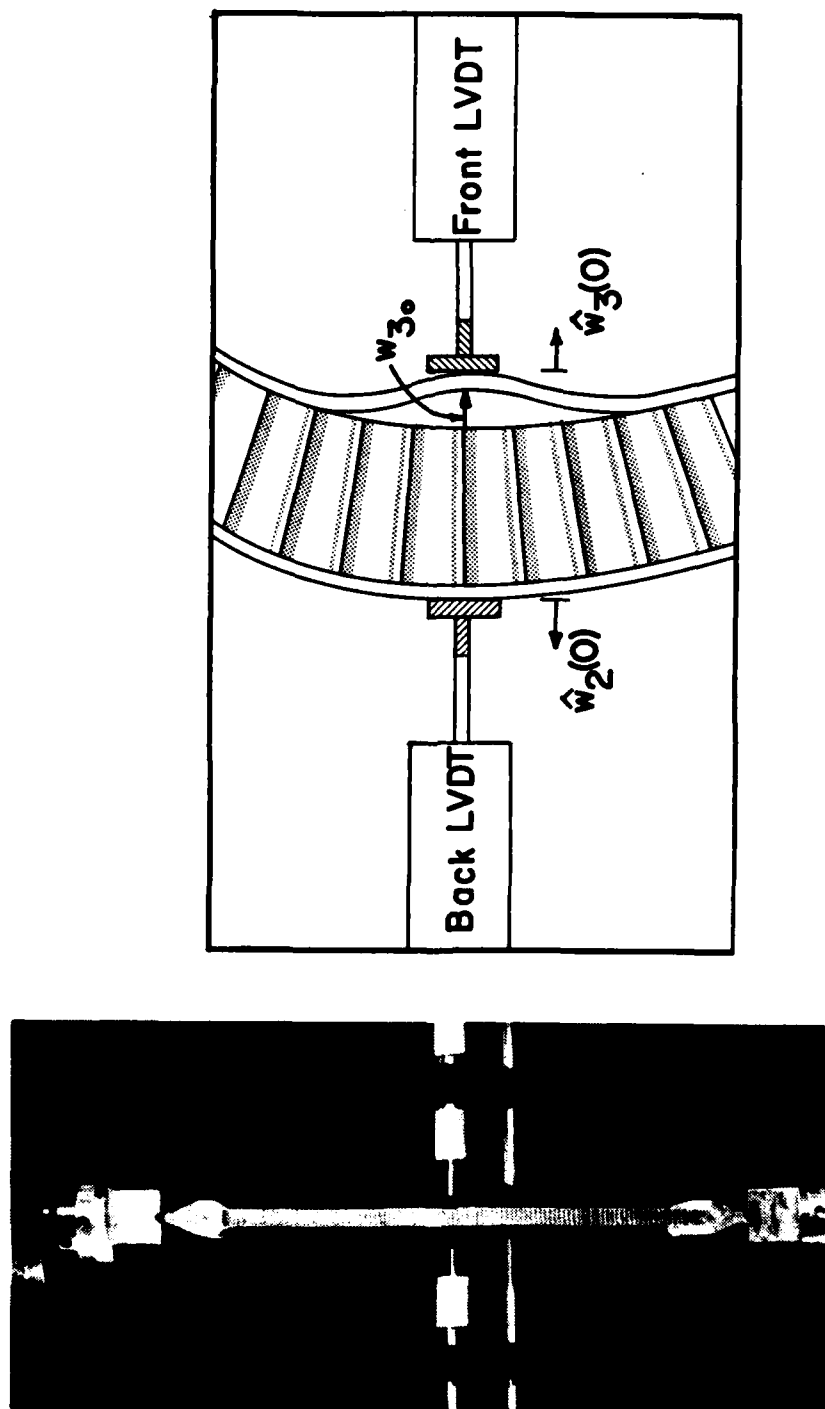
FIG 2.21 ARRANGEMENT OF THE LVDT DISPLACEMENT TRANSDUCERS
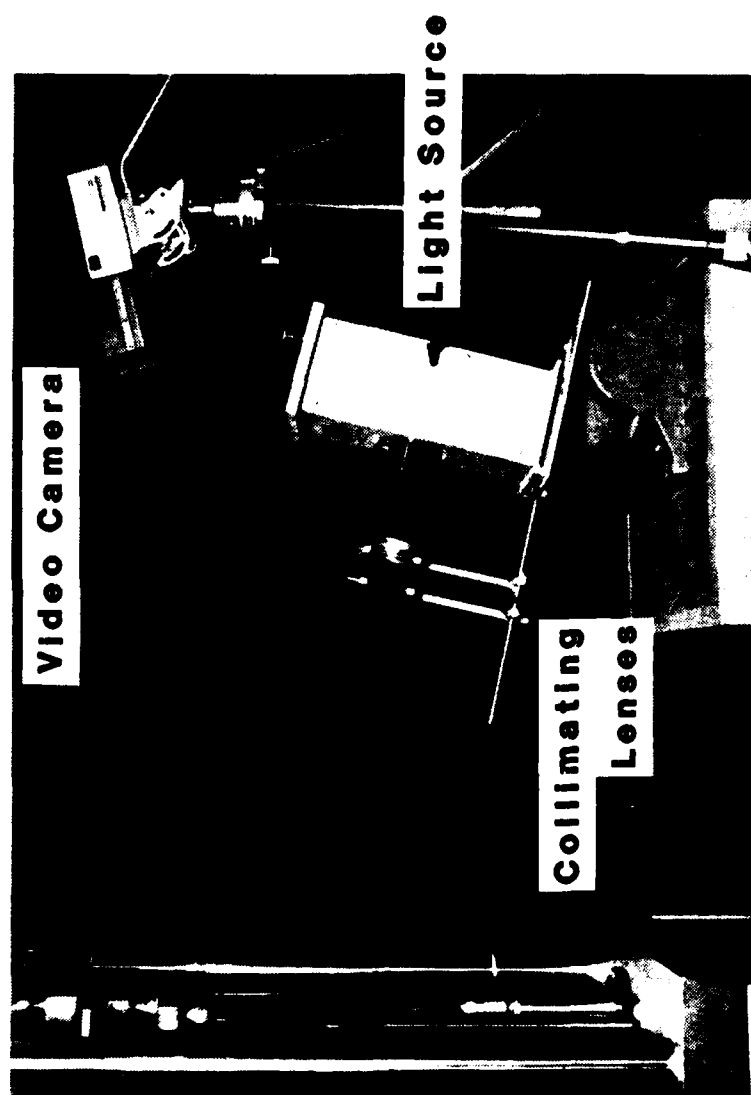
FIG 2.22 MOIRE EQUIPMENT ARRANGEMENT
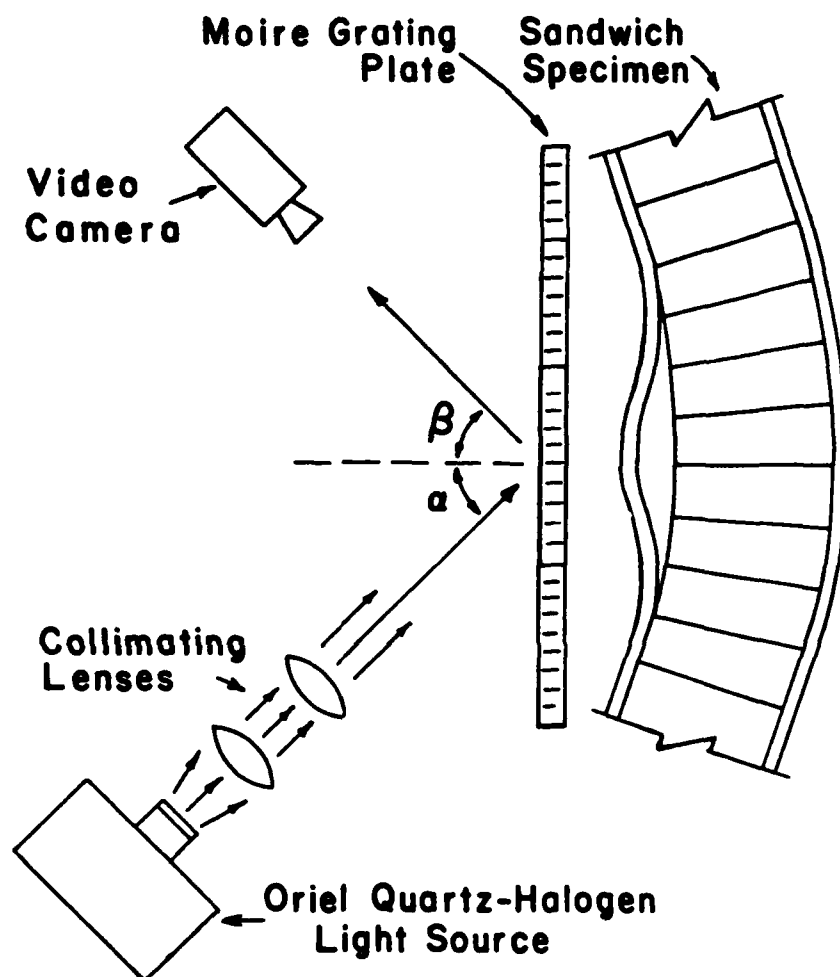
FIG 2.23 SHADOW MOIRE SCHEMATIC
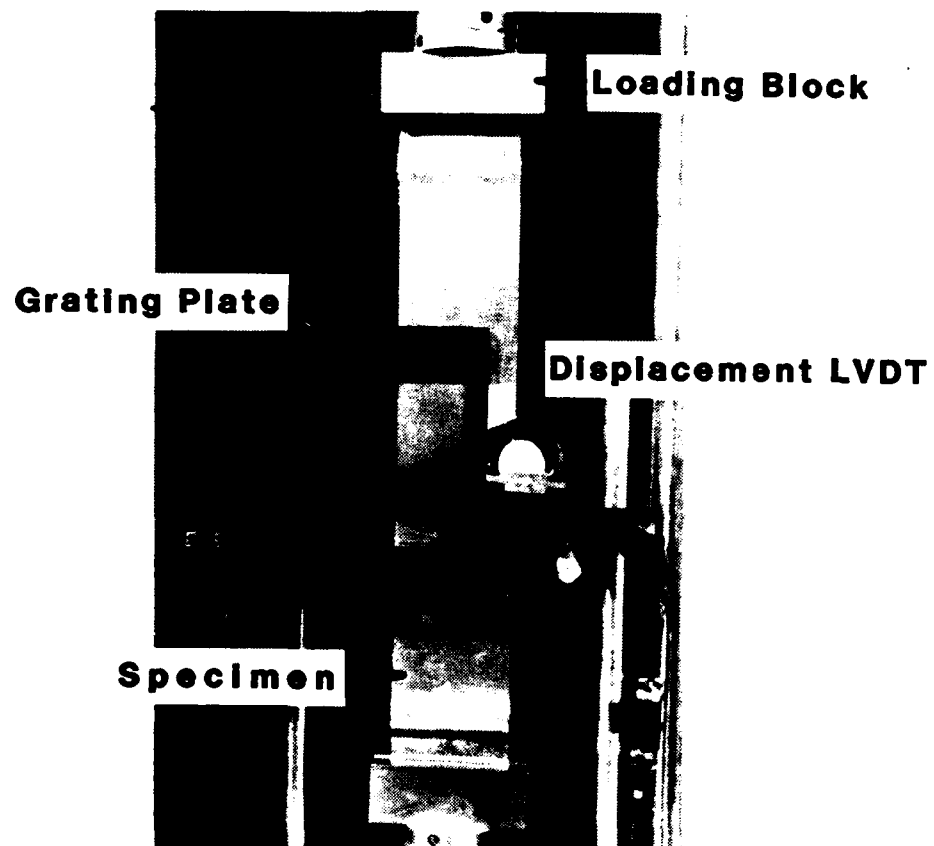
FIG 2.24   ARRANGEMENT OF THE MOIRE GRATING PLATE

Monitor

Video Analyzer

X-Y Y Plotter

Video Cassette
Recorder
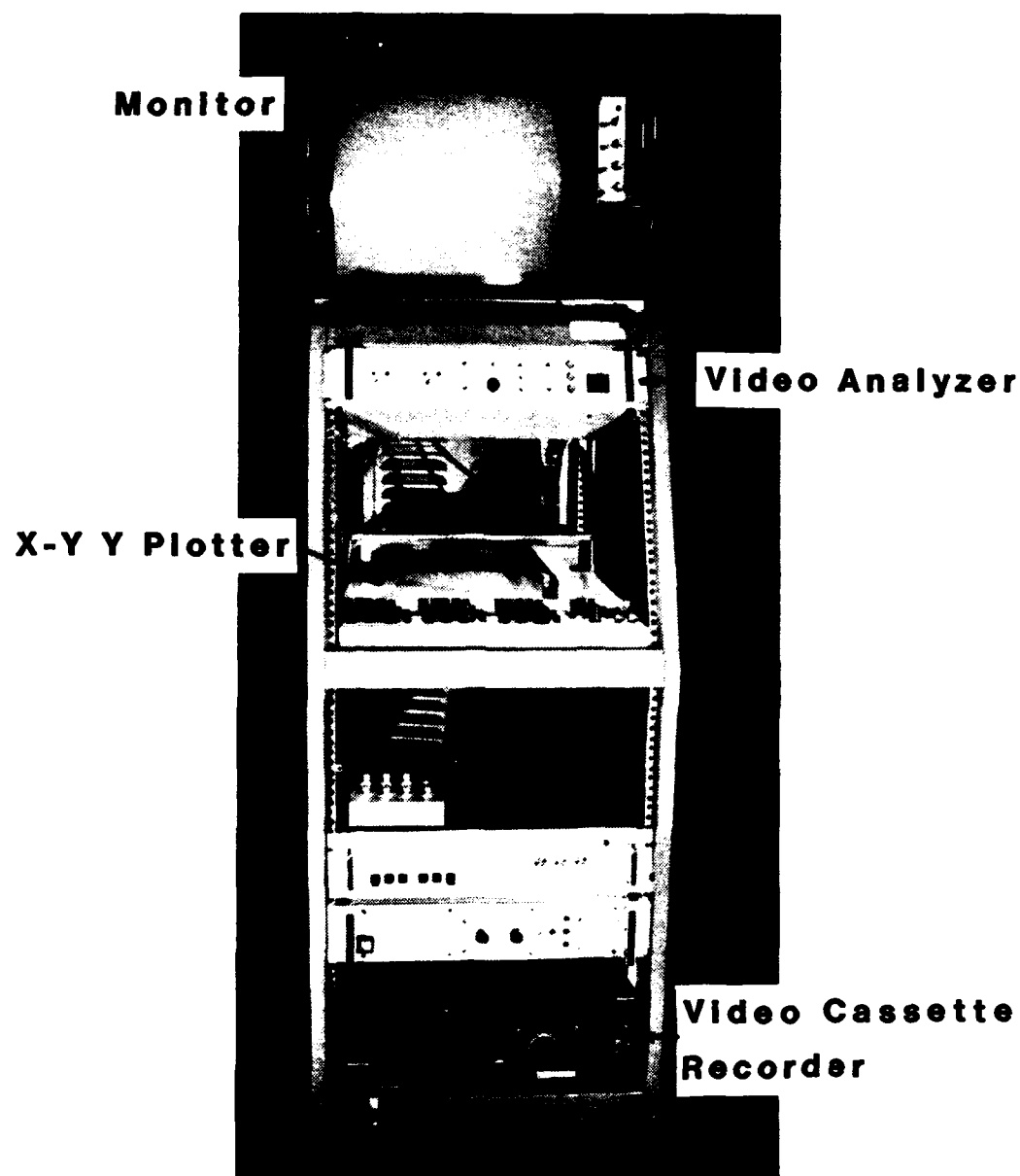
FIG 2.25 VIDEO RECORDING AND ANALYZING APPARATUS
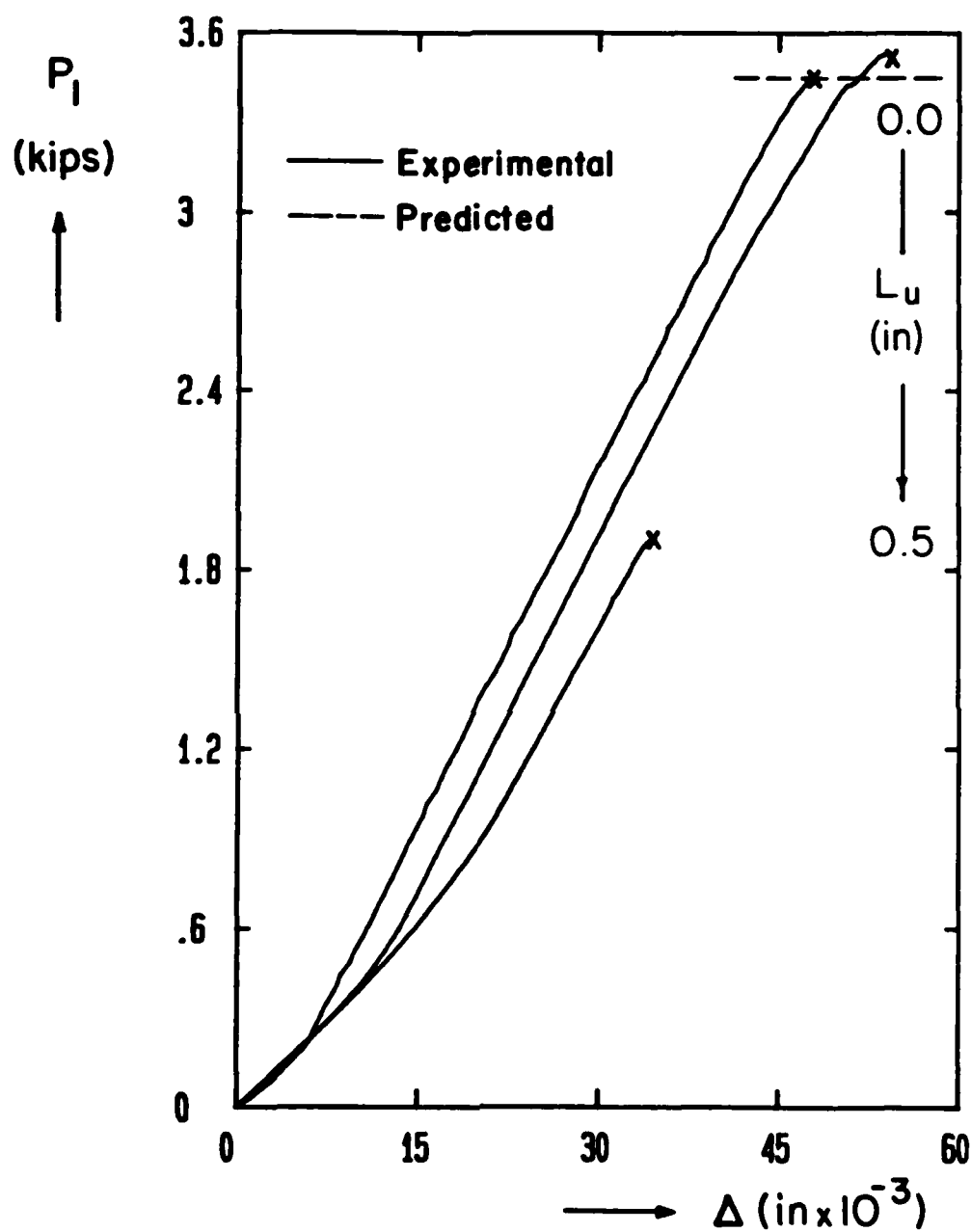
FIG 3.1 LOAD VERSUS AXIAL DISPLACEMENT
(L_u FROM 0.0 to 0.5 IN.)
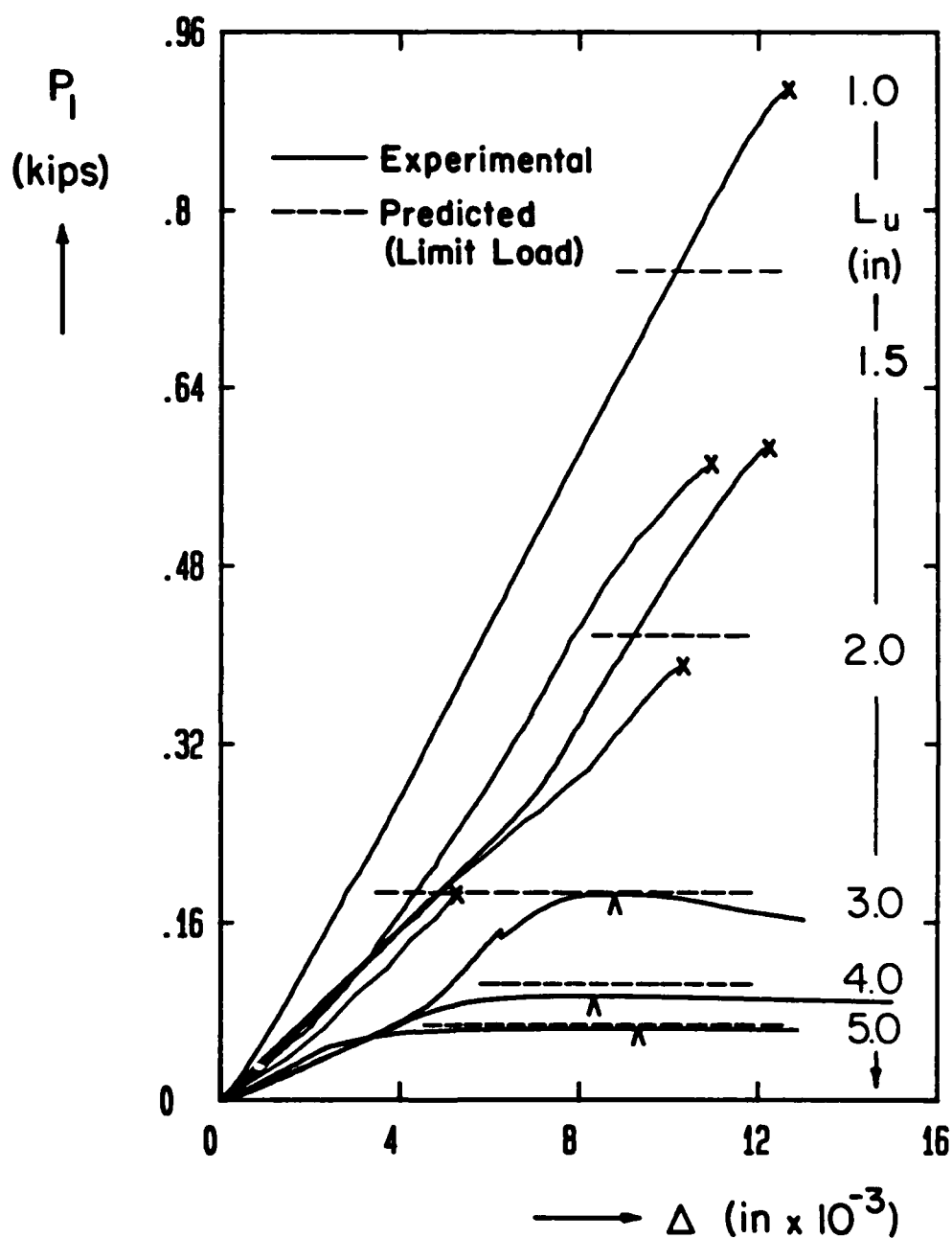
FIG 3.2 LOAD VERSUS AXIAL DISPLACEMENT
(L_u FROM 1.0 TO 5.0 IN.)
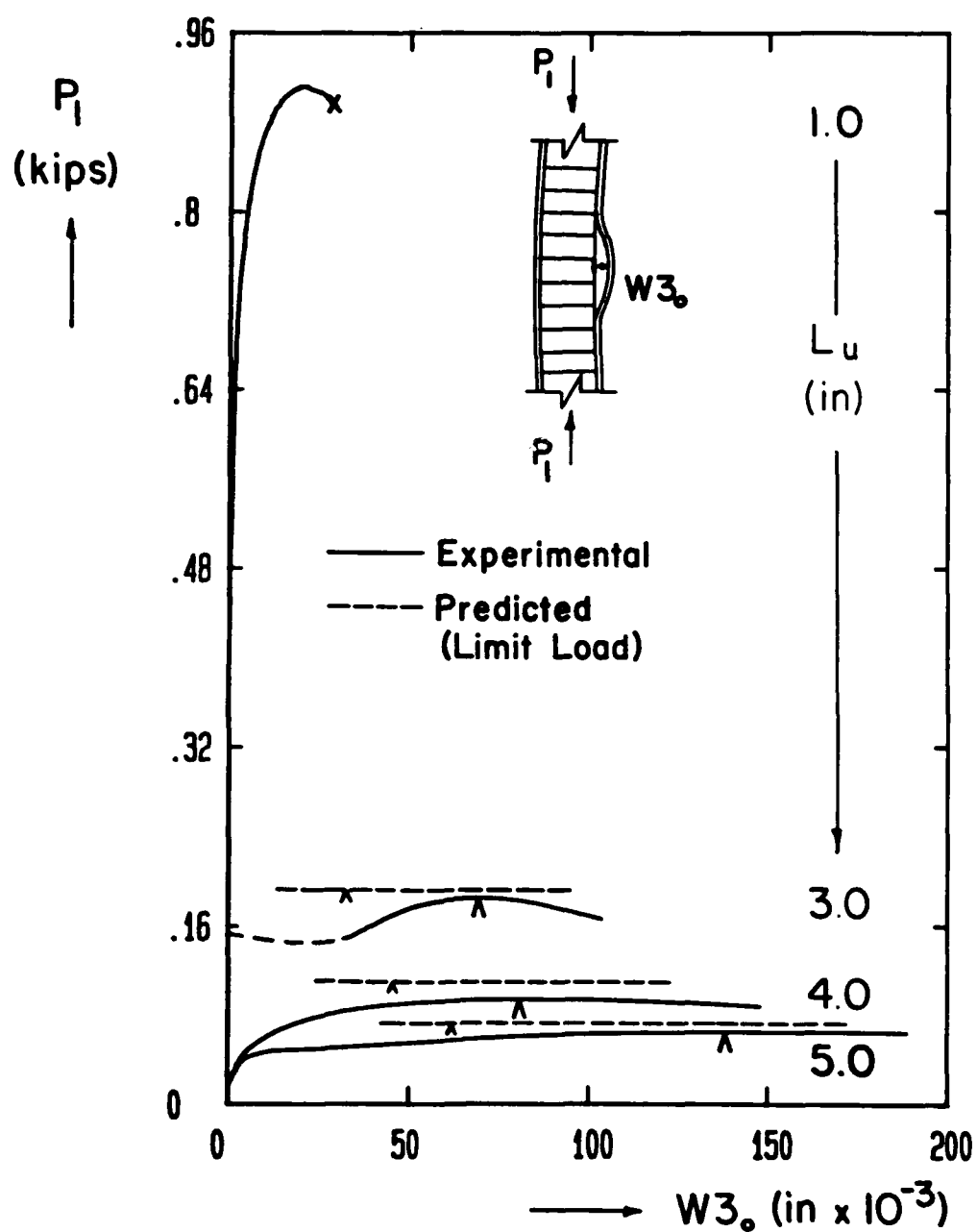
FIG 3.3 LOAD VERSUS $W3_0$ DISPLACEMENT

95
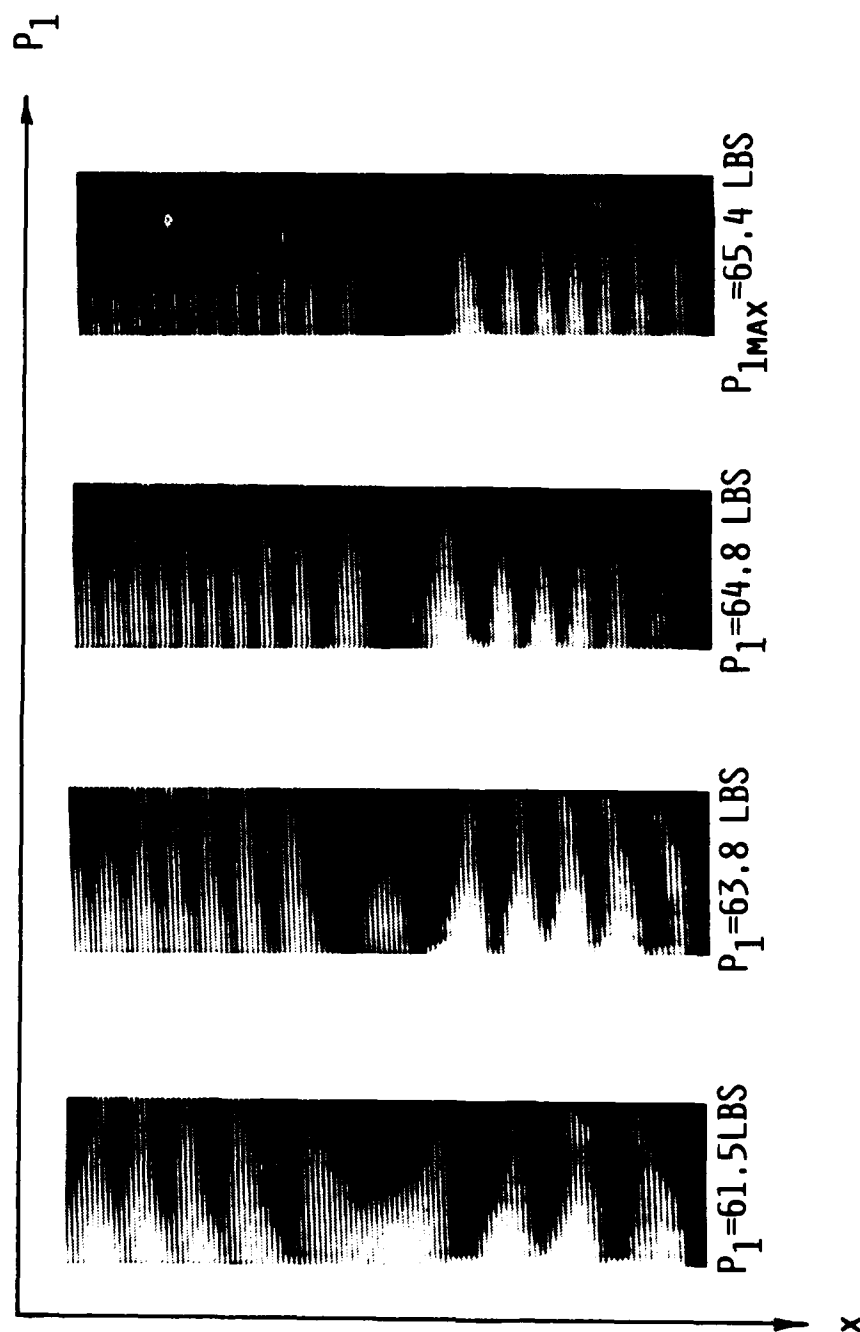
FIG 3.4 FRINGE PATTERNS OF AN UNBONDED FACEPLATE
AT DIFFERENCE LOADS (L_u = 5.0 IN.)
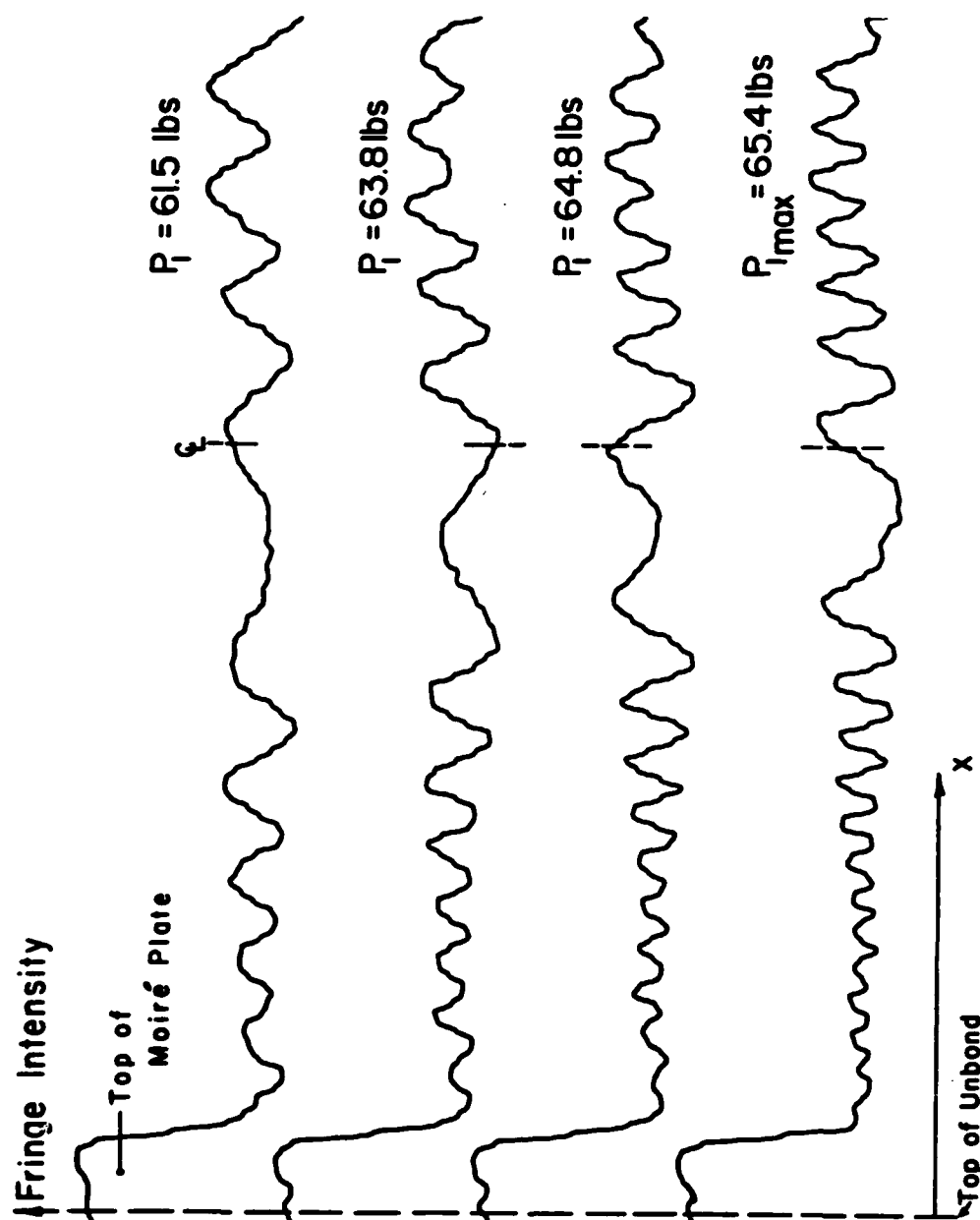
FIG 3.5 LIGHT INTENSITY VERSUS SCAN DISPLACEMENT
FOR FRINGE PATTERNS SHOWN IN FIG 3.4
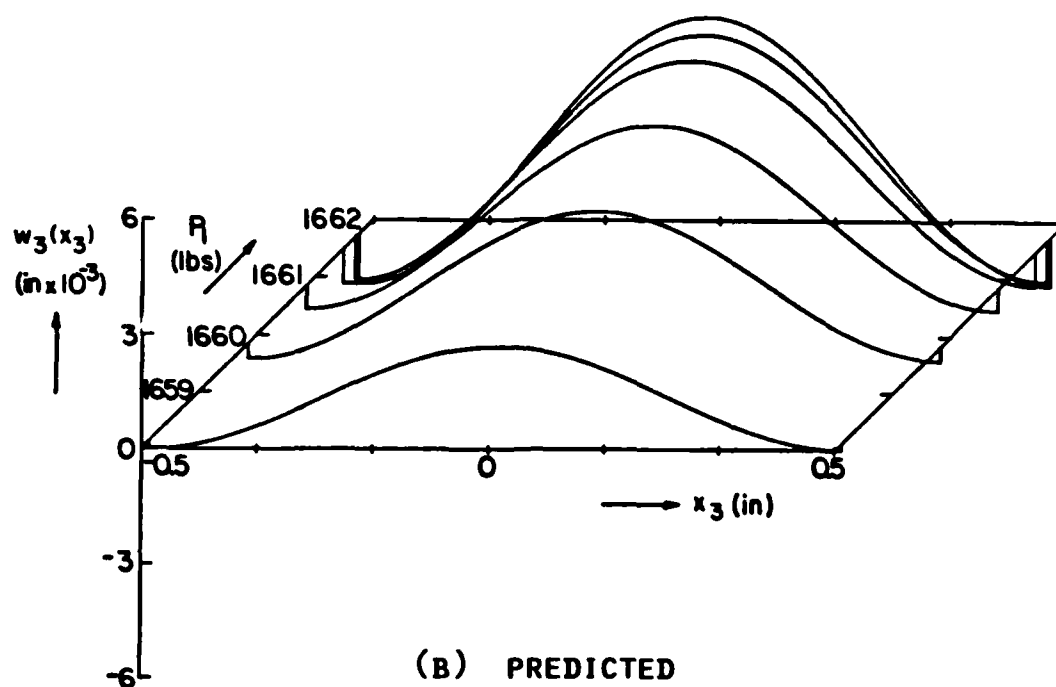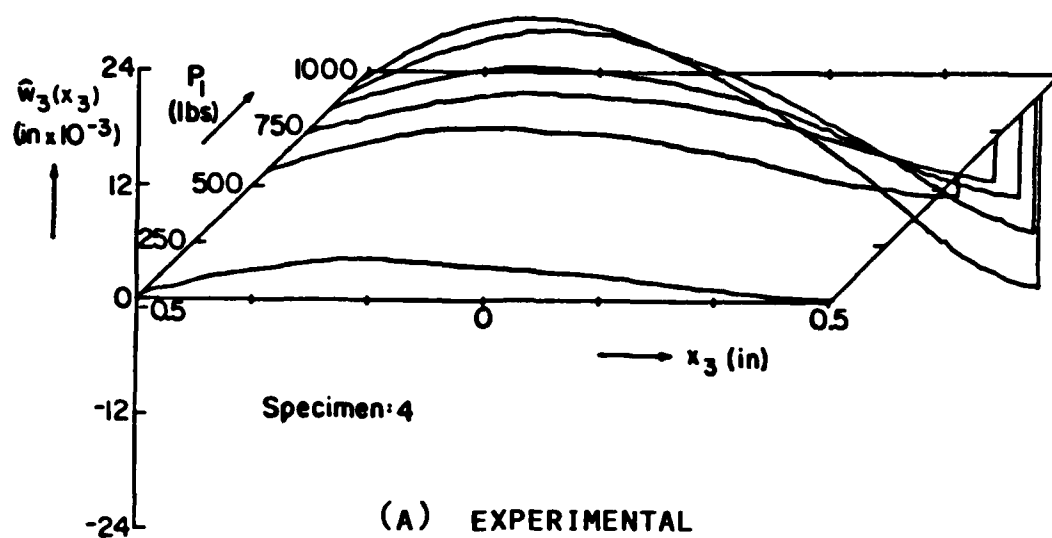
FIG 3.6 UNBOND FACEPLATE OUT-OF-PLANE DEFLECTION SHAPES VERSUS AXIAL LOAD ($L_U = 1.0$ IN.)
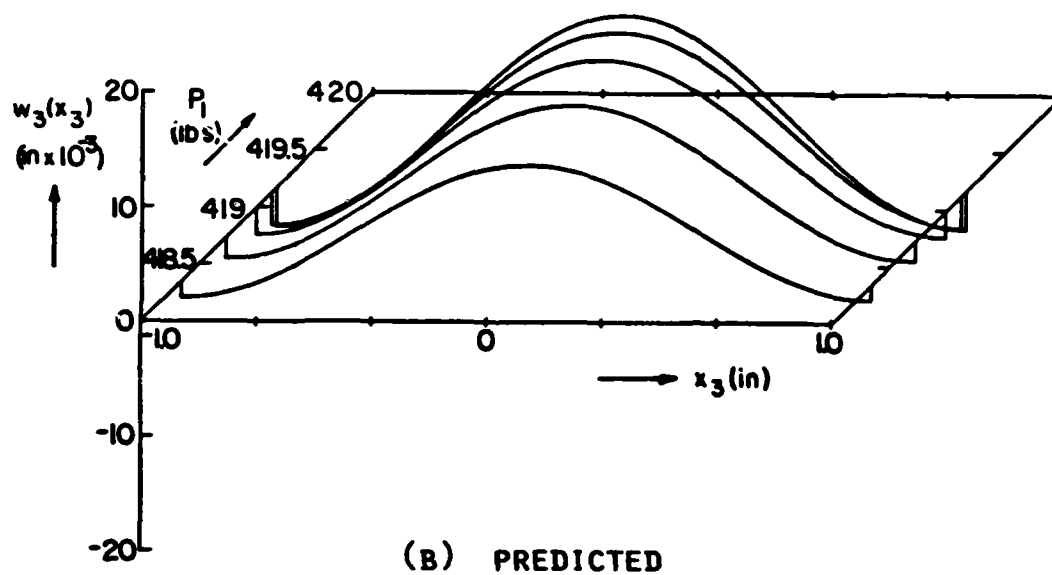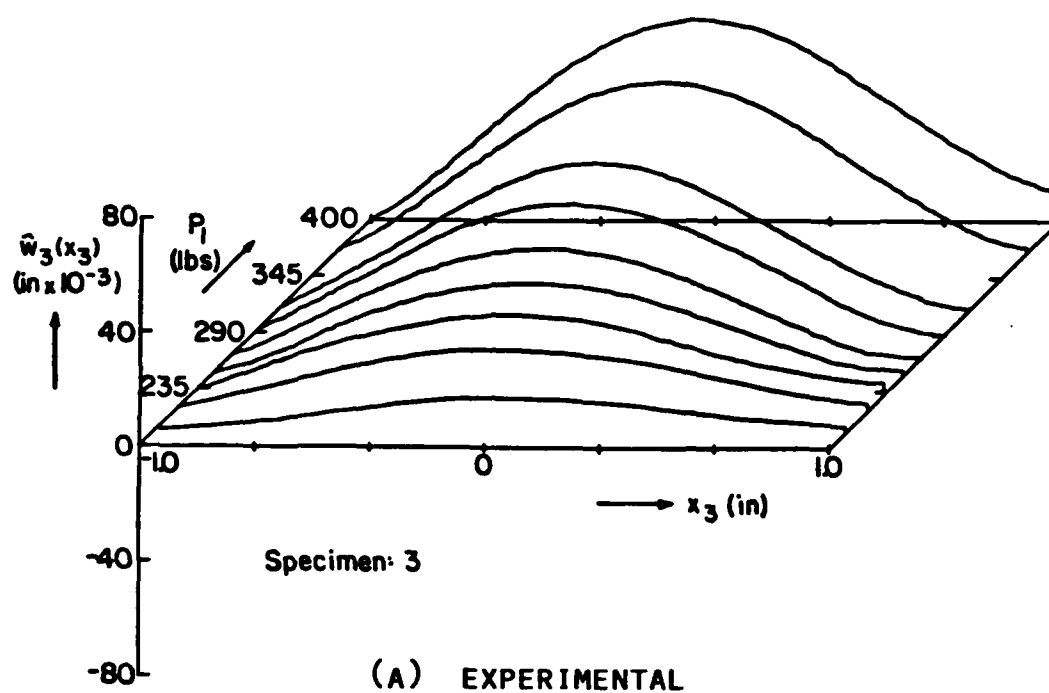
FIG 3.7 UNBOND FACEPLATE OUT-OF-PLANE
DEFLECTION SHAPES VERSUS AXIAL LOAD
$(L_U = 2.0 \text{ IN.})$
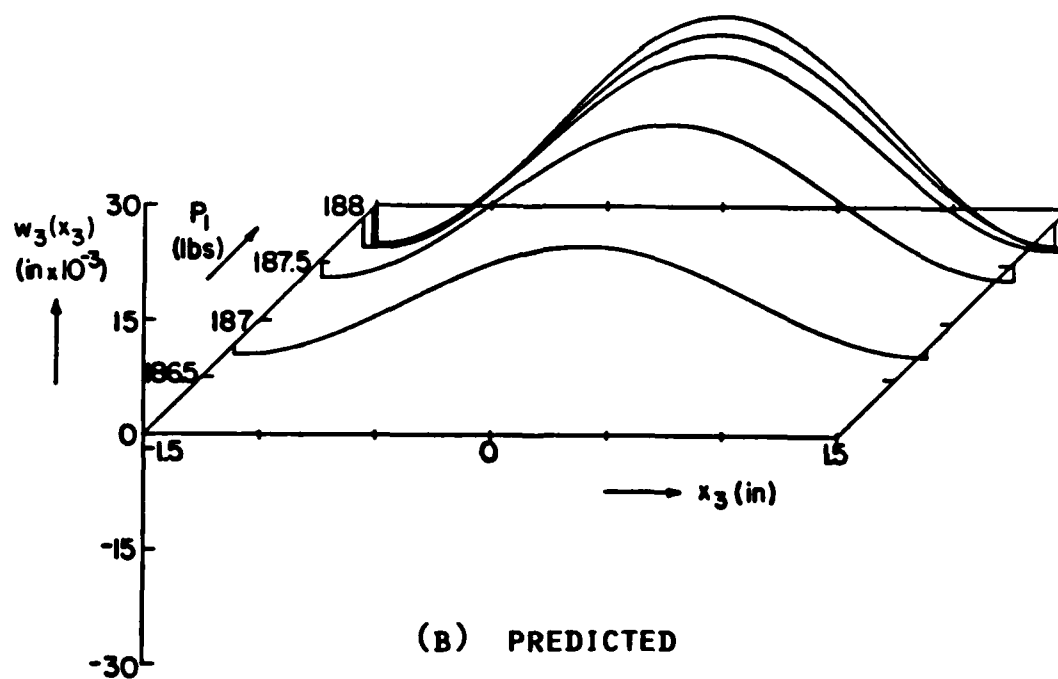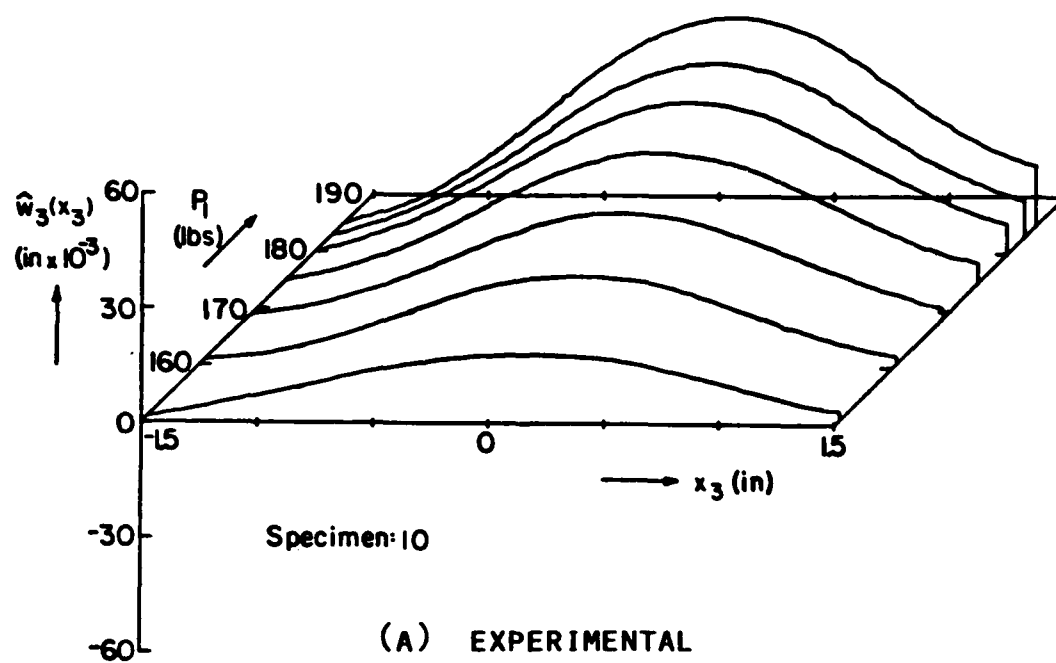
FIG 3.8 UNBOND FACEPLATE OUT-OF-PLANE
DEFLECTION SHAPES VERSUS AXIAL LOAD
(L_U = 3.0 IN.)

(A) EXPERIMENTAL

(B) PREDICTED
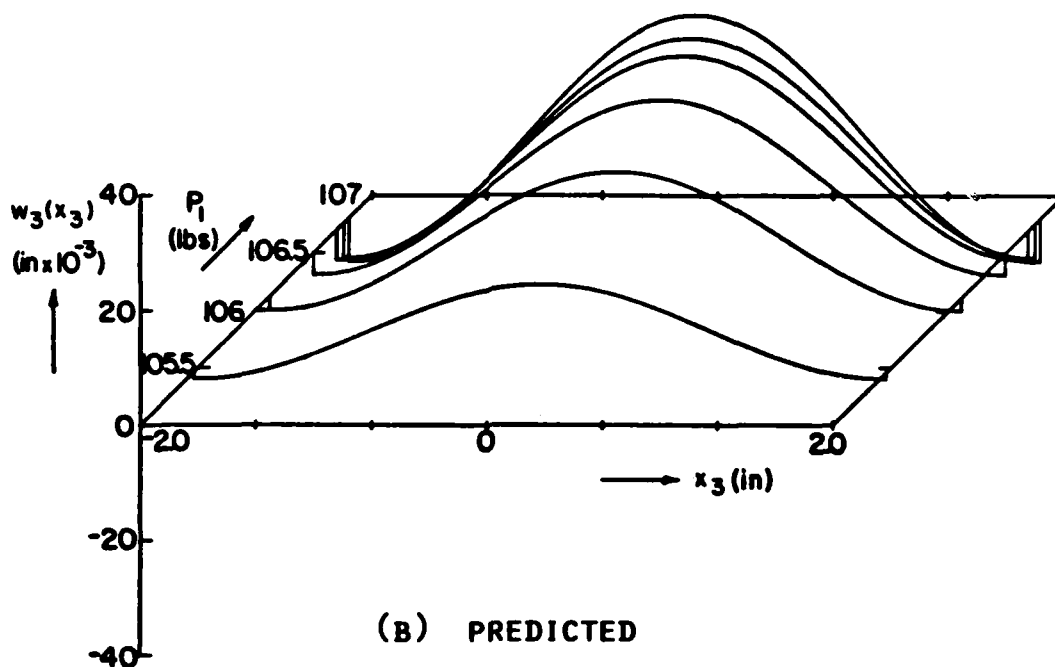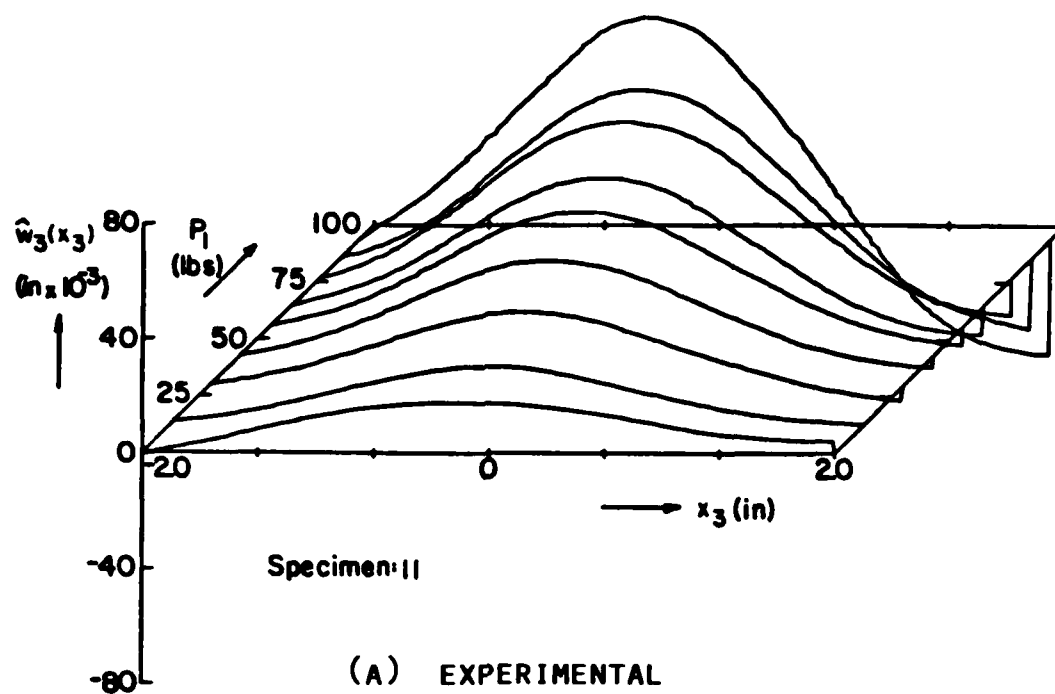
FIG 3.9 UNBOND FACEPLATE OUT-OF-PLANE
DEFLECTION SHAPES VERSUS AXIAL LOAD
(L_U = 4.0 IN.)

(A) EXPERIMENTAL

(B) PREDICTED
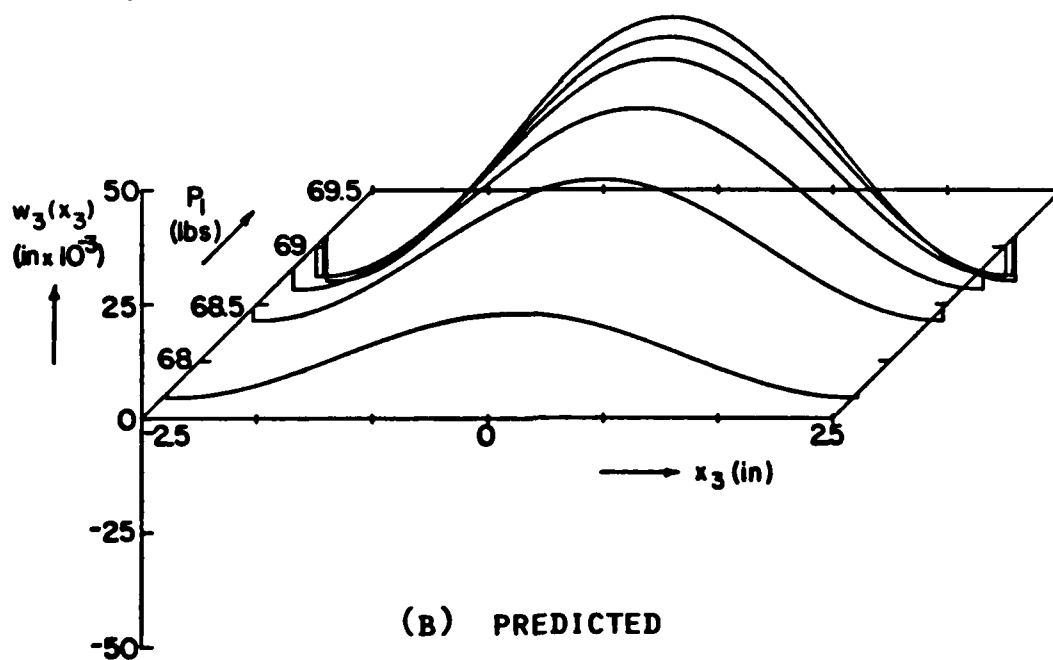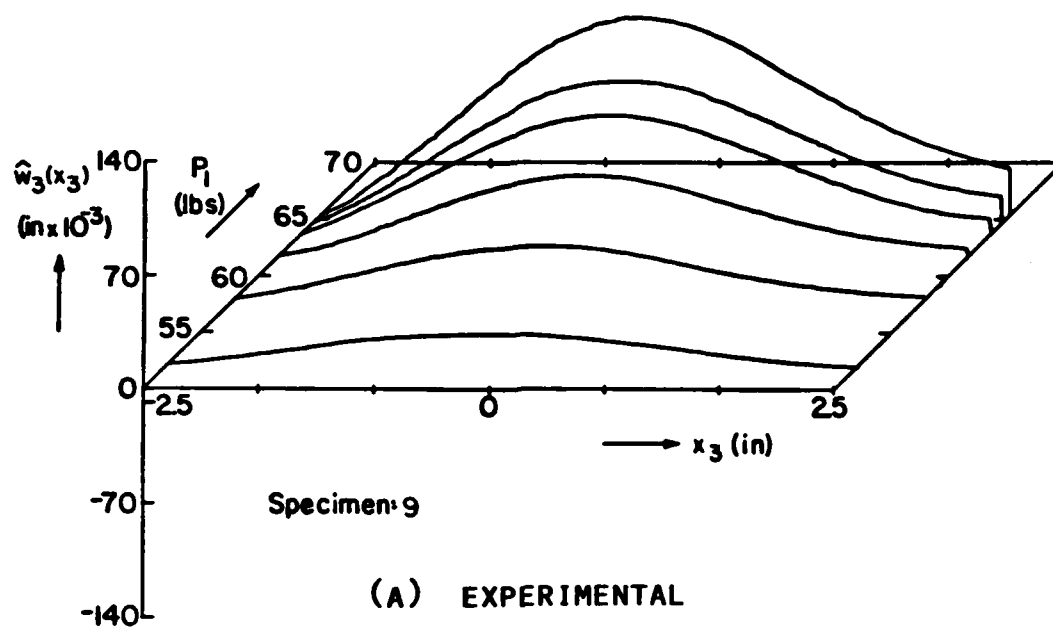
FIG 3.10 UNBOND FACEPLATE OUT-OF-PLANE
DEFLECTION SHAPES VERSUS AXIAL LOAD
(L_U = 5.0 IN.)
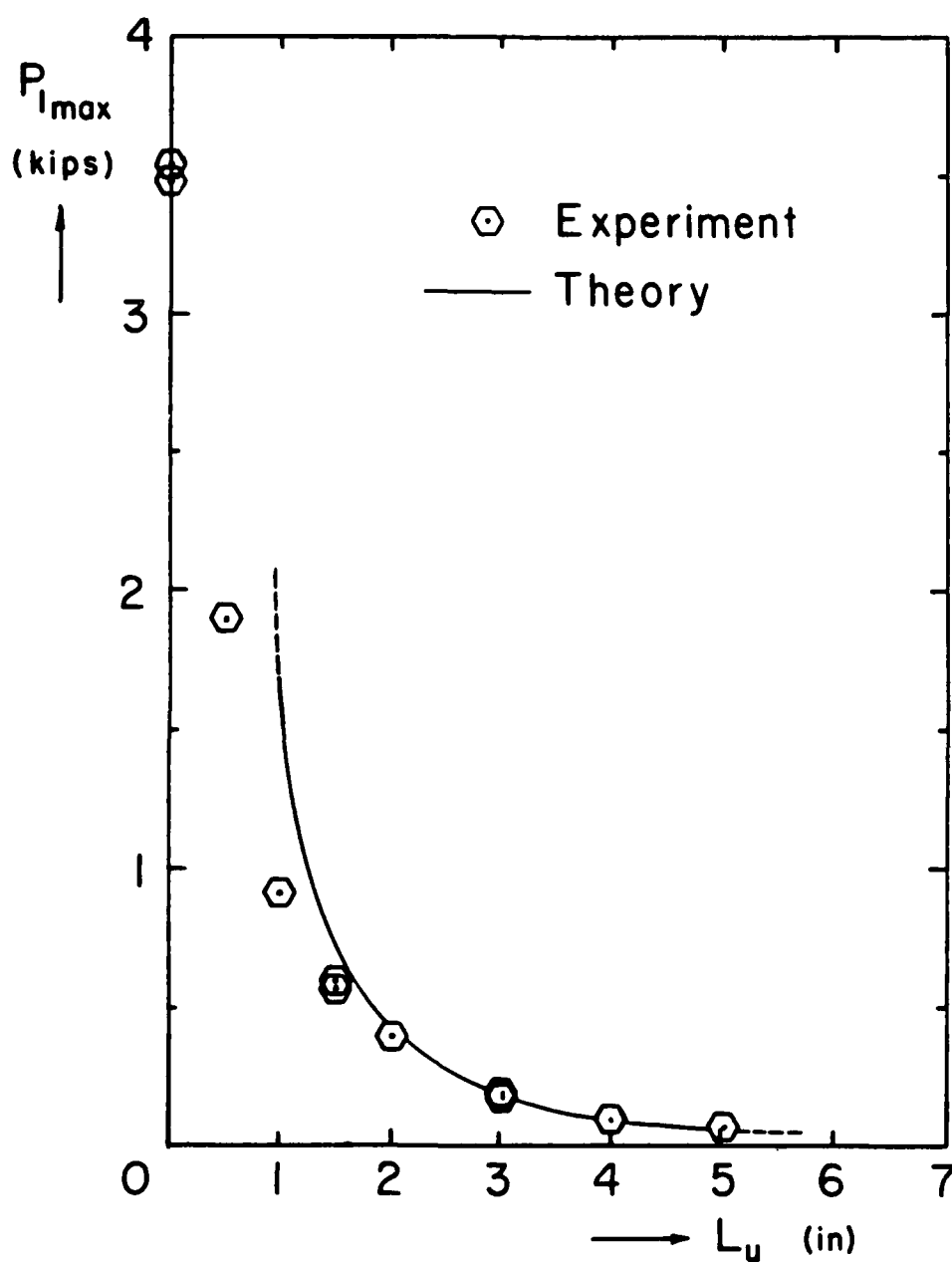
3.11 SANDWICH BEAM MAXIMUM LOADS VERSUS UNBOND LENGTH
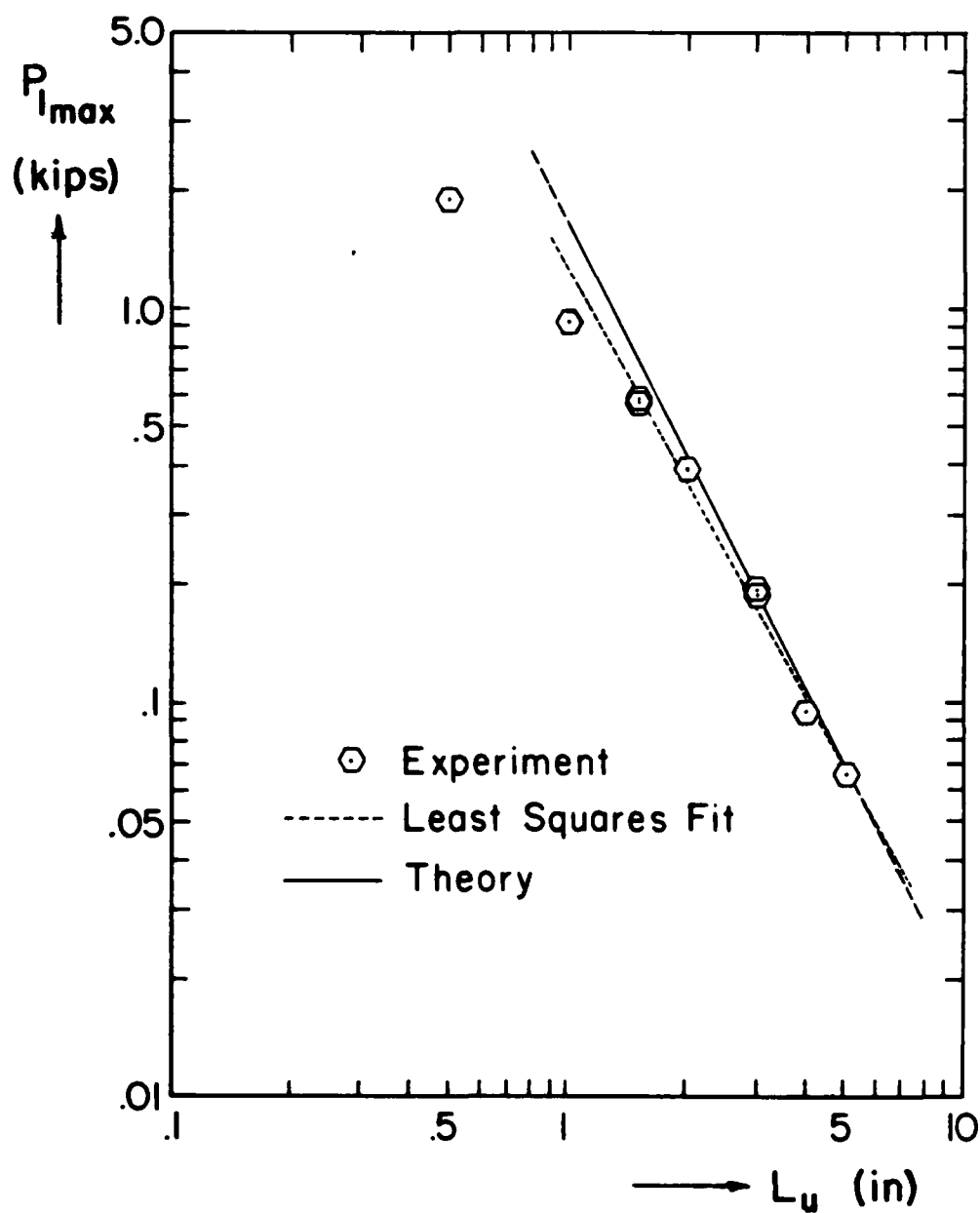
FIG 3.12   LOGORITHMIC PLOT OF MAXIMUM LOADS
VERSUS UNBOND LENGTH

A. OVERALL VIEW

B. CLOSE-UP VIEW OF FAILURE REGION

FIG 3.13 FAILURE OF A FULLY BONDED SPECIMEN
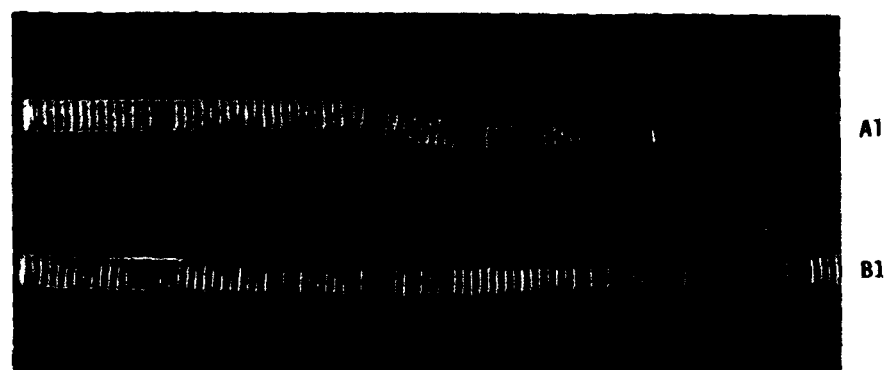
A1: L_u = 3 in.   A2: L_u = 2 in.

A. OVERALL VIEW
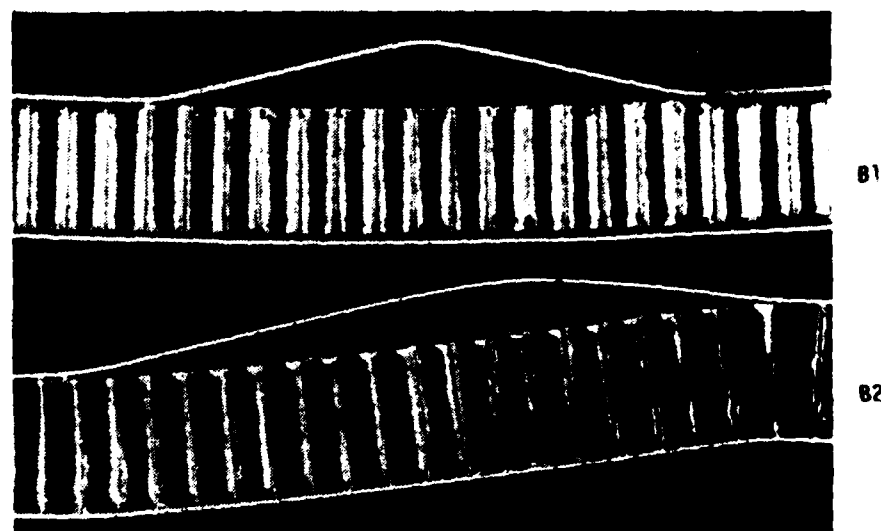
B1: L_u = 2 in.   B2: L_u = 3 in.

B. CLOSE-UP VIEW OF UNBONDED REGION
(OPPOSITE SIDE OF BEAM)

FIG 3.14 FAILURE OF AN UNBONDED SPECIMEN
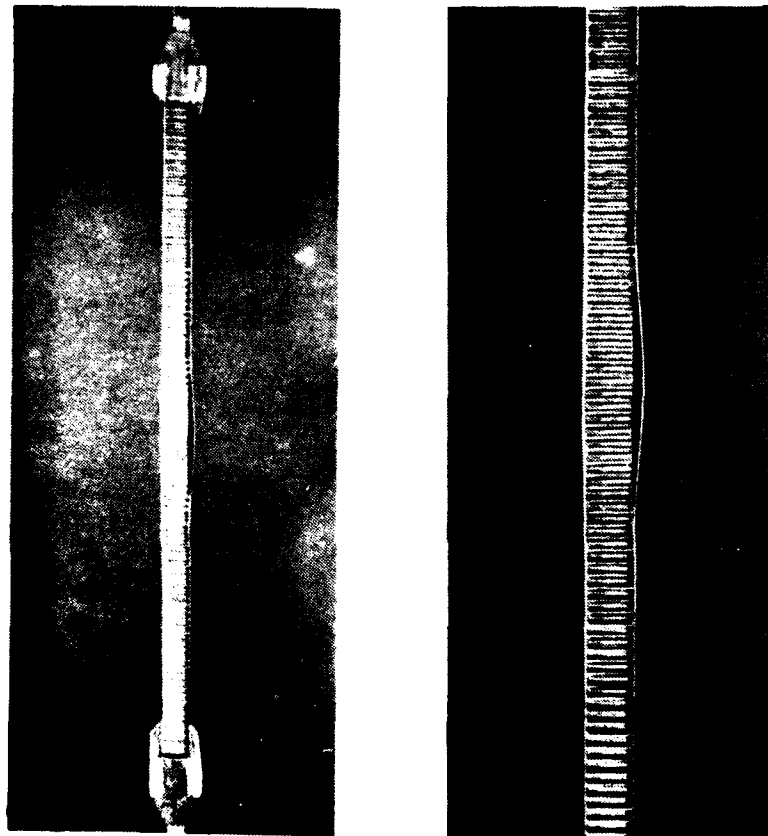
FIG 3.15   BUCKLING FAILURE OF SPECIMEN TEN
(L_U 3.0 IN.)
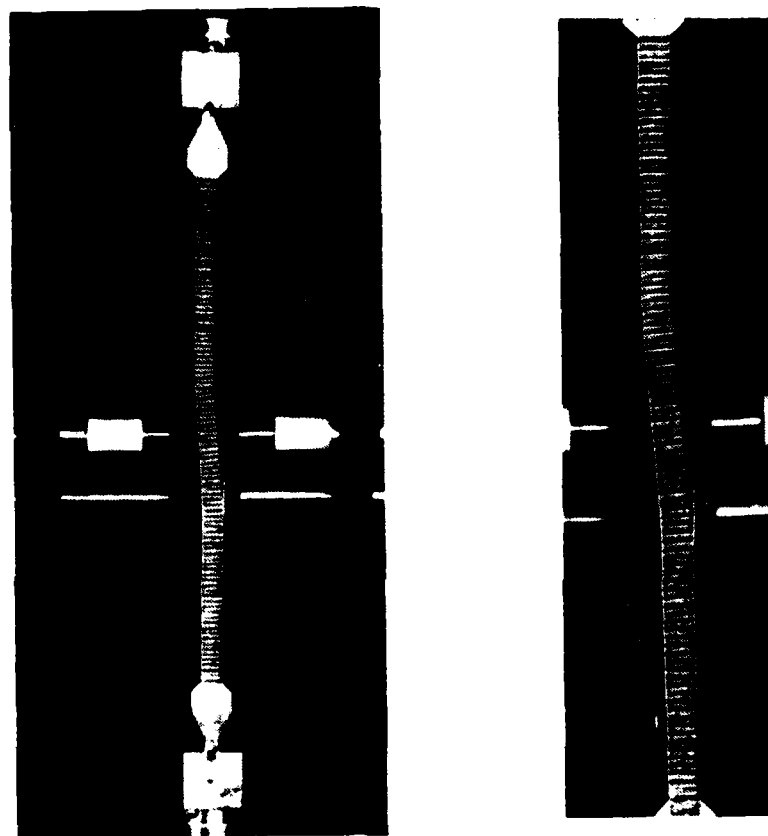
FIG 3.16   BUCKLING FAILURE OF SPECIMEN NINE
(L_U = 5.0 IN.)

Pre-Buckling Geometry

Buckled Geometry

For $\overline{oa}$

For $\overline{ab}$

For $\overline{bc}$
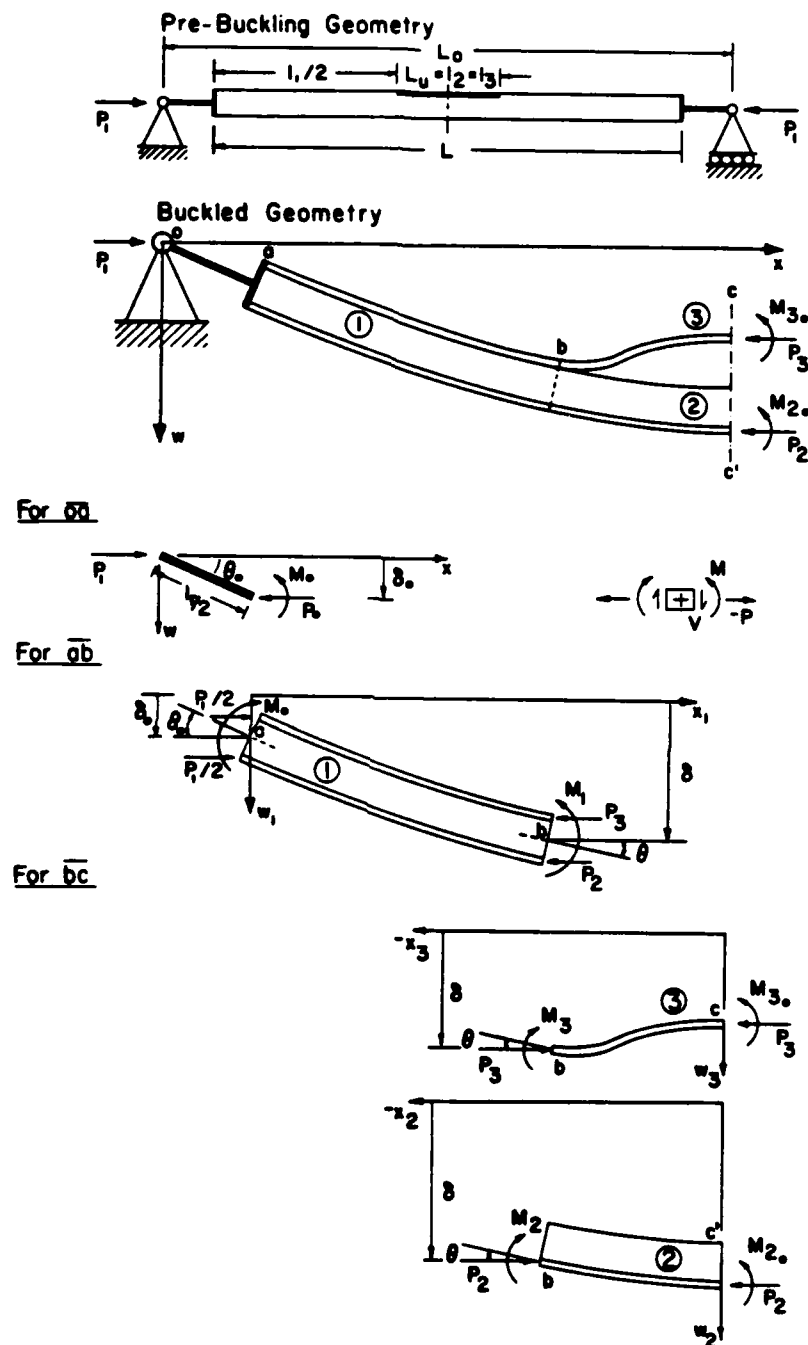
FIG 4.1 SANDWICH BEAM GENERAL MODEL
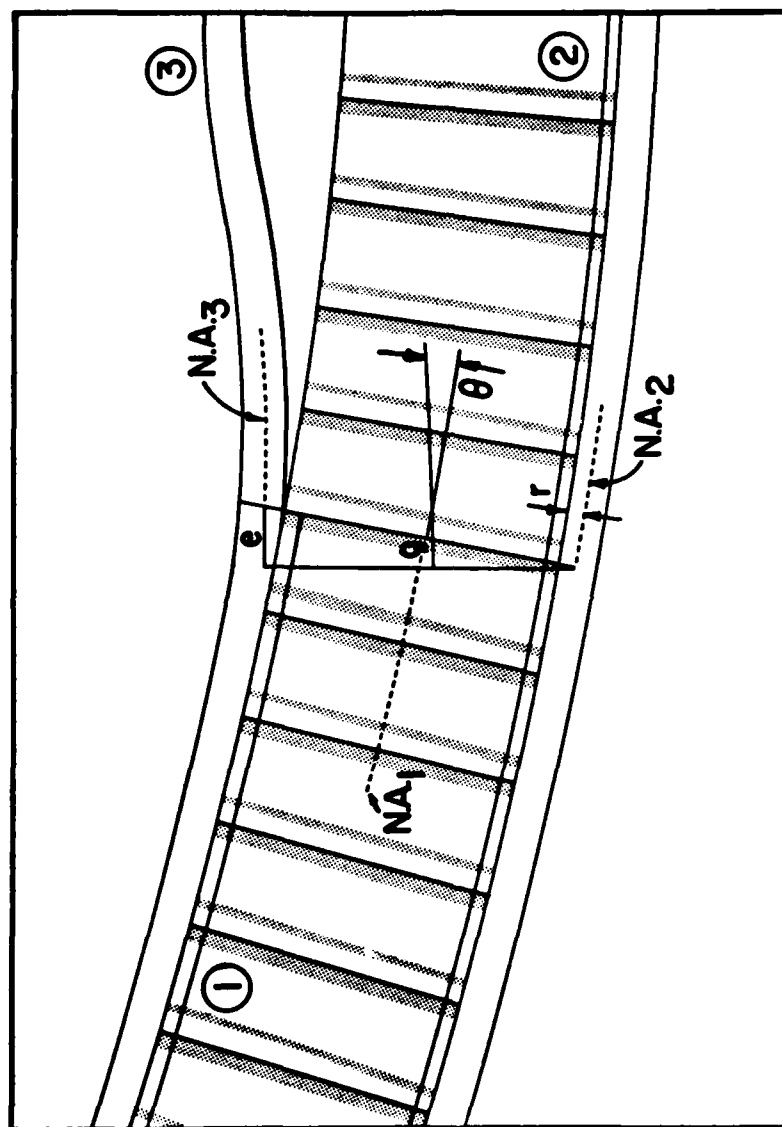
FIG 4.2 GEOMETRY OF THE UNBONDED INTERFACE

110
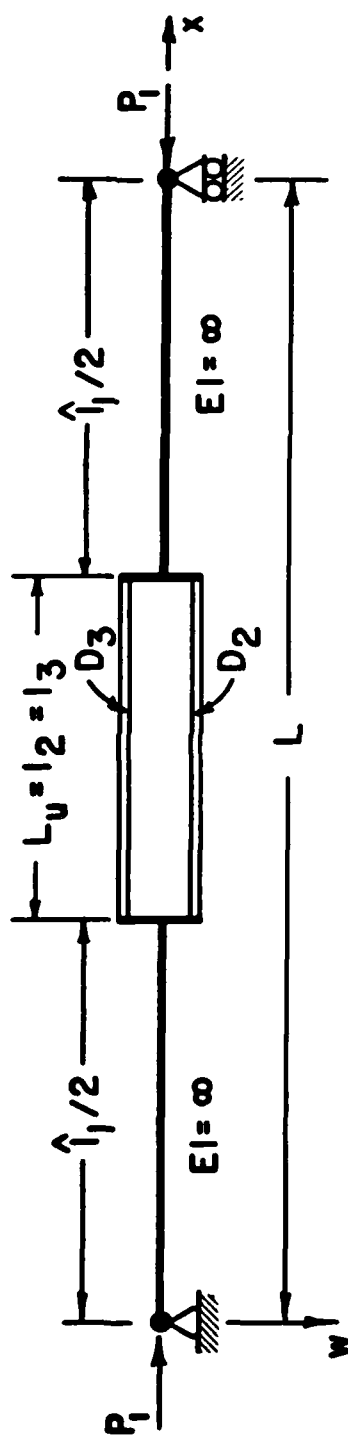
Pre-Buckling Geometry
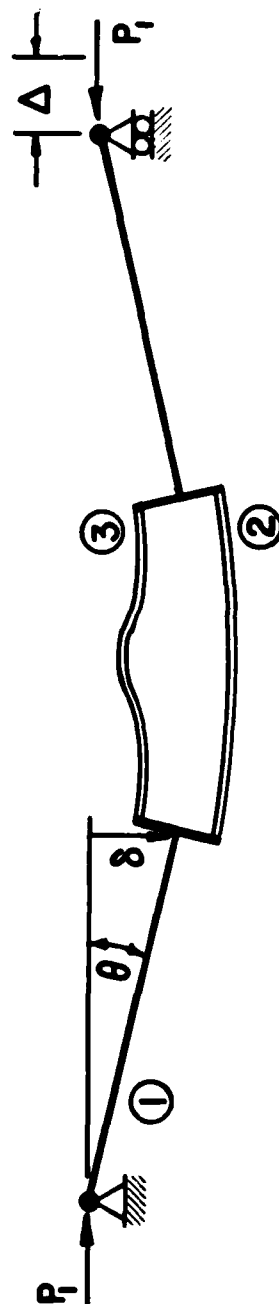
Buckled Geometry

FIG 4.3 SANDWICH BEAM SIMPLIFIED MODEL
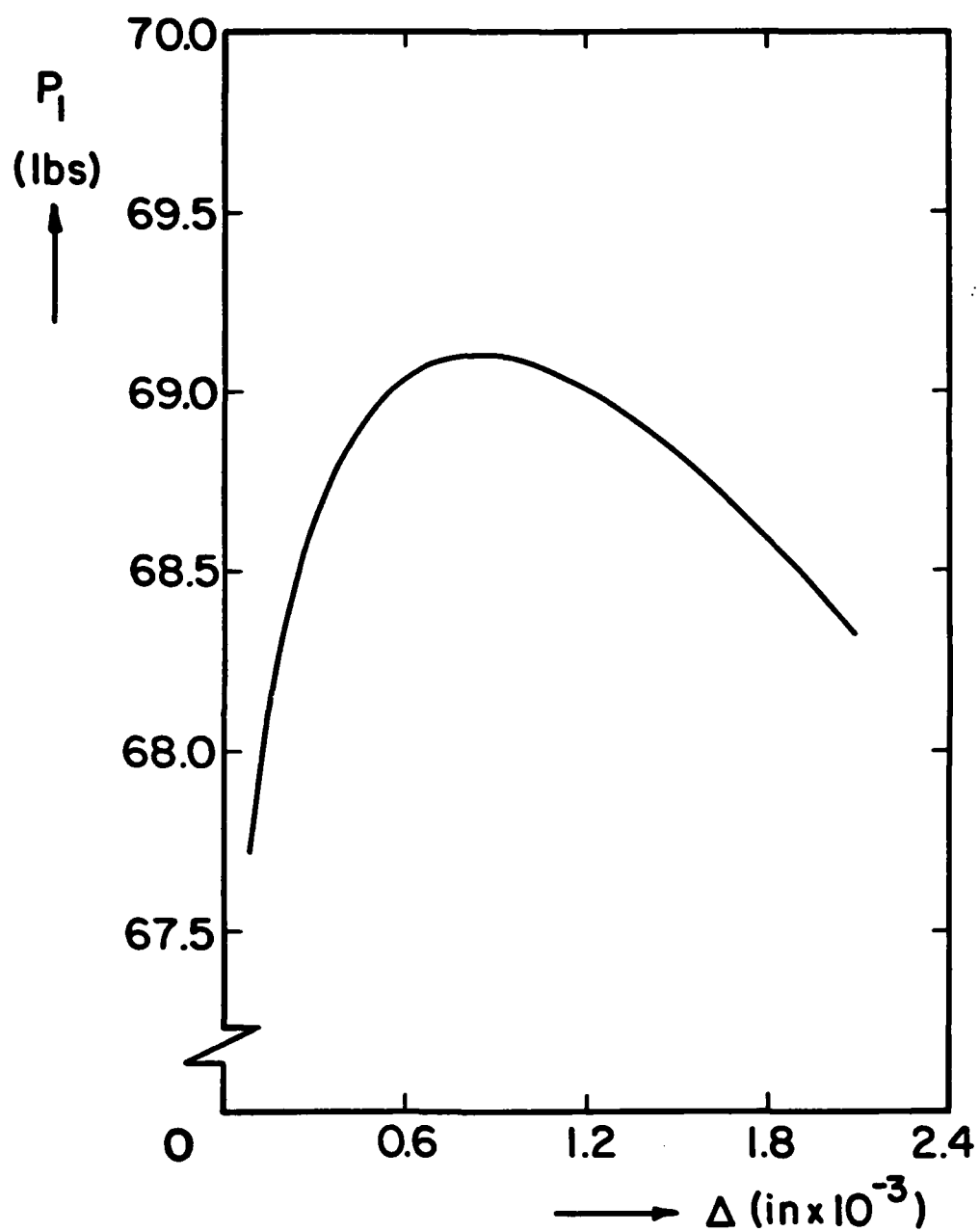
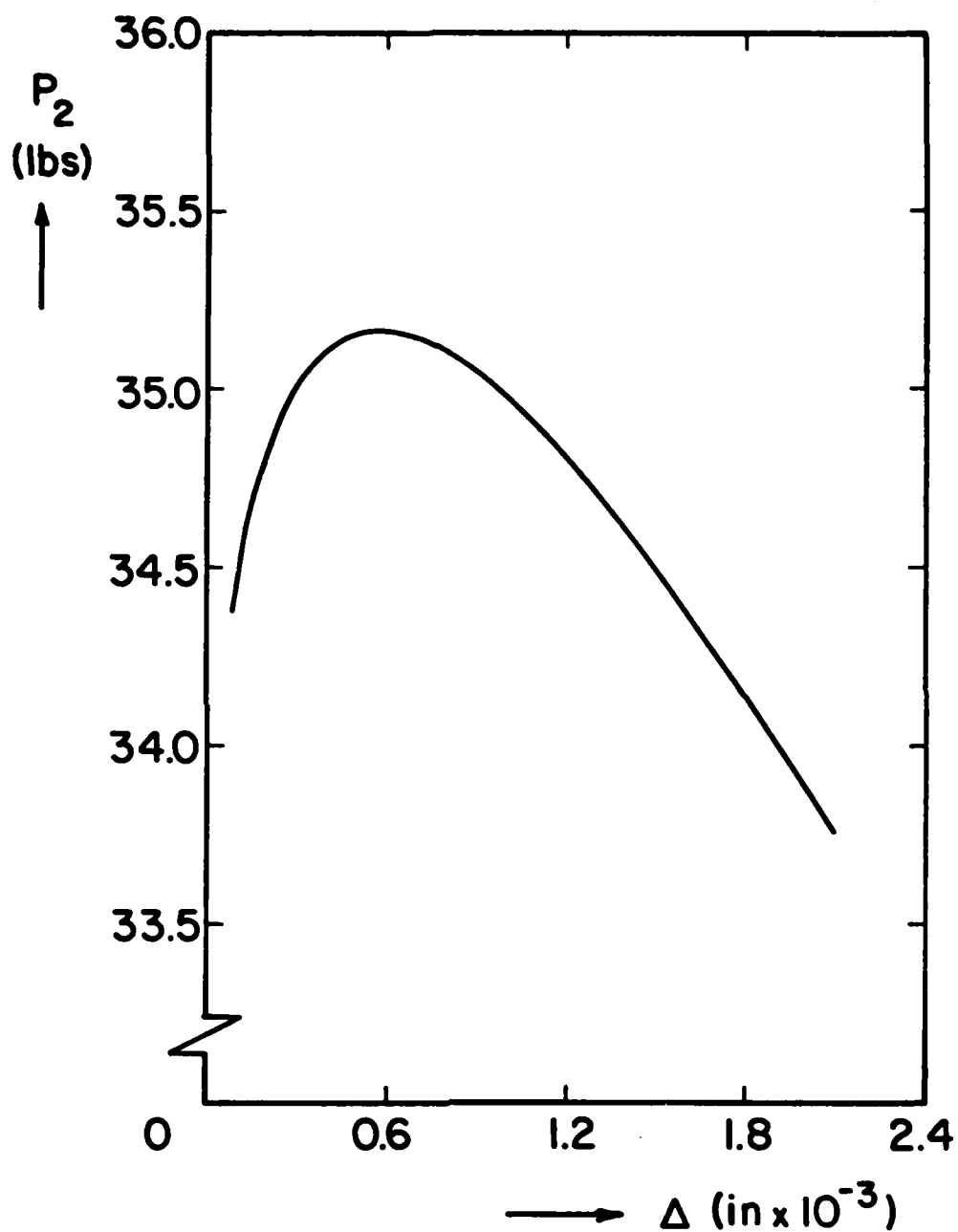FIG 4.4 PREDICTED LOAD VERSUS AXIAL DISPLACEMENT
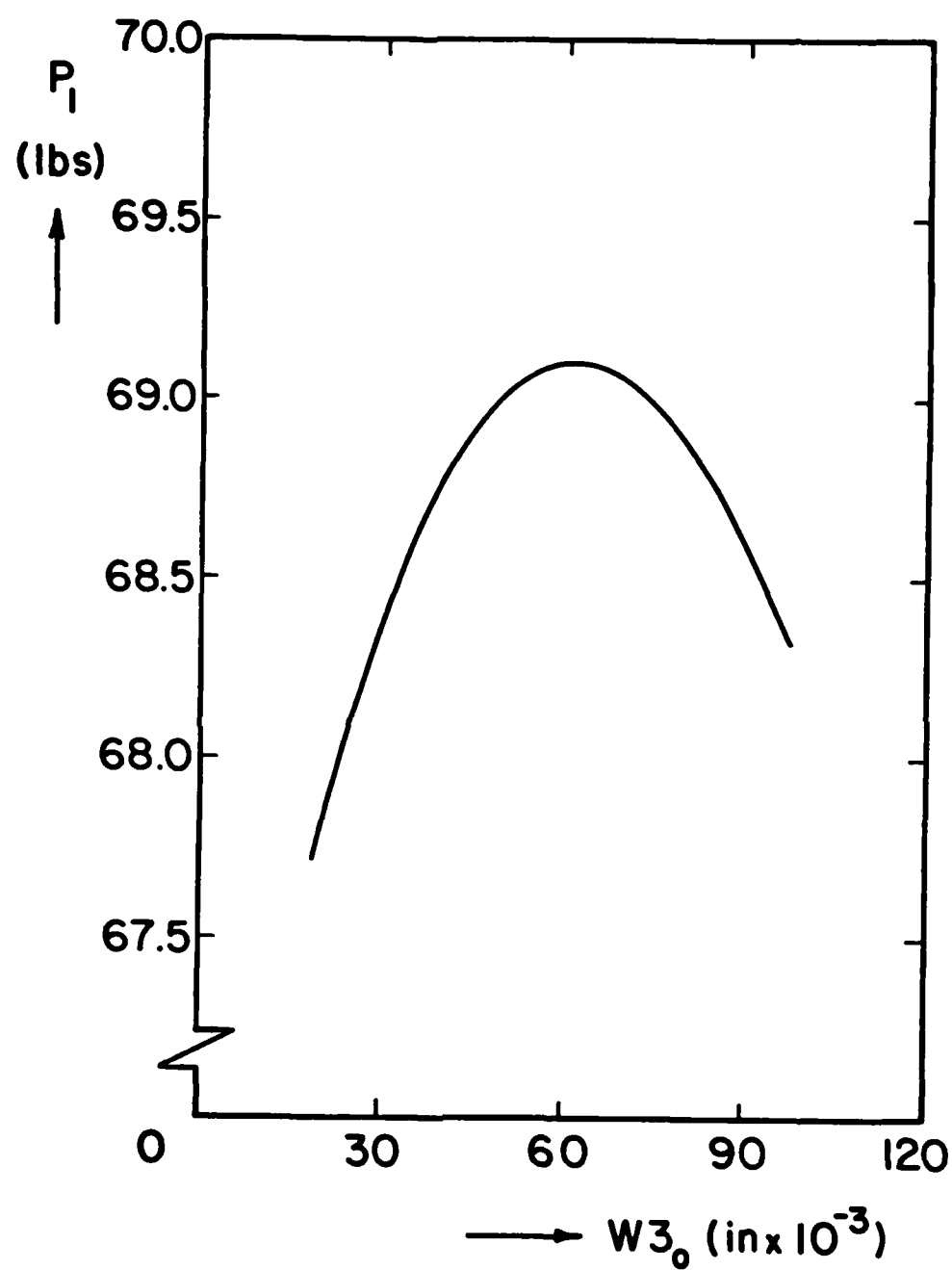(L_u = 5.0 IN.)

FIG 4.5 PREDICTED SECTION TWO LOAD
VERSUS AXIAL DISPLACEMENT (L_u 5.0 IN.)

FIG. 4.6 PREDICTED LOAD VERSUS $W3_0$ DISPLACEMENTS
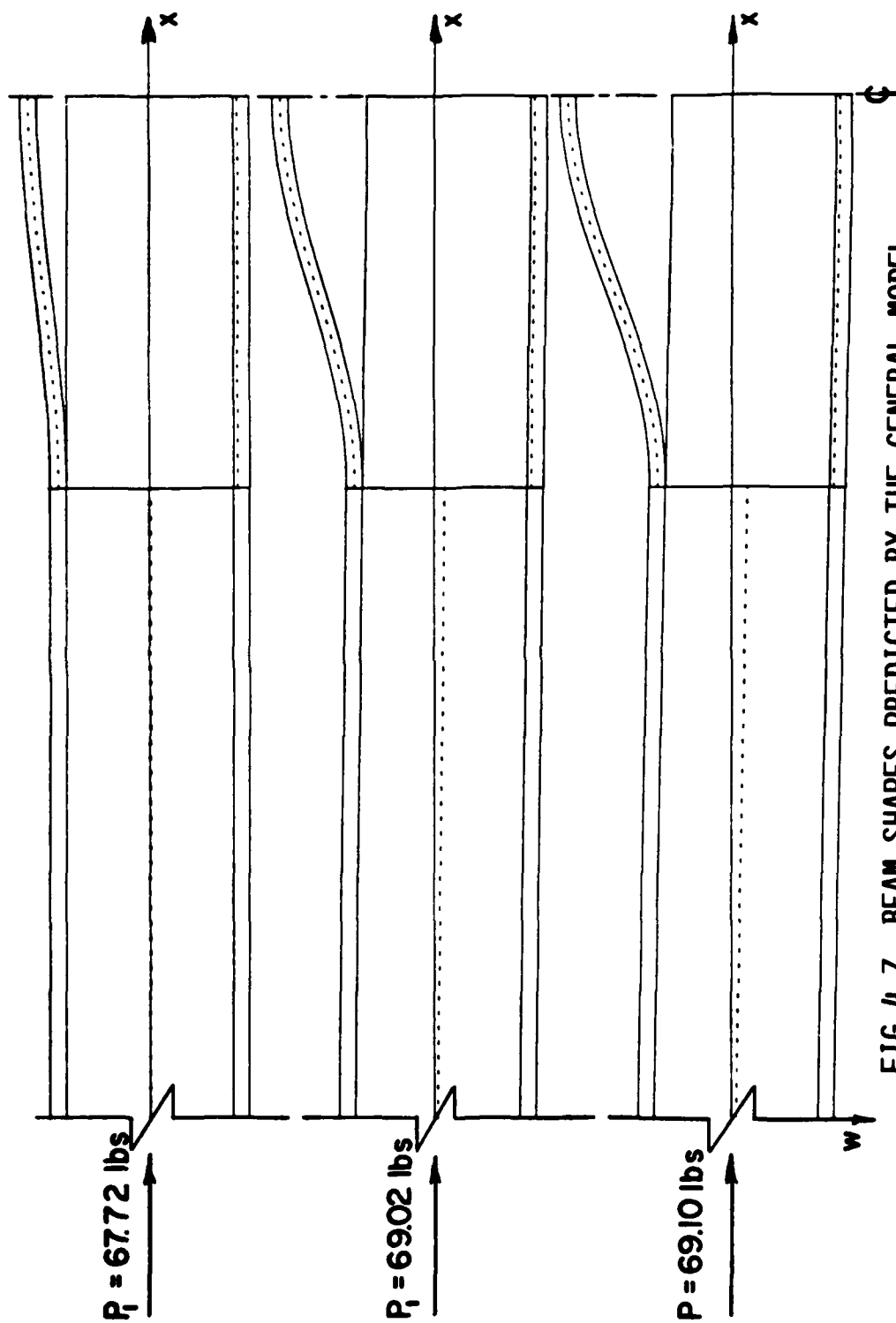$(L_U = 5.0$ IN.$)$

FIG 4.7 BEAM SHAPES PREDICTED BY THE GENERAL MODEL
AT THREE LOADS (L_u = 5.0 IN.) (NOT TO SCALE)

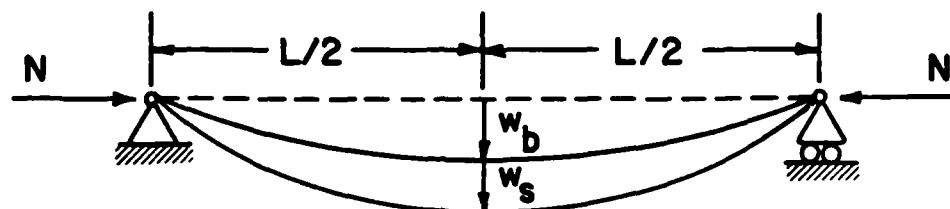P_i = 67.72 lbs

P_i = 69.02 lbs

P = 69.10 lbs

FIG B.1 BENDING AND SHEAR CONTRIBUTIONS TO
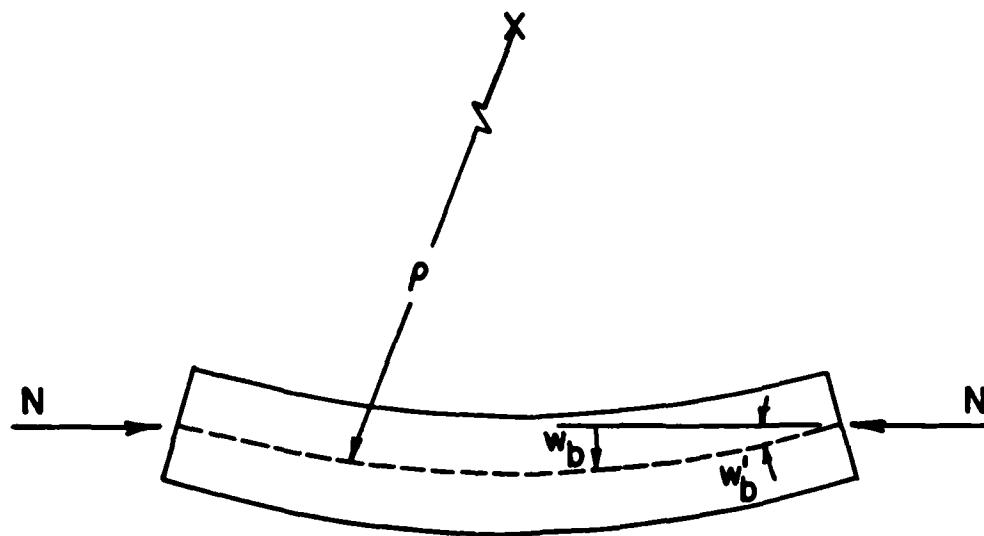TOTAL BUCKLING DEFLECTIONS

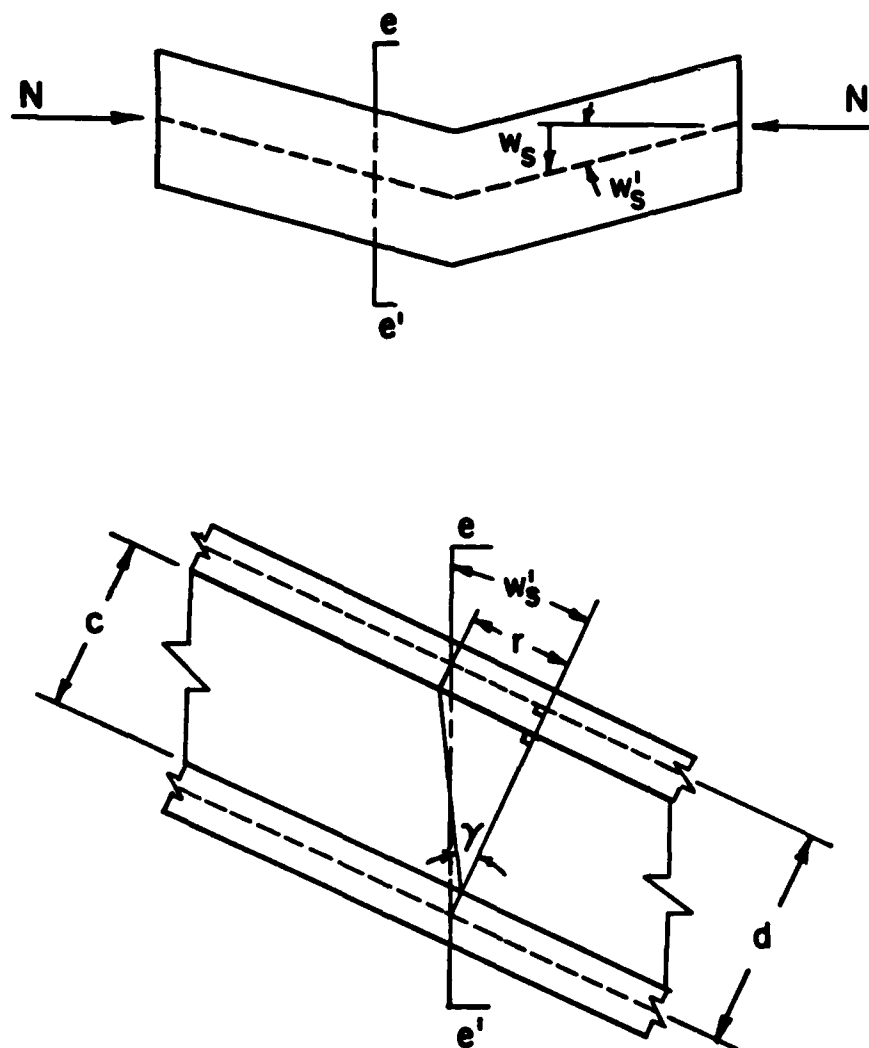FIG B.2 BENDING CONTRIBUTION TO BUCKLING DEFLECTIONS

FIG B.3 SHEAR CONTRIBUTION TO BUCKLING DEFLECTIONS

VITA

Carl Joseph Frushon was born in Wilkes-Barre, Pennsylvania, on July 4, 1962, the son of Rita Elizabeth Frushon and Carl Benjamin Frushon. After completing his work at Hereford Junior-Senior High School, Hereford, Maryland, in 1980, he entered the University of Notre Dame, Notre Dame, Indiana. While at Notre Dame, he was actively involved in the Air Force ROTC program. During the spring of 1983, he became the first Junior to hold the position of Corps Commander. In May, 1984, he received the degree of Bachelor of Science in Aerospace Engineering from the University of Notre Dame. Upon receipt of his degree in May 1984, he was commissioned a Second Lieutenant in the USAF. After acceptance into the Air Force Institute of Technology, Civilian Institutions Program, he entered The Graduate School of The University of Texas in September 1984.

Permanent address: 197 S. Southwood Ave.
                      Annapolis, Maryland 21401

This thesis was typed by the author.

END

12-86

DTIC